Aalto University
School of Engineering

Multi-metal 3D printing with extrusion method

Mehrdad Mousapour

Master's thesis, which has been submitted as a thesis for examination for a Master's degree

Espoo 28.9.2020

Supervisor: Prof. Jouni Partanen

Advisor: Dr. Mika Salmi

Aalto University
School of Engineering

Aalto University, P.O. BOX 11000, 00076 AALTO
www.aalto.fi
Abstract of the master's thesis

Author Mehrdad Mousapour

Title Multi-metal 3D printing with extrusion method

Degree programme Chemical, Biochemical and Materials Engineering

Major Sustainable Metals Processing **Code of major** CHEM3026

Teacher in charge Prof. Jouni Partanen

Advisor Dr. Mika Salmi

Date 28.9.2020 **Number of pages** 83+16 **Language** English

Abstract

3D printing has always been known as one of the most advanced technologies to produce various parts in a wide range of materials. Recently, fabrication of multi material parts has been considered by additive manufacturing technologies. The aim of this work is the feasibility study of manufacturing multi-metal parts by material extrusion technique, deposited from two different metal filaments within a single printing session.

In this master thesis, a brief description of additive manufacturing techniques, their benefits, limitations, and applications were first presented. Then, in experimental work, three stages including printing, de-binding and sintering were studied, and the results compared. According to this, two ferrous alloy filaments i.e. stainless steel 316L and high carbon iron were chosen for printing a couple and a mixed sample. The samples, after de-binding, were isothermally sintered at different target temperatures in the range of 1310-1400 °C for 1h and 6h in argon atmosphere. The sintered samples were cooled down to ambient temperature inside the furnace with slow rate. Finally, sintered density, dimensional changes, and microstructural evolution of the final parts were also investigated.

In conclusion, both couple and mixed types of multi-metal parts were successfully fabricated by fused filament fabrication. The final parts became dense up to 84% and 87% of theoretical density for couple and mixed samples, respectively. Also the amount of shrinkage was around 23% for couple sample, and 12% for mixed sample. Since the surface quality of the sintered samples were not as high as it is acceptable, a post-processing such as machining, sanding or filing is required.

Keywords 3D printing, Fused filament fabrication, Multi-metal additive manufacturing, Ferrous alloys, Sintering

Acknowledgements

First and foremost, I wish to express my sincere gratitude to my supervisor, Prof. Jouni Partanen, for all his supports. Also, I would like to express my appreciation to my advisor, Dr. Mika Salmi, for all the help and support, wise advice, and useful discussion.

I would also like to thank my colleagues at ADDLAB for having such a supportive and fun workplace. I want to extend special thanks to Tuomas Puttonen, who helped me kindly and patiently with printer and 3D models.

I would also like to thank people from CHEM, Lassi Kelemettinen, for his kind help with the furnaces and microscopes; Joonas Lehtonen for his measurements and help with XRD analysis; Ilkka Välimaa for XRF analysis; and Janne Vuori for particle size distribution analysis.

To my mom, and my brother, Farhad: you have always supported me during my whole life. Thank you for encouraging me in all of my pursuits and inspiring me to follow my dreams. I dedicate this thesis to you

Otaniemi, 28.9.2020

Mehrdad Mousapour

Symbols and abbreviations

AM	Additive manufacturing
SL	Stereolithography
DLP	Digital light processing
LOM	laminated object manufacturing
UAM	Ultrasonic additive manufacturing
PBF	Powder bed fusion
SLS	Selective laser sintering
SLM	Selective laser melting
EBM	Electron beam melting
DMLS	Direct metal laser sintering
DED	Directed energy deposition
LENS	Laser engineered net shaping
MJ	Material jetting
CS	Continuous stream
DOD	Drop on demand
BJ	Binder jetting
FDM	Fused deposition modeling
FFF	Fused filament fabrication
LPS	Liquid phase sintering
SLPS	Supersolidus liquid phase sintering

Contents

List of Figures

List of tables

1- Introduction

Additive Manufacturing (AM) is a technology that has dramatically been developed and applied to all sorts of fields in the last three decades. It has been labeled by a variety of names, such as three-dimensional (3D) printing, rapid prototyping (RP), layered manufacturing (LM), or solid free-form fabrication (SFF) [1]. Theoretically, AM is a technique in which 3D designs can be built directly from a computer-aided design (CAD) file with no further tools. The CAD model is divided into individual slices, commonly in the format of the STereoLithography (STL) and then the data sent to a machine to print the objects layer-by-layer [2].

In recent years, AM applications have widely been expanded in various fields from aerospace and automotive to biomedicine and energy [3-7]. Aerospace components usually have complex geometries and are made from specific materials, such as titanium alloys, nickel superalloys, high temperature refractories, where AM is a suitable option to manufacture. AM can also reduce product costs of some structural and functional automotive parts, such as engine exhausts, drive shafts, gear box components and braking systems for low-volume vehicles. Undoubtedly, one of the most significant applications of AM is in the biomedical fields so that this technique has a considerable contribution in production of orthopedic implants, tissue scaffolds, artificial organs, medical devices, micro-vasculature networks, and biologic chips [8-12].

AM contains 8 steps from the virtual CAD description to the final physical parts. The steps are including: 1. CAD: *all the AM parts should be first modeled by a design software so that fully describes the geometry*. 2. Conversion to STL: *the CAD model files must be converted to STL format to become readable for AM machines.* 3. File transfer to machine: *in this step, the transferred file might need some corrections in size, position and orientation for building.* 4. Machine setup: *some complementary setups need to be done related to the build parameters such as, materials constraints, energy source, layer thickness, timings, etc.* 5. Build: *the machine starts automatically building the part.* 6. Removal: *the parts should be removed after building is completed.* 7. Post-processing: *the parts might need some extra actions (including cleaning up, removing supports, etc.) before they are ready to use.* 8. Applications: *In order to make the parts acceptable for use, some other additional treatments such as, surface machining, heat treatment, etc. might be required* [13].

One of the most significant benefits of AM is producing parts in any geometry. However, there are some rules that must be taken into account per technology during printing. Beside this, AM requires no expensive tooling and high startup costs, which makes this technology profitable to produce the prototypes and low-volume production parts with required properties [14]. In contrast, low repeatability precision (due to differential cooling or warping) and also producing not fully dense parts are the biggest limitations of 3D metal printing [15].

In comparison with other technologies, which usually have multistage processes (including hand carving, molding, forming techniques, CNC machining, etc.), AM reduces the number of processes and prevents making them difficult and prone to error. For instance, molding technology needs building molds, careful planning required for CNC machining and also some fixtures must be built before the part itself can be made. Although CNC parts are often more homogeneous and predictable in quality than AM parts, CNC machines can be only used for those machinable materials such as metals. There are many options in both CNC and AM machines that must be set, but the range and complexity in the case of AM are relatively less than CNC [13]. Based on the experimental results, AM is much more environmentally friendly than machining, with an impact reduction of about 70%. In the case of energy consumption, however, there is no firm evidence yet to prove that AM has an edge over conventional manufacturing processes [16].

Although AM emerged in the 1980's for creating models and prototypes with shorter time and lower cost (well known as rapid prototyping), this technique has recently become an important commercial manufacturing method for all types of materials. Among them, many research studies have been focused on manufacturing metal parts in order to develop the link between processing, properties and microstructure. According to literatures, metallic AM systems can be classified, based on feeding system, to three categories: (a) powder bed systems, (b) powder feed systems, and (c) filament feed systems [17-19].

Fused filament fabrication (FFF) is one of the most common forms of AM technology that uses a continuous material. FFF was first proposed by the company Stratasys as fused deposition modeling (FDM) and used for thermoplastic materials. Although the primary idea of using FDM for manufacturing of metal and ceramic parts was suggested in the 1990's, there were only a few attempts carried out until the middle of the 2010's. Nevertheless, some metal parts (such as, stainless steel, copper, aluminum, etc.) have been built in the past few

years, thanks to the composite filaments in which highly filled polymers are mixed with metal powders [20, 21]. Beside this, some studies have been done on additive multi materials manufacturing e.g. building multi-color polymer parts. It seems that, however, there is still lack of information on manufacturing multi metal parts (metallic alloys) from different metallic filaments by this technique.

The aim of this work is the feasibility study of manufacturing multi metal parts by material extrusion technique, deposited from two different metal filaments within a single printing session. In this study the different types of AM, their history, mechanisms, and effective parameters will be first covered. Then the research methods and materials will be introduced in detail, and finally the results including microstructure, some physical properties, dimensional changes, and sintering conditions of final parts will be analyzed and discussed.

2- Background

It is important to become familiar with different aspects of AM and the prominent factors, which might affect the production properties, in order to choose the best type of it for specific applications. Basically, the effective parameters on AM can be divided to 4 key factors: input, method, materials and applications. Figure 1 indicates the AM wheel including these 4 parameters. Input implies on the electronic information that describe the part. It can be either a computer or physical model, in which both surface and solid models are used. Although many methods have been introduced for AM systems, it generally can be categorized into: cutting and joining, melting and solidifying or fusing, joining or binding, and photo-curing. The latter one can also be divided further to single laser beam, double laser beam and masked lamp [22].

The initial categorization for materials in AM systems is in the following forms: solid, liquid or powder state, where solid materials are in the form of pellets, wire and laminates. General materials used in AM are including paper, polymer, wax, resins, metals and ceramics. Applications are classified based on manufacturing and tooling, engineering and analysis, and design in a wide variety of industries [22].

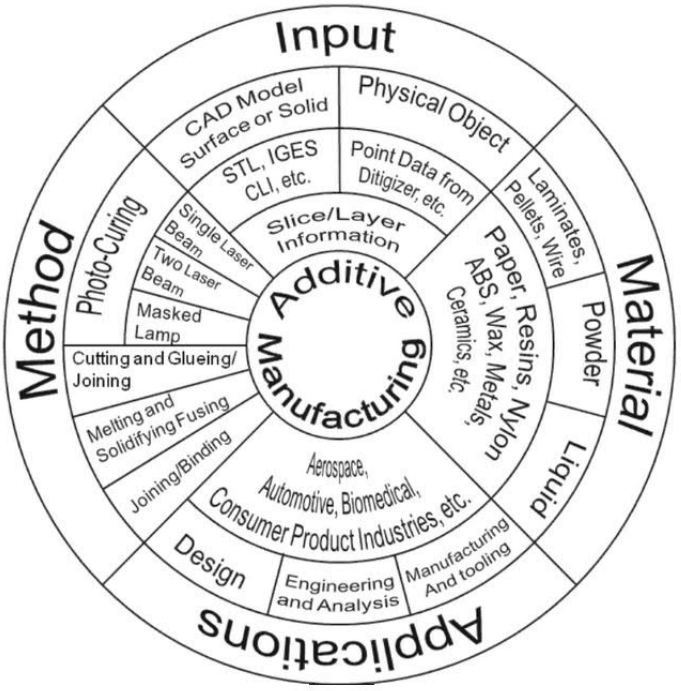

Figure 1: The Additive Manufacturing wheel including 4 key factors [22].

2-1- AM technologies

There are a few ways to classify the technologies based on their tools, sources and applications. The most common way for categorizing AM technologies, however, is based on ISO/ASTM standard 52900:15 system [23] in which the technologies mentioned as follows: 1) Vat photopolymerization, 2) Sheet lamination, 3) Powder bed fusion, 4) Directed energy deposition, 5) Material jetting, 6) Binder jetting, 7) Material extrusion. Each technology is including various techniques that will be expanded in detail later in this thesis.

Stereolithography apparatus (SLA) was the first AM technology that used for fabrication of parts from UV photopolymerizable materials. In order to increase the build speed of parts and save time, another method called digital light processing (DLP) was derived from SLA to produce 3D models. This technique, which in some literatures known as film transfer imaging (FTI), considered as subclassification of vat photopolymerization technology. The other technology is laminated object manufacturing (LOM), which is a rapid prototyping process so that a part is built from layers of paper [24].

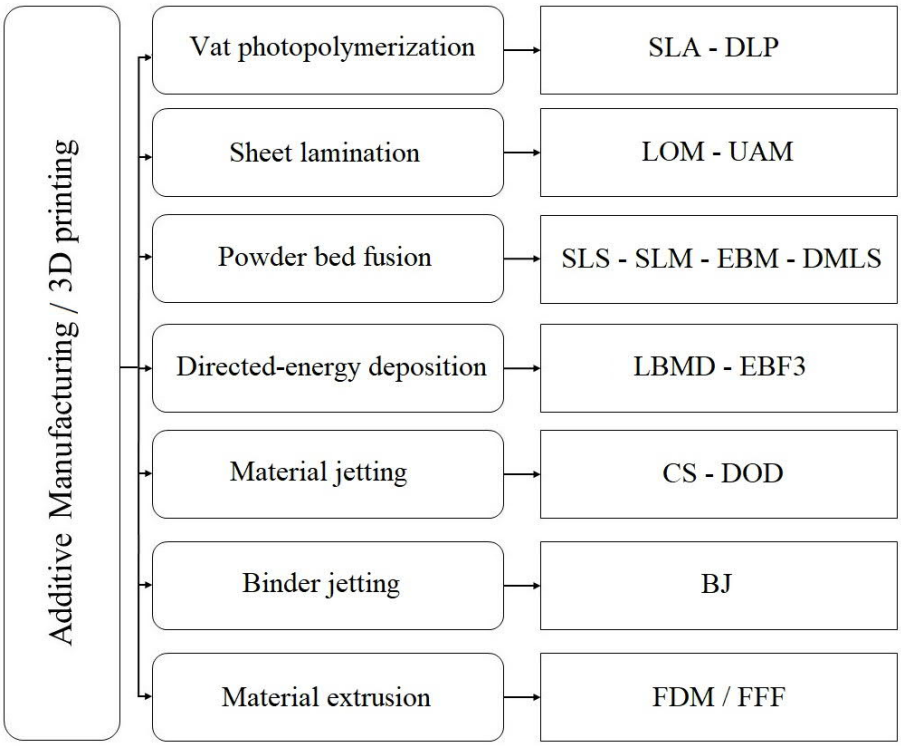

Figure 2: Standard classification of AM technologies based on ISO/ASTM 52900:15 [23].

Powder bed fusion technology can be divided to selective laser sintering (SLS), selective laser melting (SLM), electron beam melting (EBM) and direct metal laser sintering (DMLS). The main methods in extrusion technology are categorized, based on how materials are deposited, to directed energy deposition (DED) and material extrusion (ME). Also jetting technology can be described by two major techniques: material jetting (MJ) and Binder jetting (BJ), where the main materials and binder are deposited, respectively, by a jet system [24]. This classification is shown schematically in Figure 2.

Each of these technologies, depending on their mechanism and the amount of used materials in one part, has different response to productivity and production time. For example, adding more parts in material extrusion technology increases the production time, while more parts will reduce the time for producing a build in PBF, VAT, MJ, BJ, and LOM [25].

2-1-1- Vat Photopolymerization

The primary materials used in vat photopolymerization process are liquid, radiation-curable resin, or photopolymers. A chemical reaction due to irritation resulting in solidifying the primary materials. This reaction is well known as photopolymerization. Although most photopolymers react with various types of radiation in the range of gamma rays, X-rays, electron beams, and ultraviolet (UV), visible light is also being used in some cases. For instance, photomask materials are irradiated by far UV and electron beams, while visible lights are more common in dentistry [13].

Photopolymers were widely used in various areas from coating on paper and cardboard to sealing the teeth surface by photo curable resins. The process changed, when solid polymer patterns were produced by lasering UV curable materials. Thanks to this invention, stereolithography (SL) technology was introduced so that 3D parts can be fabricated based on curing a layer over another [13].

The most two significant benefits that vat photopolymerization has compared to other AM technologies are dimensional accuracy and surface finish. These two advantages have resulted in expanded use of this technology in rapid prototyping field. The dimensional accuracy for SL machines is usually introduced as a ratio of an error per unit length. For instance, SLA-250 has an accuracy of 0.002 in./in, however, modern machines are even more accurate. Regarding surface finish, SL parts have ranges from submicron to over 100μm Ra for up-facing surfaces and surfaces at slanted angles, respectively [13].

The other advantages of vat photopolymerization are the adaptability of this technology with different machine configurations, flexibility and size scales. The various types of sources from lasers and lamps to LEDs, as well as different patterns including scanning galvanometers or DMDs can be used in this technology. One of the most interesting features of vat technology is a great variety in size range, which can produce the parts from the 1.5 m vat in the iPro 9000XL SLA Center to the 100 nm features with two-photons photopolymerization. High resolution is one of the characteristics of the parts fabricated by this technology, where there is a balance between resolution and the size of the pattern. For example, the resolution of DMDs is 1024×780 or 1280×720, however, the newer HDTV DMDs have higher resolution (1920×1080). In spite of that, to build a part with resolution of 50μm or better, the projected area of maximum 96×54 mm is required [13].

Although vat photopolymerization is a suitable technique to manufacture high resolution parts, the most important drawback of this process is limitation in materials selection so that only photopolymerizable materials can be used. In order to expand the application of this technique, some attempts have been done to produce multi materials. such as nanocomposites by adding nanoscale reinforcements to resin [26]. According to literatures, there are two main formats for photopolymerization process describing as follows:

2-1-1-1- Stereolithography (SLA)

The laser lithography is one of the most common methods in AM technology. Currently, SLA is being used for fabricating not only photopolymerizable materials, but also direct making of ceramics. In fact, ceramic powders (mostly silica and alumina) can be added to a fluid UV curable monomer to form a composite solution. Then composite layers are fabricated using a laser beam and photopolymerization reaction similar to conventional SLA process [24].

In some references, another photopolymerization format that is introduced called two-photon. In this method, reaction occurs at the meeting of two laser beams. Unlike SLA, no recoating needed in two-photon method, and the part will be built below of resin that makes the process faster and less complicated. Another important benefit of using 2 scanning beams is to greatly increase the resolution of photopolymerization, where the photon density becomes high enough for the process [13].

2-1-1-2- Digital light processing (DLP)

Although two-photon method could, to some extent, reduce the producing time and increase the built speed, film transfer imaging (FTI) technology was introduced to produce 3D models

with high resolution using a photomask system to reach a layer thickness of 30µm. Unlike SLA, masking technology uses a UV flash of light instead of a laser beam so that this flashlight projected by a DLP projector to cure the resin (UV photopolymerized material) and produce each slice after another. By projecting to the entire layer rather than lasering lines or points, DLP enables to produce the models much faster than other methods of rapid prototyping. Another difference of DLP is the direction of build platform movement, where the part pulled upward out of the resin, while the part movement is downward into the resin in SLA [24]. Figure 3 schematically shows the process of all 3 types of vat photopolymerization technology.

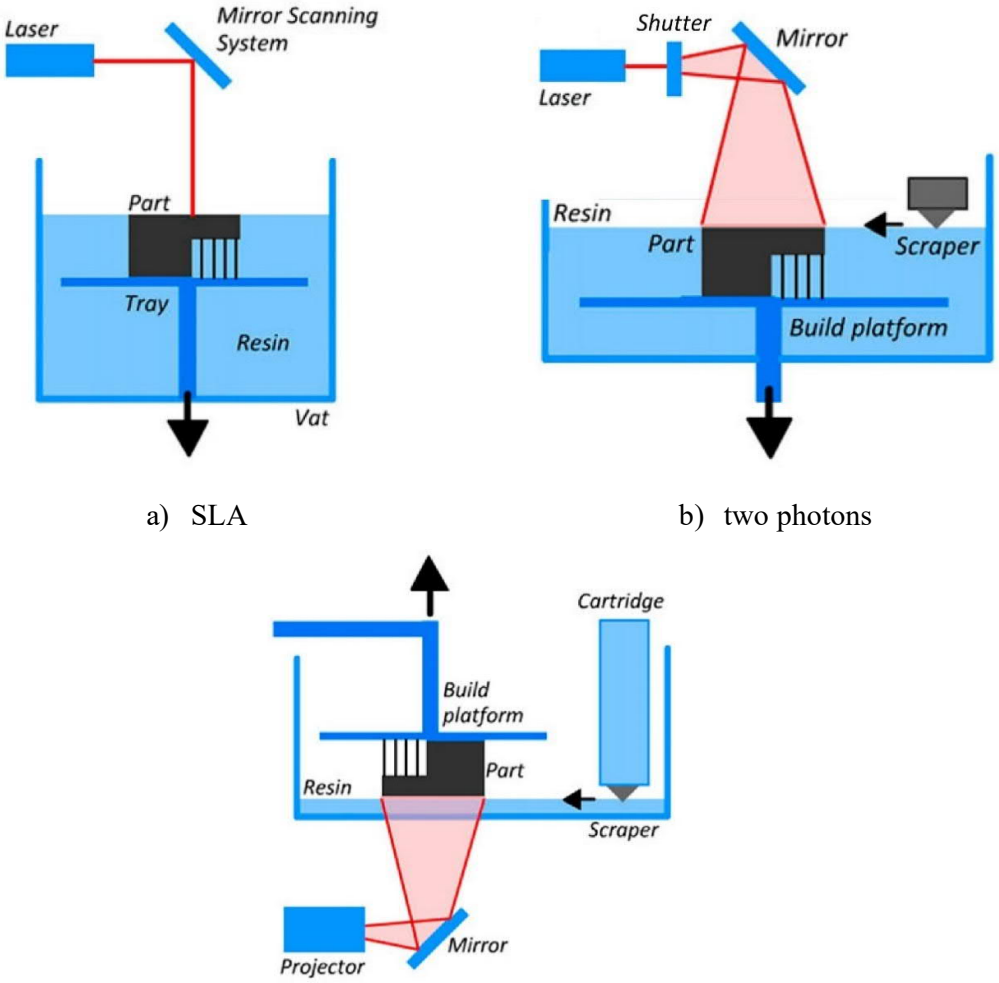

a) SLA

b) two photons

c) DLP

Figure 3: A schematic of 3 types of vat photopolymerization technology [24].

2-1-2- Sheet Lamination

This AM method involves cutting and bonding the materials, where a part is built from layers of sheet. This technique, well known as laminated object manufacturing (LOM), consists of cutting a pattern of paper layers (uniform thickness) using a CO_2 laser and the thermal adhesive bonding. There is a x-y plotter device above the worktable creating a layer from the material sheet. The formed layers are bonded by heat-sensitive adhesives and an applied lamination force. The layers placed over each other to build the final part so that the resolution can be defined as the thickness of the paper sheet [24]. One of the advantages of LOM is that this technique can be used for various materials including ceramics, polymer composites, paper and metal-filled tapes [27]. The technology of LOM is schematically indicated in Figure 4a.

Depending on the type of materials, some post processing such as heat treatment might be required. LOM is also the only AM method capable for manufacturing metallic parts at low temperature. Furthermore, this technique can lead to reduction in tooling costs and manufacturing time, and one of the best choices for larger structures. Since LOM uses relatively low processing temperature, this is an appropriate technology for electronic encapsulation and embedded electronic system applications [27].

In spite of mentioned benefits for LOM, the parts manufactured by this technique have poor surface quality, which often makes post-processing necessary. On the other side, compared to other AM methods (specifically powder bed), has lower dimensional accuracy, and also more time needed to remove the excess parts from the main object. One of the most critical problem of LOM is delamination between the bonded layers. Solving this problem should be taken into account to increase the application of sheet lamination processes [28].

Other sheet lamination processes have been derived from LOM and developed based on different cutting strategies. Depending on the mechanism of layer bonding, these processes can be classified to a) gluing or adhesive bonding, b) thermal bonding, c) clamping, d) ultrasonic welding. In the case of gluing, a polymer-based adhesive is used for bonding the sheet layers. According to the order in which the layers are cut and bonded, the processes can be categorized to “bond-then-form” and “form-then-bond”. The latter approach is suitable for construction of the parts with small internal channels, where removing excess materials from the internal features is difficult or impossible. Among these developed processes, however, ultrasonic welding has several features that make it even more interesting [13].

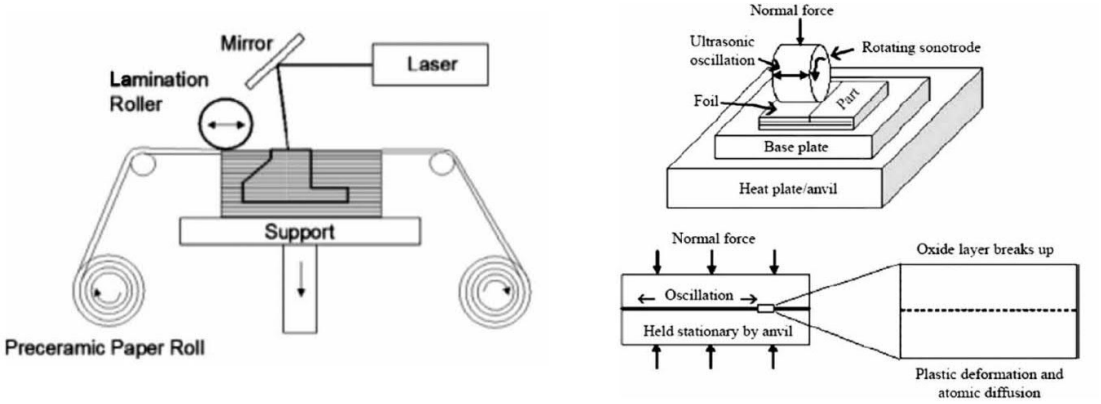

a) LOM b) UAM

Figure 4: A schematic of two sheet lamination processes [28].

2-1-2-1- Ultrasonic additive manufacturing (UAM)

UAM, also known as ultrasonic consolidation (UC), is combining ultrasonic metal seam welding and subtractive contour milling. A low energy ultrasonic frequency is applied using rotating sonotrode to bond sheet materials and build the object onto a heated platen. The objects are constructed from bottom to top with relatively low temperature between room temperature and 200°C, which makes UAM one of the most suitable techniques to build metallic parts with the least changes in properties. The object eventually is trimmed by CNC milling to provide the desired shape. Nevertheless, UAM can be considered as a bond-then-form process, where forming of the object happens after ultrasonic bonding. The UAM system is shown in Figure 4b.

The most significant process parameters effective in the quality of bonding in UAM can be named as oscillation amplitude, normal force, travel speed, and temperature. Oscillation amplitude is a criterion for the amount of ultrasonic energy so that the higher amplitude, the greater energy. Based on literatures, a better welding (bonding) quality is achievable by greater ultrasonic energy input. There is, however, an optimum level for input energy depending on thickness, material and geometry that should be applied in a balance with welding traveling speed. In order to reach the best metallurgical bonding, a sufficient load (normal force) is required to be applied on the layers by sonotrode. Although heating can facilitate bond formation in metals, excess heating will create harmful effects [13].

2-1-3- Powder Bed Fusion

Powder bed fusion (PBF) process is a type of AM that uses a thermal energy (laser or electron beam) to melt polymer, metal or ceramic powder materials. A layer of powder material is fed on a build plate by a blade or wiper mechanism. The thickness of each layer is defined by the distance between the surface of finished layer and the bottom edge of the blade. This thickness could be different depending on the type of material so that for metal powders it is between a few tens of microns and 100 μm, while the range of 50-150 μm has been reported in polymer systems. Alongside the layer thickness, there are other effective parameters and factors such as power, geometry, powder particle size and size distribution that must be carefully selected and calibrated.

Once the layer is fed on the plate, the energy beam applied on the powder bed and build a slice of the object based on the 3d data. After completion of one layer, the machine repeats similar processes for the following layers to finish the whole object. An important point in PBF technology that should be taken into consideration is that the lower layer is affected by the energy beam exposure so that a certain depth of previous finished layer is melted, and a full fusion occurs in two layers [29].

Some of the advantages of PBF are fine resolution, high quality of printing and great dimensional accuracy of the final part. With these features, a widespread range of parts with complex structures can be built by PBF technology. This process is widely used for advanced applications in different industries such as aerospace, electronics, lattices, scaffolds for tissue engineering, etc. Also, various types of materials including polymers, ceramics, metals and composites are printable by PBF. Since powder bed can be used as a support, this technique has diminished the challenges of removing supporting materials after printing [27].

In contrast, PBF is a slow process with high costs that limits utilizing of the method. In the case of the powders that fused with a binder, high porosity in the final parts is the other drawback of this process. As well as this, the particle size and shape, and size distribution are the other limiting factors that must be carefully selected, where spherical particles with a certain size are used to gain the best result [11].

There are several types of powder bed fusion technology. Although all the types follow the same working principle, a few differences can be mentioned in process capability, conditions and part characteristics. The most common four types of PBF process are described below in more details:

2-1-3-1- Selective laser sintering (SLS)

In this method, the small particles are fused by a high-power laser so that not completely melted but heated up to the temperatures in which molecules are able to fuse together. Therefore, the used energy beam for this process must be carefully set. The SLS machines, for instance, use laser powers in the range of 30-200W in a CO_2 chamber controller. Also, a variety types of powder materials such as polyamid, steel, titanium, metallic alloys, ceramic powders, etc., were formerly sintered by SLS. However, recently this method is not being used to produce metal parts anymore [24].

Since the diffusion rate as the most important parameter in solid state sintering dramatically increases with temperature, sintering becomes rapid when the temperature reaches close to melting point. It basically happens at temperatures between a half of absolute melting point and the melting point. On the other side, this is an accepted fact that the sintering rate slows with decreasing the total surface area to volume ratio for a set of particles. In the case of PBF, the total surface area to volume ratio is directly dependent on particle size. Hence, smaller particles lead to increase in driving force for necking, and consequently sintering with lower laser power.

One of the methods for construction of polymer parts is laser sintering. Although most commercial polymers are being processed by injection molding, there is a difference in thermal and stress conditions for polymers when they are built by laser sintering. In the case of injection molding, the polymer is heated slowly, conveyed into a mold under high shear forces, and cooled with high rate. Whereas, in laser sintering process, the material is heated with high rate, flows by surface tension, and cooled very slow. Since the polymer microstructure is related to temperature and time processing, the properties of final polymer parts made by laser sintering are different than those by injection molding [13].

Due to shortage of appropriate machines for laser sintering of ceramic parts, SLS has not been widely used for ceramic powders [30]. Since ceramic materials have much higher melting point than polymers and metals, high energy input needed that makes them difficult to become sintered. Another interesting parameter in laser sintering process of ceramics is atmosphere. Argon gas and vacuum atmosphere are the most common inert environment being used during laser sintering of polymers and metals. Although these mentioned atmospheres are also options for ceramic laser sintering, oxidation and reduction reactions

may occur in ceramic powders (oxide) depending on the oxygen and nitrogen containing atmosphere [31].

2-1-3-2- Selective laser melting (SLM)

Similar to SLS, the powder is fused by a powerful laser beam layer by layer based on the points defined by CAD file data, while these layers are completely melted and consolidated over each other to build the final 3D object. Thermal energy induced by laser beam is sufficient to melt the thin powder layer and bond it to the previous solidified layers. Recently, some modern machines have been introduced with multi laser technology in which layers can be printed with the thickness of 75-150 μm [24]. Figure 5 shows a schematic of SLS/SLM processing.

Physical phenomena that occur during SLM can be introduced as follows: adsorption and scattering of laser radiation, phase transformation, heat transfer, fluid flow within the molten pool due to surface tension gradient, emission and evaporation of material, and chemical reactions. During the process, a part of radiation is adsorbed by the outside surface of particles, and the rest is penetrating through the pores and interacts with particles in the lower layers [32].

The most common materials used in SLM are metallic alloys and semi-crystalline polymers. Nylon polymade, as a prevalent semi-crystalline polymer, must be fully melted during the process to present the highest strength. In the case of metal parts, cobalt chrome, steel, stainless steel, aluminum and titanium alloys are some of the materials being used in this process. High rate of melting and solidification in SLM processing of these metallic alloys leads to specific desirable properties that might be unreachable with conventional casting methods [13].

However, high temperature in SLM might result in part growth and consequently reduce dimensional accuracy. As well as this, since a wide area in powder bed is affected by high energy laser, it is difficult to build a part with thin walls. On the other side, the heat induced by laser beam influences the particles near the printed part, which results in reduction of surface quality [33,34]. In this situation, it seems to be necessary to create a balance between accuracy and strength of the part.

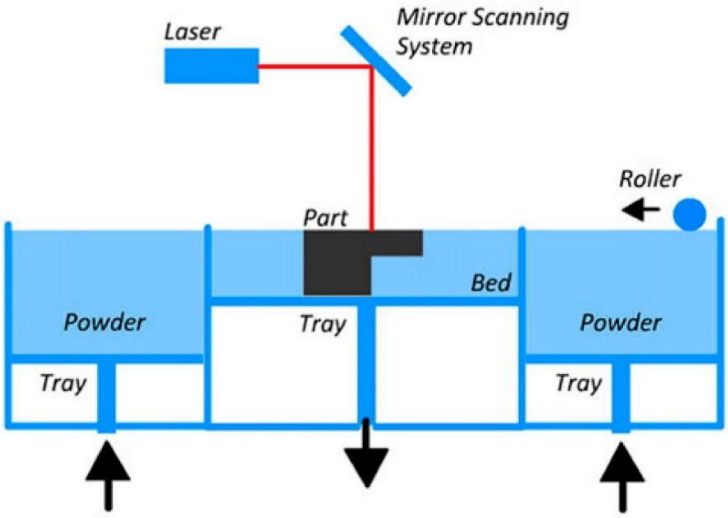

Figure 5: A schematic of SLS/SLM processes [24].

The main differences that make metal powders more difficult than polymers to process in laser melting are high thermal conductivity, high surface tension, high tendency to oxidize, and high laser reflectivity. Fraunhofer Institute for Laser Technology developed the process with using Nd-YAG laser instead of CO_2 laser. They showed that Nd-YAG laser considerably increases the metal powders absorptivity [13].

The main challenge during melting process of metallic powders is oxidation. For instance, the formed oxide on the surface of molten metal particles reduces the wettability. Another problem of oxides in SLM processing is the possibility of being entrapped within the molten metal and creates weak sites inside the part, which reduces mechanical properties. As well as this, higher laser powers are needed in SLM compared to SLS for some metals with high reflectivity (e. g. aluminum). High thermal conductivity of metals can also result in higher laser powers demand that can increase energy consumption and product costs [35].

2-1-3-3- Electron beam melting (EBM)

This method, as one of PBF processes, is a similar process to SLM with different energy sources, where electron beam used to fuse powder bed layers instead of high energy laser. In fact, the electrons are emitted from a heated tungsten filament and focused by two magnetic fields to a required point with desired diameter of 0.1 mm. The kinetic energy of these high-speed electrons becomes converted to thermal energy in order to melt the powder, when the beam hits the powder bed [29]. Figure 6 schematically indicates EBM system.

EBM system includes an electron beam gun, build tank, vacuum chamber (~10-4 torr), and powder distribution system. The first step is preheating the powder bed by electron beam, where the powder is fed via a raking system. In this situation, the particles are disorderly placed alongside each other with gaps so that the thickness of layer is 2-3 times greater than it must be. With melting the powder layer, the thickness reduced to the suitable amount. The platform is moved down up to a layer thickness (0.05-0.2 mm), when layer printing is completed. Then, a new powder layer is fed, and the process continues until the whole object is printed. Depending on the size and material of the object, cooling down might last up to 6 h with the help of helium.

EBM has been used to fabricate a variety range of devices in different fields such as medical and aerospace industries. Based on the structure and mechanism of this process, EBM is a technology to build metal parts including Inconel 718 superalloys, titanium and cobalt alloys. Inco 718 is a nickel-chromium-based superalloy that has been recently considered due to its desired unique properties. This superalloy has perfect corrosion resistance with excellent mechanical properties at high temperatures [29].

One of the advantages of EBM compared to laser processing is its low energy consumption. In EBM, most of the electrical energy turns into electron beam, while only 10-20% of the input energy in laser process converted to beam. Beside this, producing a beam energy from electron beam is much cheaper than that by laser with the same input energy. The modern laser sintering machines, however, have introduced higher conversion efficiencies (70-80%) that significantly reduce the costs. Another advantage of EBM is rapid movability of beam, which dramatically increases the production speed. Nevertheless, low residual stress is probably the most interesting benefit of EBM compared to laser processing due to higher bed temperature.

In contrast, the biggest restriction of this technology is materials selection. Since conductivity of powder bed is essential, EBM is only being used for metal powders. Another disadvantage of EBM is need of support to provide electrical conduction through the powder to the plate in order to eliminate electron charging [13].

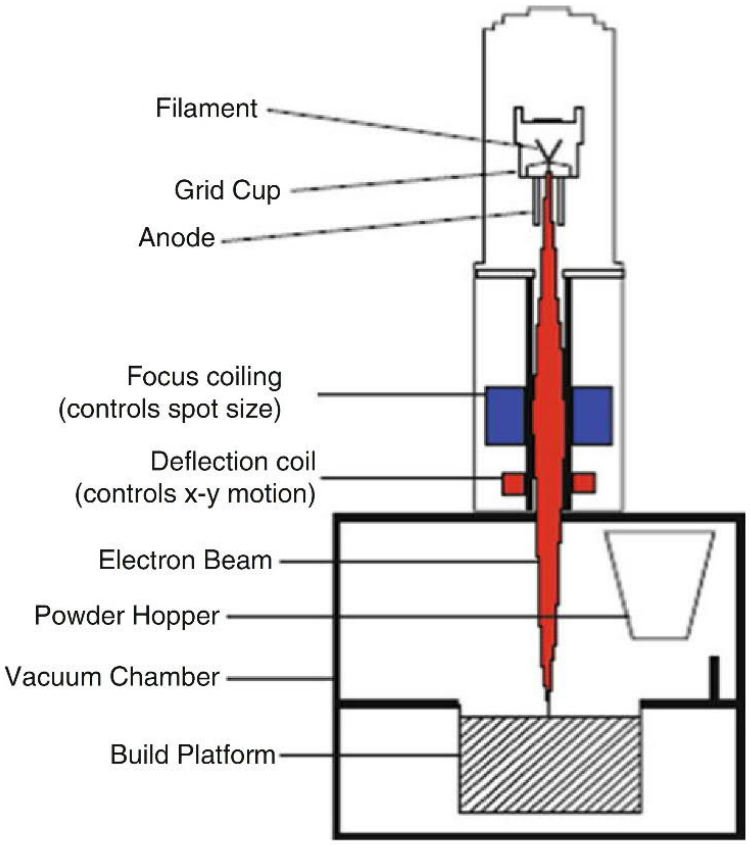

Figure 6: A schematic of EBM system [13].

2-1-3-4- Direct metal laser sintering (DMLS)

DMLS is a known process to build metal alloys used in different industries such as aerospace, medical, dental, etc. Due to formation of liquid phase during the process, the powder is not able to act as a support, and consequently the external support is necessary to use [24].

There are four ways to prepare the mixed powder from binder and structural materials. a) separate particles: both binder and structural particles are well combined and used as the final powder. According to literatures, the binder particles with smaller size can lead to less shrinkage and lower porosity in the final parts. b) composite particles: each particle has both binder and structural materials. Mechanical alloying is a common method to produce composite particles. The benefit of this type of particles compared to separate particles is having better surface quality after the process.

c) coated particles: in these particles, structural material can be coated by binder, where better flow properties, better absorption of laser energy, and more effective binding of structural particles is achievable. d) pre-alloyed particles: each particle is an alloy and mixture of binder and structural particles. The point that distinguishes this type from composite particle is that there is no separability of sections in particle. In this case, only a certain percentage (partially) of particle is melted, and the formed liquid phase fragments the particle into smaller pieces [13]. Figure 7 shows four types of particles used in liquid phase sintering (LPS) for PBF process.

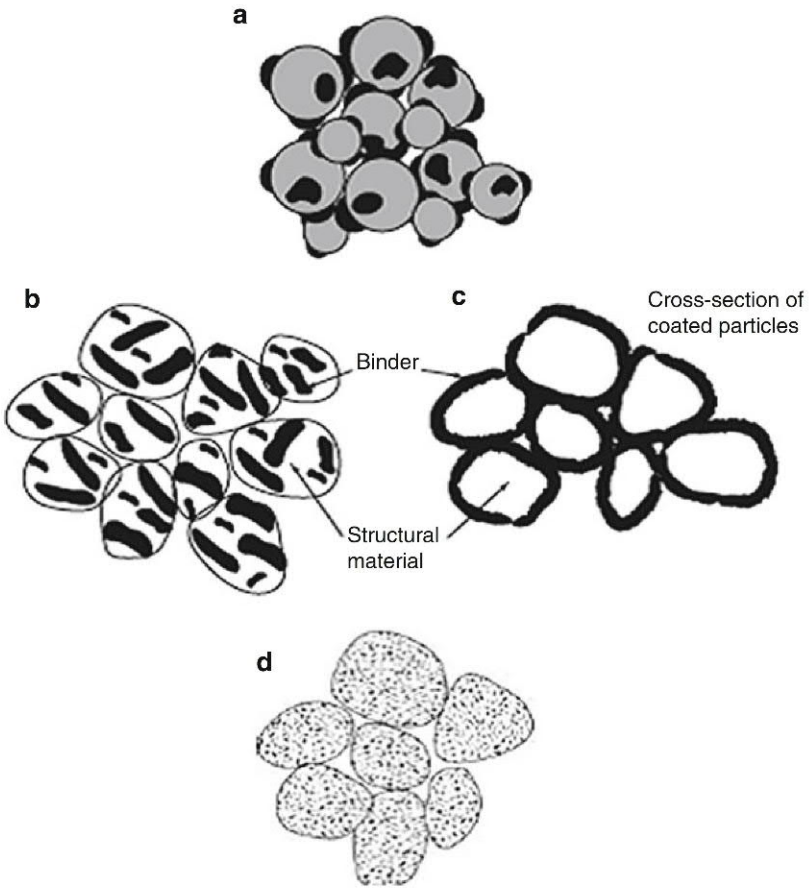

Figure 7: Different types of particles used in PBF: a) separate particles, b) composite particles, c) coated particles, d) pre-alloyed particles. Darker areas represent binder material, and lighter areas represent structural material [13].

2-1-4- Directed Energy Deposition

Directed energy deposition (DED) is a type of AM that build a part by deposit of molten material on former layer. In this process, the feedstock materials (in the form of either powder or wire), are melted by a heat source that can be a high-power laser or electron beam. This is a similar technology to welding, a new layer deposited on a target material by flowing a protective gas over the formed melt pool. Although different types of materials including ceramics, polymers, and metal matrix composites are usable in DED process, this technique is mostly used for metal parts. For this reason, this process also known as direct metal deposition (DMD) [36].

Depending on the type of feedstock materials and heat source, there are several different subsets for DED process, however, the general procedure is the same. Figure 8 schematically indicates DED process with different heat source and material feed systems. One of the most common type of DED systems is laser-based metal (powder) deposition (LBMD). In this technique, a small molten pool (diameter of 0.25-1 mm and depth of 0.1-0.5 mm) is created by laser beam, while the powder added into the pool. The laser beam melts the target points in substrate and create a small molten pool, while the powder can be melted either during flight from feeding head to substrate surface or after entering the molten pool. However, the latter way is more common when the added powder into the pool is melted, and both substrate and powder solidified once the laser beam moves away [13].

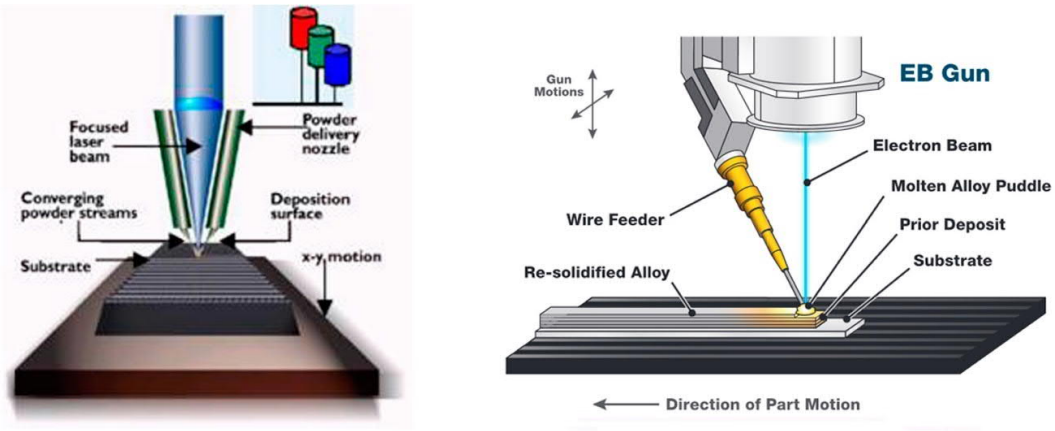

a) Laser powder feed system b) Electron beam wire feed system

Figure 8: DED process with various heat sources and feed systems [36].

Due to specific mechanism of DED, some unique features might appear during the process including very high cooling rates (10^3-10^5 °C/s) and thermal gradients that affect the microstructure. These features, which emerge as a result of rapid speed of laser beam moving and small size of created molten pool, can help to gain desired properties that are not achievable from traditional processes. Furthermore, using higher beam powers (typically electron beam) considerably decreases cooling rate, which leads to grain growth, and consequently weakens mechanical properties of metal parts.

The most interesting application of DED process, which makes it different from other AM technologies is possibility of repair and renovation of metallic parts [37]. Recently, DED has increasingly been used to build near net structure of new material alloys, wrought billets, biomedical implants, etc. Also, DED is a common technique for coating or adding materials and features to the parts with different structures in order to improve surface properties. For example, wear-resistant materials can be deposited on injection molding and casting dies to protect the high-wear sites [13].

Despite the numerous applications of DED in different fields, this process has an intrinsic limitation in dimensional accuracy and surface finish. Thus, surface machining is needed after building the part, which is not economical. On the other side, it is difficult to produce the complex geometry parts with DED and more dense support structures are required to facilitate it [29].

As it mentioned above, there are some subsets for DED process based on the type of feedstock materials and heat sources. The most two important of these techniques are named and described below in more details:

2-1-4-1- Laser-based metal deposition (LBMD)

One of the most common DED processes that using laser beam as the heat source and typically metal powder as feedstock. The first commercialized machine was LENS, which originally had an Nd-YAG laser. Then, it developed, and the modern machines launched with dual laser head and fiber laser. The process occurs in a chamber including an inert gas atmosphere (typically argon) with oxygen concentration of below 10 ppm. This inert gas system is several times cleaner than that in powder bed fusion machines.

In order to gain the desired deposit conditions, a few process parameters such as powder flow rate, deposition speed, and laser power should be carefully adjusted. Previously, LENS machines were using CO_2 laser, which was economically desirable. However, since the

absorptivity of most materials are low at CO_2 laser wavelengths, Nd-YAG or fiber lasers were replaced [13].

2-1-4-2- Electron beam freeform fabrication (EBF3)

The other common method of DED is electron beam freeform fabrication (EBF3) that using metal wire as the feed material and an electron beam as heat source. The technology was first developed by NASA in order to repair or fabricate of aerospace structures. Some features that make EBF3 a suitable method for aerospace applications are: high efficiency of converting electrical energy into a high energy beam that significantly reduces electrical energy consumption compared to most lasers, possibility of work with electron beam in vacuum environment (similar to space conditions), and also the advantages of using wire feeds because of limitations in the use of powder in vacuum conditions [13].

2-1-5- Material Jetting

Material jetting (MJ) is a process in which photopolymer materials in the form of droplets are deposited on the build platform by multi jets (Figure 9). Two types of photopolymer materials in this technology are used for: a) actual model, and b) supports (gel like material). Similar to Vat photopolymerization technology, UV lamps are used to cure deposited photopolymer material layers. After printing, the soluble support material is removed by water jet, and the final object with a very good surface finish remained. The parts produced by MJ have high resolution, and the machines can print the layer with the thickness from 50 to 25 μm [24].

In comparison with vat photopolymerization process, MJ gives higher productivity, and wider range of part size and materials selection. The reason is having large arrays of nozzles so that each of them acts as a separate channel. Typically, a normal commercial material jetting system has fifty to several hundreds of MJ nozzles that deposit the materials. Due to mechanism of the process, the materials used in MJ should be photopolymerizable, which are including: engineering plastics and elastomers, and conductive inks. Nevertheless, in order to produce a metal part via MJ process, a composite of metal and a photopolymerizable material must be used. Currently, however, material jetting does not widely apply in metal technology, and only some works have done in electronics applications such as soldering, where low temperature is required to melt the metallic material and create droplet for deposition [29].

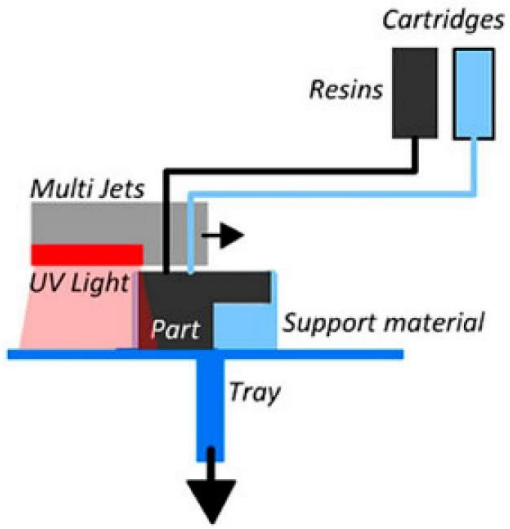

Figure 9: A schematic of material jetting system [24].

The mechanism of MJ is much easier than other processes, where complex components are not required for printing machines. Another advantage of this process is high speed in production. In fact, hundreds or thousands of nozzles enable this process to build the parts so quickly with high resolution and sufficient surface finish. As well as this, the capability of printing both multi material and multi-color parts with material jetting, makes it a unique process among the other AM technologies.

In contrast, the most important disadvantages or limitations of MJ can be mentioned as: material selection, and limited durability. As it mentioned before, only waxes and photopolymer materials are useable in this process. On the other side, since waxes are not the materials with desired properties, the parts manufactured by MJ are not suitable to be used in long-term purposes [13].

Based on the type of creating and expelling of droplets, two main categories can be described as follows: continuous stream (CS) and drop on demand (DOD).

2-1-5-1- Continuous stream mode (CS)

In this mode, a continuous column of fluid is ejected from the nozzle by a steady pressure so that after abandoning the nozzle, the fluid stream is broken into droplets. This splitting may occur as a result of vibrating, perturbing or modulating the jet. In order to controlling the deposition rate, the droplets pass through a charging field, and then the charged droplets deviated to the desired destinations by deflection plates (with high voltage). The advantage of

this mode is high rate of deposition that can develop its application in pharmaceutical labeling. The limitations, however, are firstly the type of material that should be able to carry the charge, and secondly disposing or reprocessing of the deflected droplets, when the fluid is expensive, or waste management is important [13].

2-1-5-2- Drop on demand mode (DOD)

Unlike continuous mode, separated droplets are made directly from the nozzle in DOD. The pressure pluses in each nozzle lead to formation of droplets at certain time by thermal, piezoelectric, electrostatic, acoustic or other actuators. In printing industry, the first two actuators (i.e. thermal and piezoelectric) are more common than the others, however, thermal is less used than piezoelectric due to formation of vapor bubble or possibility of damaging sensitive materials. In general, almost all commercial printers are using DOD system in MJ process [13].

2-1-6- Binder Jetting

Binder jetting (BJ) technology can be described as a combination of powder bed fusion and material jetting processes that was first introduced by Saches et al. In this technology, a liquid binder is injected on the powder bed by one or several nozzles to stick the particles together based on the 3D model. A schematic of binder jetting system is shown in Figure 10. There are two chambers in the system: one is powder tank and the other consists of a building platform. After bonding a thin layer of powder, the platform moves down and new layers are subsequently added by a levelling roller to build the whole object. After finishing bonding process, the built object (called as the “green body”) is taken from the building platform for further post-processing.

Post-processing is a complicated step in BJ that should be carefully done especially for metallic parts. In order to produce a metallic object via BJ technology, the “green body” must be first de-binding for 6-12 h, and then heat treated at certain temperature and time depending on the type of metallic material. The heat treatment is including sintering, consolidation, and infiltration. The density of metal part increases during sintering so that this densification improves the strength and mechanical properties. In some cases, depending on the composition of powder material, metal particles with lower melting point can be melted and diffuse through the particles with higher melting point. This can result in improvement of ductility of final product [38].

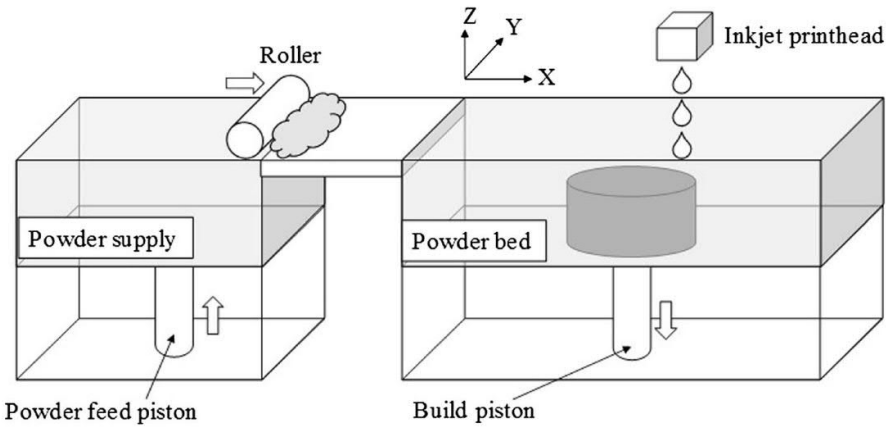

Figure 10: A schematic of binder jetting process [38].

In addition to metals, ceramic powders are also widely used in BJ technology. A similar process is done for ceramics, where a thermal decomposition is used to remove polymer binder. Also, it is possible to be used with metal powders to fabricate a ceramic-metal composite part after sintering. In the case of polymer powders, the "green body" is often ready to be used without any further post-processing [29].

As it mentioned above, BJ is similar to material jetting process. Therefore, it not only has many advantages of MJ, but also has some extra benefits. Unlike MJ, a small volume fraction of the total part (binder) is required to be deposited, which makes it faster process. On the other side, the mechanism of BJ facilitates manufacturing of composite parts by combination of powder materials and additives in binder liquid. In this process, some material compositions might be achieved that are impossible or hard to reach by conventional processes. Furthermore, binder slurries with higher solid volume fraction can be used in BJ, compared to material jetting process, which leads to production of metal and ceramic parts with better quality. Also, BJ is a suitable process to add various colors during the printing to build multi-color parts.

Some of the disadvantages of BJ are the accuracy and surface finish of the parts produced by this technique is lower than that with MJ. Also, in post-processing step, partially melting of the powder in sintering process is required in order to produce dense parts with reliable mechanical properties [13].

2-1-7- Material Extrusion

This technology consists of melting and loading the materials through one or more nozzles (extruders) by pressure or force to produce the 3D object layer by layer. After printing each layer, the build platform moves down, and the next layer is deposited and bonded on the top of former layer. Basically, the 3 different types of extruder used in this technology are plunger-based, filament-based, and screw-based, where material extrusion of filaments is more common among the others. This type of material extrusion technology is called fused filament fabrication (FFF). However, FDM is generally used for all types of material extrusion process [20]. Figure 11 schematically indicates material extrusion system, where a filament feedstock is fed by a pair of electric motor-controlled rollers.

The basic principles for all types of material extrusion process can be mentioned as follows: loading of material, melting the material, conveyor system to move the material through the nozzle, extrusion, plotting according to the 3D data, printing and bonding the material layer by layer, building support structures for complex shape parts, and post-processing if needed. Although there are 3 types of materials loaded into FDM machines including rods, filaments, and pellets, the most prevalent type used in industry is filaments. The filaments can be continuously fed into the extruder by electrical rollers, while powder or pellet materials are fed by either gravity or screw. The material conveyed into the extruding system becomes liquid by heating the chamber to be able to be passed through the nozzle. The temperature should be carefully chosen to prevent burning the material (polymer) inside the chamber. Also, the liquid material is solidified quickly after extrusion.

In extrusion step, the diameter of nozzle plays a significant role, where defines the shape and size of extruded material. Larger diameter leads to more material deposited on the build platform, while reduces production accuracy. The pressure applied from rollers moves the molten filament through the nozzle for deposition. With solidification of molten filament after extruding, the size and shape of the layer are affected by cooling rate. To minimize this effect, the difference in the temperature of chamber and surrounding atmosphere must be as low as possible. In order to bonding the new layer to previous ones, there should be either a residual heat energy or wetting agent in the filament to activate the surface of layers. In the case of support structures, a different (secondary) material should be used to build the support, if the part has complex shape. Using different materials for supports helps to remove them easier [13].

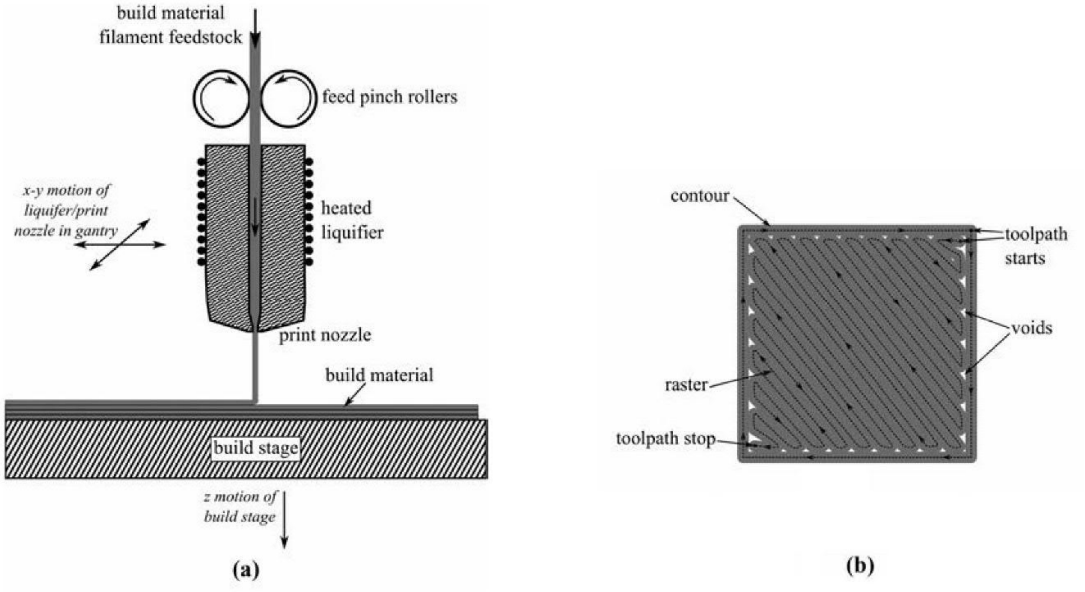

Figure 11: A schematic of a) material extrusion process, and b) a toolpath with one contour and internal raster for one layer [39].

The largest applications of FDM process are producing rapid prototype parts and presentation models. These applications need the requirement related to surface roughness, general appearance and dimensional accuracy. As well as this, other applications such as fabrication of different types of tooling, and manufacturing of finished and end-use parts have been recently growing up in AM markets. Another area using FDM technique is manufacturing cast molds, where leads to reduction in production costs up to 50 percent and shortens time from nine weeks to only one week [39].

The most important advantage of FDM technology is its accessibility and flexibility in the case of cost and production rate. With this process, various parts with complex geometries can be easily produced by home-user printers at very low costs. On the other side, this is a reliable technology to produce engineering structural parts in meter-scale from fidelity materials such as ULTEM and PEEK [29].

Although FDM has been successful method in manufacturing of parts in different fields, there are some limitations in terms of accuracy and surface finish, material density, and production velocity. In the best conditions, the thickness of printed layer is around 0.078 mm, which possible with modern high-cost machines and normally longer time. Since the nozzle opening is circular, it is difficult to produce parts with completely sharp external edges, which may affect the final shape and limit some sensitive applications [13].

Since melting the feedstock material in the chamber of FDM machines is one of the most principle steps in this process, those materials with low melting point are suitable to be used. Therefore, a considerable share of polymer parts in the market is supplied by FDM with lower production costs and time. Other types of material parts, however, can be produced by this method, when a combination with polymer is provided as the feed material. Under this condition, metal and ceramic parts are producible via FDM, of course with a few more post-processing steps. The features of each of these materials are described in more details as follows:

2-1-7-1- Polymer parts

A wide range of polymers can be used feedstock material in FDM process. Polylactic acid (PLA), acrylonitrile butadiene styrene (ABS), polycarbonate (PC), and polyamide (PA) as thermoplastic polymers are examples of polymer materials being used in this technology. Thermosetting polymers such as epoxy resins need heat or UV light to become polymerized. Hence, the thermosetting polymers are more suitable to be used in thermal or UV curing processing such as vat photopolymerization technology. Some of the applications of polymer parts produced by FDM are manufacturing lightweight structures with complex shapes for use in aerospace industries, structural models in architectural industries, organs and tissues in medical industries, artifact replication in art, and conceptual prototypes. However, weak mechanical properties (low strength and functionality) of polymer products might limit the industrial applications in some cases [40].

One of the most common polymers used in FDM machines among the other materials is ABS/ABS plus owing to their desirable chemical, thermal and mechanical properties. At low temperatures, it is easy to manage ABS in its pre-fusion state as well as return it back to the primary properties during cooling [41]. Furthermore, recently some studies have been carried out to develop mechanical properties of ABS parts using some microfibers, nanofibers, and carbon nanotubes via FDM technology [42].

Another most applied polymer in FDM technology is PLA, which has low melting point as well as non-poison, non-irritation, and biocompatibility features. These properties make PLA a desired material to be used in medical industry as drug sustain-release material and spare parts in tissue engineering. On the other side, the toughness and plasticity of PLA does not change in the long-term service. Furthermore, since this type of polymer is made from

renewable crops (not petroleum), there is no environmental pollution during its decomposition to water and carbon dioxide [43,44].

According to literatures, amorphous polymers have better performance in FDM technology rather than crystalline polymers, which are more suitable for powder bed fusion technique. The reason is that amorphous polymers are more viscous than crystalline, which enables materials to maintain their shape after extrusion. Since there is no distinct melting point in amorphous polymer, the material easily softens with increasing temperature as well as solidifies quickly after extrusion. Moreover, a new layer is more easily bonded to the former extruded material in the case of amorphous polymer, while high crystallinity in the powder material used in laser technology is required to enable to transformation from solid state to liquid phase within a well-defined temperature region [13].

2-1-7-2- Metallic and ceramic parts

Although FDM is well known as a deposition method for plastic objects, recently some studies have been done to produce metal and ceramic parts by this technology. Therefore, several ideas have been proposed by some researchers to fabricate the parts from a filament of green ceramic or composite of metal-polymer filaments. Also, ceramic clay and metal slurry have been investigated, however they still have some restrictions, particularly in the case of minimum diameter of nozzle. One of the most important parameters in deposition process of metal/ceramic parts is powder volume fraction, which directly affects the possibility of successful production of the part [45].

Different types of ceramic/metallic powder materials such as aluminum oxide, PZT, hydroxypatite, silicon nitrate, and stainless steel can be mixed with plastic (organic binder system) and used as feedstock filament material in FDM technology. In order to have a successful processing, some properties of the mixed filament including stiffness and flexibility are required. The printed object needs to be sintered at high temperature to eliminate the plastic (organic binder) and gain a dense ceramic/metallic part. Recently, researchers have been used thermotropic liquid crystalline polymers (TLCP) fibers instead of ABS, which have the tensile modulus and strength up to 4 times higher than those of ABS [46,47].

The fabrication of metallic and ceramic parts via deposition process are well known as fused deposition of metals (FDMet) and fused deposition of ceramics (FDC), respectively. The idea is that a combination of metal/ceramic particles with highly filled polymers (45-65 vol %)

extruded on the platform to build the object. The extrusion of the mixed filament occurs at a temperature higher than melting point of polymer (binder) to facilitate the flowing of solid particles through the nozzle. After shaping step, the binder is removed from the object by solvents, catalyzers or thermal decomposition (debinding step). Eventually, a full dense metallic or ceramic part is achieved by sintering process at certain temperature and time. Figure 12 shows the whole steps of FDM process for metal/ceramic parts.

The binder should be completely removed in the way that the part shape remains intact. The most prevalent way for debinding is thermal decomposition, where debinding process conditions such as temperature, time and atmosphere differ with the type of used binder. Another debinding method is to use a solvent to remove a part (type) of binder as primary step, and then continue the process by thermal degradation. The last step of producing metallic/ceramic parts by FDM is sintering, which is a thermal treatment to remove the porosity created in debinding step. Similar to BJ technology, depending on the composition, there are different types of sintering (solid stat or liquid phase) can be used to densify the "green body" [20].

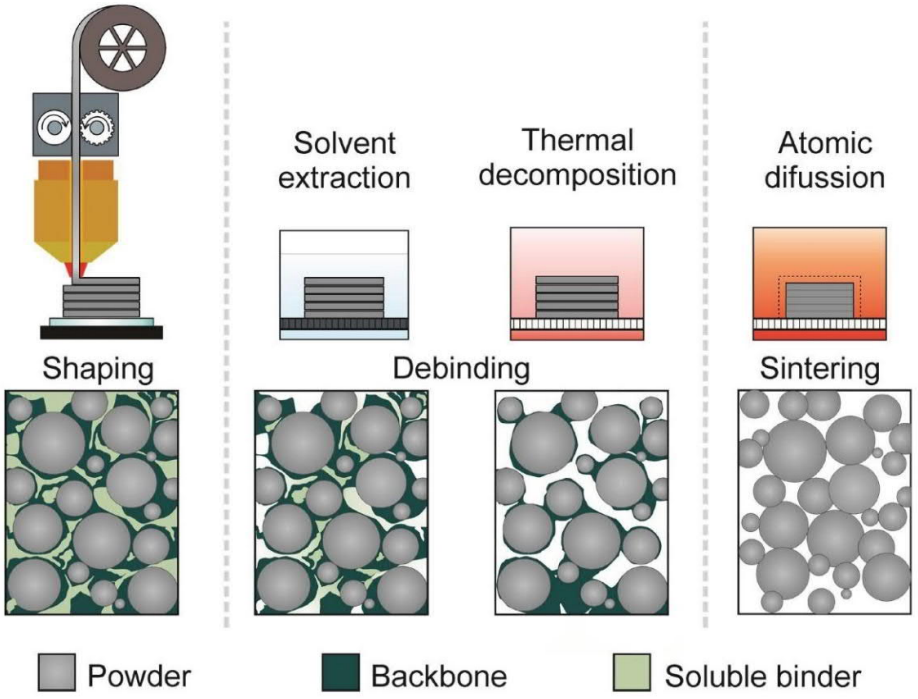

Figure 12: A schematic of shaping, debinding, and sintering steps in FDMet and FDC, and morphology of components [20].

2-2- Multi-materials AM

It is more common to use single material in AM technologies, while fabrication of parts from multi materials might have some benefits. Recently, multiple material additive manufacturing systems have been noticed to improve the functionality and performance of AM parts. In fact, multi-materials AM can be considered as an economical package to build high value products with desired properties. multi-materials AM enables to use various types of materials in a single layer of parts, while it is too difficult or even impossible in common conventional manufacturing methods [28].

In addition to ability of multi-materials AM to produce the parts with various properties, the most important feature is creating the desired composition in specific location of the product with a single manufacturing step. For example, instead of doing multiple steps of conventional welding process to join two metals and build an alloy, functionally gradient materials (FGM) can be made by deposition of those two metals at specific areas to locally increase the product properties. This can be used to build various multi materials from metal-metal to metal-ceramic parts, and even food materials (e.g. chocolate bar that is a combination of chocolate and caramel) [48].

Another important topic in fabrication of multi-materials AM is modeling and design. In order to take the best result, it is necessary to develop the design using solid modeling techniques and mathematical modeling. The used algorithms for multi-materials AM including random sequential adsorption (RSA), spatial segment shortest distance (SSSD), lattice boltzmann modeling, collective rearrangement models, monte carlo simulation, and distinct element method (DEM) are suitable for investigation of thermal, mechanical and electrical behavior of composites. As well as this, these algorithms can be used to control shape, size, distribution and volume fraction of reinforcement in the composite, which directly affect mechanical properties of multi material parts [49].

FGM was first introduced in 80’s to build heat-resistant products used in aerospace industry, and particularly airframe of space plane. However, by developments in FGM system, more fields such as biomedical industry were concerned. First studies for producing metallic and metal-ceramic multi materials were carried out in the middle of 90’s and early of 2000’s, respectively. Since then, many research have been done in the case of characterization of material phases, micro-structure, macro-structure, mechanical and biological properties of multi materials parts produced by AM technologies [50]. Inkjet printing technology (Connex

500^{TM}) was the first method that efficiently demonstrated the high capacity and interest of multi materials products in commercial, which resulted in more attempts to develop the processes [51].

Although many attempts had been made to use different AM technologies, some challenges in each process limited fabrication of multi materials parts. Alongside AM limitations, multi-materials AM has some extra challenges that should be addressed. One of the limitations is this fact that the parts produced by multi-materials AM have unpredictable properties due to their non-isotropic nature, which make them difficult to be accepted by customers. Other challenges can be mentioned are fabricating parts in larger scales, material modeling software, CAD restrictions, designers unfamiliar with the techniques, etc. These challenges must be first overcome, then multi-materials AM is able to be considered as a modern technique [52]. The biggest challenge, however, is material selection that should be not only usable, but also multi-functional. Jettable materials are more suitable to be used in multi-materials AM, which may limit other AM technologies. In comparison with single material AM, bonding of different materials in multi-materials AM is much more challenging. Two types of bonding are classified as thermal (sintering/melting, contact fusion, ultrasonic welding), and non-thermal (polymerization or adhesive). In fact, the difficulty of bonding is because of differences in properties of used materials including physical (e. g. melting or sintering temperature, thermal expansion rate), chemical (e. g. chemical bonds, Van der waals forces), and also the type of bonding method (e. g. polymerization, laser technology) [28].

2-2-1- Motivations

There are many reasons to encourage researchers to study on multi-materials AM including its applications in medical field, and the positive impacts on environment and commerce. Tissue engineering is one of those attractive fields that has been paid most attention, where commercial sales increased from $1.4 billion to $3.5 billion from 2007 to 2011. One of the most important products in this field is building scaffolds for cell growth, which are similar to human bodily subsystem (e. g. a blog vessel, a bone or other complex systems). These types of cells are most commonly produced by PLA using fused deposition modeling (FDM) technique. Therefore, development of multi materials deposition can effectively and efficiently help to promote growth of various cell types with more complex scaffold structures [53]. As well as this, materials extrusion technique is an affordable way to produce multi metal parts, due to its cheap equipment.

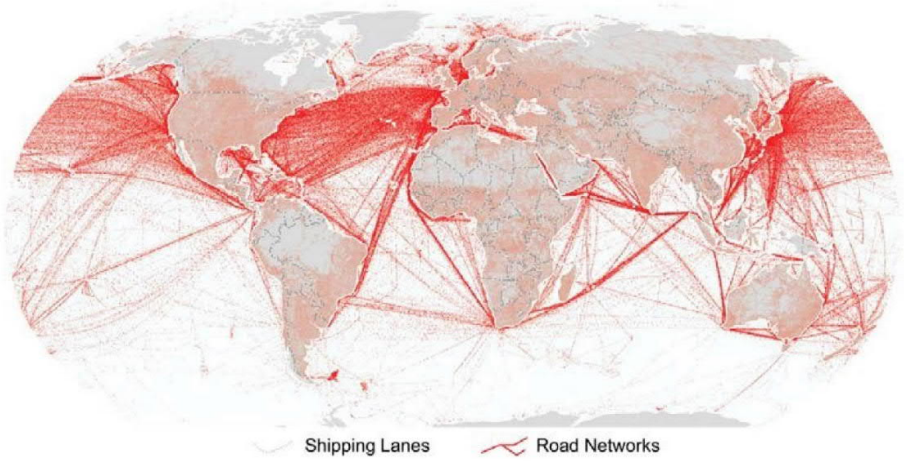

Figure 13: A map of global shipping routes in production chain [53].

Another motivation for working on multi-materials AM is reducing the human footprint on the environment. For example, in order to produce steel, iron ore must be first extracted in one country and then shipped to another country for further processing. Therefore, investigation of the shipping routes (Figure 13) can clarify how much of the natural resources are used to make various products, and subsequently how much impacts it has on earth ecosystem. Thanks to additive manufacturing technology, not only steel parts can be easily produced, but also other elements can be added to steel to make alloy steel with more desired properties. If other materials such as polymers and ceramics can be combined with the main materials (steel) during deposition, it will either decrease the consumption of natural resources or allow to produce complex materials with high functionality. Furthermore, multi-materials AM can reduce global pollution by eliminating most of operations of the production chain [53].

2-2-2- Classification

multi-materials AM can be categorized based on the type of production including a) discrete multiple materials, b) composite materials, and c) porous materials that usually used in secondary infiltration. A schematic of each type is shown in Figure 14. In discrete materials type, there is an obvious boundary separates component from each other. In the case of composite materials, a mixed material used as raw material, where material composition is varied at each location. One of the subsets of this type is FGM that is suitable for alloying. The last type is used when a second material (often in liquid form) can be penetrated to a porous part, where a specific matrix structure is required [28].

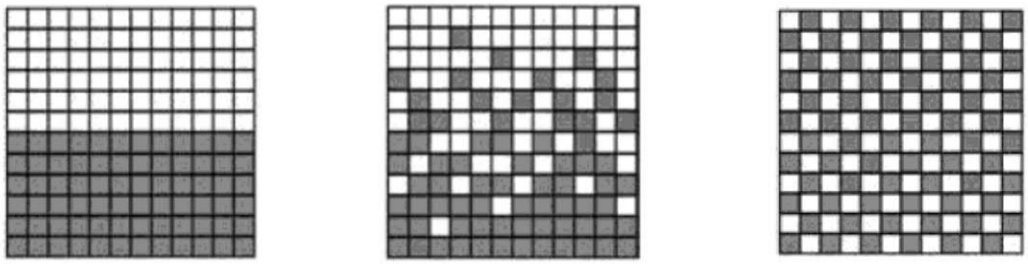

a) Discrete multi materials b) Composite materials c) Porous materials

Figure 14: Multi-materials AM classification based on type of production [50].

Since materials selection, as it mentioned, is one of the most critical factors in multiple materials fabrication, another classification for multi-materials AM can be described based on the type of materials. The three general types in this assortment are multi-materials AM of a) polymers and composites, b) metals and alloys, and c) multifunctional materials. Each category is explained in more details as follows [48]:

2-2-2-1- Multi-materials AM of polymers and composites

Since production of polymer parts is simpler and cheaper than metals and ceramics in AM, fabrication of one part from various colors or different materials has been paid more attention. These multiple colors or materials parts are often printed by FDM technique, where each polymer material extruded from a specific nozzle and the whole part is complete. In some specific cases, other methods such as SLA and material jetting can be combined and cure the part by UV light. In general, multi-materials AM of polymers as an interesting process can mix droplets of different polymers on the building platform in an effective way so that the final part includes a wide range of rigidity, flexibility, transparency properties. For instance, according to the literatures, 22 various resins can be combined in different ways to give 360,000 distinct material options [48].

Although the type of polymer as a significant factor can enhance the properties of the final product, processing parameters can have similar effects. Therefore, creating a balanced relationship between material-processing parameters is difficult and of course necessary to gain the best result. In this regard, the researchers showed that some mechanical properties of a single acrylic-based photocurable resin (De Solite SCR-300) such as strength, Young's modulus, and toughness can be improved by increasing scanning power from 100 to 250 mW and decreasing the layer thickness from 300 to 150 μm [54].

In this category, fiber-reinforced polymer composites (FRPC) are even more important than simple multi-polymers parts due to their high strength and light weight. FRPC contains small fibers, which are laid into the polymer matrix. They are usually built over each other in different directions (lattice-like) through the main polymer matrix. In fact, the deposited polymer layer is first cured by UV radiation, and then the fibers continuously sealed into the mat shape until the whole composite is built. Furthermore, in order to obtain different desired properties of final part, various types of fibers can be used in each layer. Some of the most common examples of polymer-based composites are ABS-carbon fiber, ABS-Fe/Cu, PCL-TPC, and PLA-carbon fiber [55].

2-2-2-2- Multi-materials AM of metals and alloys

Unlike polymers that can be manufactured at relatively low temperatures, most metals and alloys need high energy in order to supply sufficient heat for melting or sintering. Therefore, high power laser or electron beam technologies play a significant role in manufacturing of these types of materials. Although one of the most common and reliable laser methods for production of single metal parts is powder bed fusion, this technique might be faced with some limitations to process metallic multi materials due to characteristics of this technology. However, in addition to PBF, other processes such as “wire fed direct deposition” and “powder based direct deposition” are capable of being used for metallic multi-materials AM.

Some suitable methods for fabrication of metal alloys can be mentioned as direct metal laser melting (DMLM), laser engineering net shaping (LENS), direct laser/energy/metal deposition (DLD/DED/DMD), electron beam melting (EBM), and hybrid additive manufacturing (HAM). The latter method that has been recently noticed is a combination of additive process with subtractive CNC machining to enhance dimensional accuracy. Some alloys are being produced by these processes are Ti6Al4V-Ti-Al, Ti6Al4V-Nb, Ti6Al4V-CoCrMo, In718-Ti6Al4V, In718-Cu, SS316-SS430, SS316-Ti6Al4V-NiCr, etc. Some special properties such as hardness, wear resistance, and thermal performance can be improved by producing these alloys [48].

In “wire fed direct deposition” system, depending on the number of nozzles, several metals can be easily fed or changed under the beam to produce a multi-metal part. However, the ability of alloy to be fed in the form of wire and its ductility are two restrictions that might limit material selection in this process. Titanium, aluminum, Inconel, cobalt, nickel, nickel-copper, tantalum, and niobium alloys have already been produced in the form of wire

feedstock. The considerable advantage of this system is high deposition rate. Nevertheless, this quick deposition process leads to low dimensional accuracy and high surface roughness in final part, which can be solved by changing the feedstock from wire form to powder-based form [56].

LENS, DLD and DMD are examples of "powder based direct deposition" process in which multi-metal powder can be deposited on platform by laser beam. In this process, there are two ways for deposition: a) using a pre-mixed powder from a single nozzle, or b) using different powders from each nozzle to produce composite materials and discrete materials structures, respectively. These types of deposition are shown in Figure 15. As it mentioned before, one of the biggest challenges in multi-materials AM is whether different metals with various properties can bond to each other during the process. Difference in melting temperatures, thermal expansion, thermal conductivity and laser absorptivity are some of issues that are being studied in order to expand multi-materials AM applications [48].

One of the solutions to reduce the effect of mismatch in properties is producing a gradient structure so that a transitioning zone is laid between two pure materials at the end sides. This method improves the entire properties and integrity of the product by decreasing weld-seam stress concentrations, which is the agent of reducing the strength of joints. An example in this case is building a FGM part from stainless steel 304L to Inconel 625. The analysis shows that the stress concentration at transitioning zone is 10 times less than that in friction stir welded joint in the same processing conditions [57].

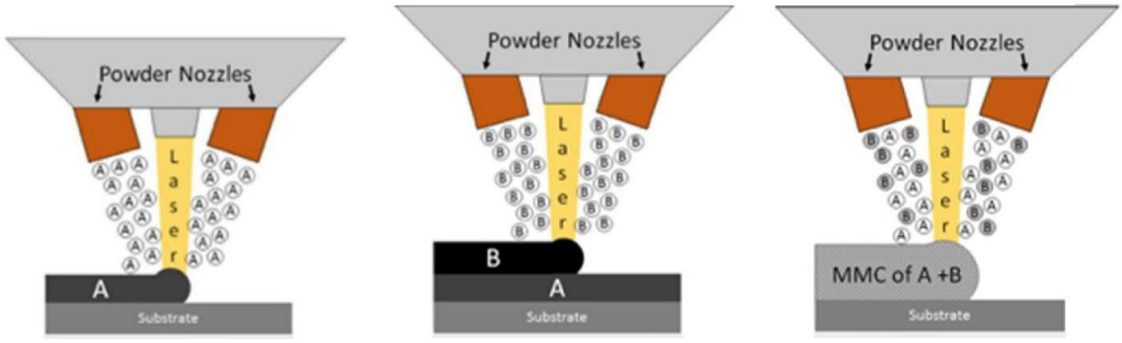

a) Single powder b) Discrete powders c) Pre-mixed powder

Figure 15: A schematic of the way powders can be deposited in multi-materials AM [48].

2-2-2-3- Multi-materials AM of multifunctional materials

Undoubtedly, the most famous multifunctional system in multi-materials AM is metal-ceramic structure, where depending on the application, one of them considered as matrix and the other as reinforcement. Metal matrix composites (MMCs) are widely used in various fields due to their remarkable properties such as high strength and hardness, acceptable wear resistance and conductivity, and light weight. In fact, a second phase (ceramic) can improve mechanical properties of MMC, while remains desired features of matrix phase. Some of the composites used in different industries are SS316-Al_2O_3, SS316-BN, Ti6Al4V-TiC, 16NCD13-TiC, AZ91D-Al-SiC [58].

Despite of MMC advantages, there is a huge mismatch between ceramics (often inorganic, crystalline oxide, nitride or carbide materials) and metals, which arises some challenges for multi-materials AM. One of these challenges is dramatic difference in melting temperature so that in some cases the metal component is evaporated, while ceramic still remained in solid state. In this situation, it is very difficult to bond the components to each other. One instance for this case is Ti6Al4V-Al_2O_3 composite, where high enough laser power applied to the materials. Then, the absorbed energy results in evaporation of Ti6Al4V alloy, while alumina particles remained solid [48].

Due to the difference in properties of metals and ceramics, processing parameters are also matter of great importance. One of the ways to build a metal-ceramic composite is coating various ceramics onto metal parts to increase hardness. For example, titanium-ceramics composites are common products used in biomedical applications. It has been reported that the thickness of coating increases by increasing powder feed rate from 9 to 13 g/min or laser power from 400 to 500 W, while an increase in laser speed decreases the thickness. On the other side, adding calcium phosphate in coating increases the hardness from 882 ± 67 to 1049 ± 112 HV, and develops a tribofilm in terms of wear by decreasing coefficient of friction. Furthermore, calcium phosphate can change the microstructure of titanium from columnar to equiaxed grains [59,60].

As it described, different types of materials, despite of various features, can be additively manufactured in order to improve the final part properties in less operation steps. Figure 16 shows a number of multi materials products fabricated using different additive manufacturing techniques.

a) Multi-polymers

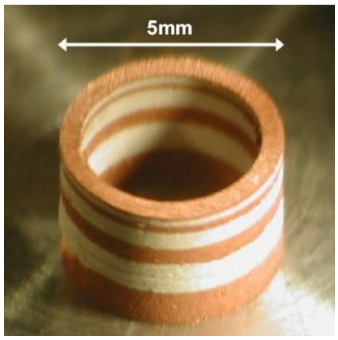

b) Multi-metals

c) Multi-functional materials

Figure 16: a) Six vertically altered resin combinations produced by multi material stereolithography (MMSL) system [51], b) a cylinder containing copper-silver segments [61], c) coating ceramics on a metal part by LENS process [62].

2-2-3- Assessment of technologies for multi-materials AM

Based on what described in this section, the type of materials and bonding mechanism between them are of the most important issues in multi-materials AM. In order to have better understanding of multi materials production, it is necessary to investigate each AM technology, their features, limitations, and facilities in more details. Each AM process has its own unique features, which are suitable for a specific type of materials. Finding the appropriate method for multi materials manufacturing is another significant step in the process that must be carefully chosen. In the following, AM technologies will be assessed in respect of material type [53]:

SLA – this is a technology in which a photopolymerization reaction occurs, when photo monomers exposed to UV or visible light. The technology has a reputation of manufacturing the parts with high-resolution and high surface quality. For multi materials production, the biggest challenge in this technology is contamination, when the object is transferred from one material reservoir to another. In fact, the residue resin of material A is dropped from built object to material B tray. There are some ways to minimize this cross-contamination such as designing a mechanical wiper to remove the residue from the bottom of object before transition, however, it is almost impossible to completely prevent contamination. Another type of multi materials production is using different resins in the same tray, where some other challenges arise. Each resin material needs specific wavelength of light, which means that

even if the same base resins used in tray, there is no guarantee for successful photopolymerizing all resins.

SLS/SLM – these are the most common techniques in powder bed fusion process that a wide range of powder materials from metals and ceramics to thermo polymers can be produced using laser technology. One possible way for multi materials production is sintering or melting of powder materials so that each layer can be set from one material. The challenge is how to separate different powders from each other inside the chamber in order to recycle materials for reusing purposes. The other way is using two or more powders within a single layer, which homogenization of the final part would be the issue.

FDM/FFF – these are types of deposition technology that the materials need to be melted during processing in order to make it possible to extrude through the nozzle. Therefore, thermo-polymers with low melting points are most common materials used by this technique. However, it is possible to print other materials such as metals and ceramics (in powder form), if they are mixed with thermo-polymers and fed as composite filaments. Since most of industrial FDM machines have multiple extruders, it is easy to deposit different materials in a single layer to make multi-colors polymer, metal-metal alloys, or metal-ceramic composites products.

LOM – this method is one of the earliest processes in additive manufacturing, and appropriate one for multi materials production. The mechanism of this technology enables to use different material sheets and build multi materials layers. However, it is difficult, if not impossible, to make different materials in the same layer.

Binder jetting – this technology is similar to SLS/SLM and the difference is that instead of applying laser energy, a binder (polymer) is used to bond the powders. Although different types of powders from metals to ceramics can be used in this method to build discrete multi materials parts, separation of these powders from each other for recycling is a big challenge. As well as this, it is much difficult to create multi materials in the same layer.

Material jetting – this technology is a combination of SLA and FDM processes, where curable materials extruded from a nozzle and photopolymerized by UV lights. In order to make multi materials objects, they must be first mixed with curable materials and then fed through the nozzle to print. Although it is possible to deposit multi materials in the same layer with this method, this is not suitable technique for manufacturing of metal alloys, metal-ceramic, and ceramic-ceramic composites.

LENS – this technology usually used for repairing and coating of different industrial parts. Mostly metals and ceramics in the form of powder deposited onto the main object with the help of high energy laser technology. Multi material powders can easily deposited either within the same layer or separate layers, especially to enhance the surface hardness or improve wear resistance [53].

Evaluation of all AM technologies shows that one of the most suitable methods for production of multi materials parts is FDM/FFF, which enables to build discrete, gradient and composite parts in a wide range of materials. Since this project is focusing on producing multi metallic parts from metallic filaments, FFF technology was chosen and studied. The investigations and results are presented in the next sections.

3- Research material and methods

In this section, materials and methods used in this study including technologies, equipment, preparations, experimental steps, and performed tests in order to characterize the properties of final samples will be described in more detail. The main "aim" of experimental work is first to make sure that multi-metal parts can be successfully fabricated by FFF technique, and then investigation of possible scenarios to achieve adorable properties using microstructural studies and some measurements at various production parameters.

Figure 17 indicates the trend of experimental work in this study, based on AM procedure steps and analyzing tests. According to the chosen AM method for this study, FFF technique, the procedure chain contains materials selection, printing and effective parameters on the built part, de-binding and sintering processes in which temperature and time have a significant role in production. In addition to fabrication chain, characterization of fabricated parts will be taken into account in order to analyze the final parts properties such as density, shrinkage, microstructural evolution, chemical composition changes, the possibility of formation of intermetallic compounds, etc. The methods for measuring and analyzing of each part will be discussed later in this section.

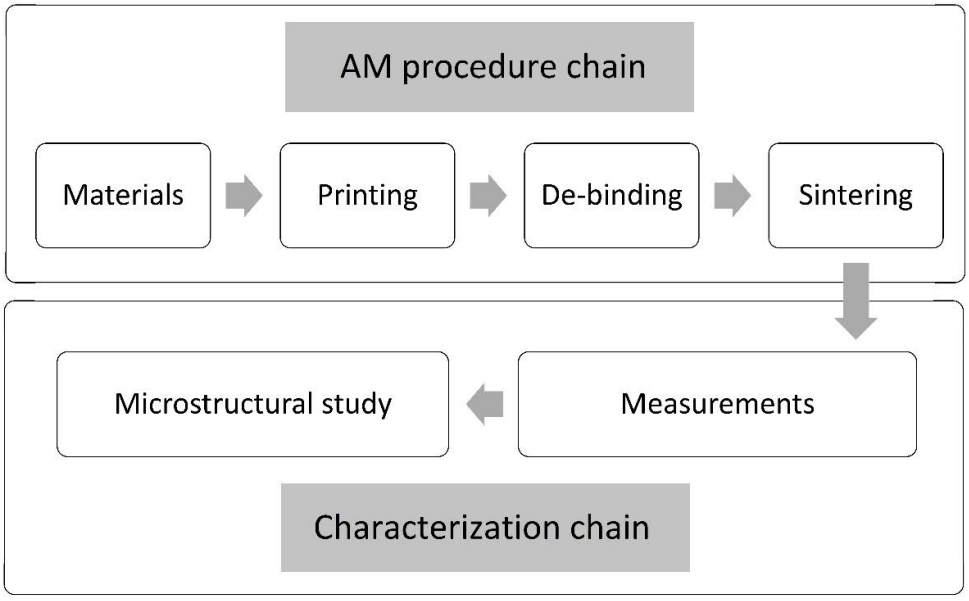

Figure 17: The experimental design for fabrication of multi-metal parts.

3-1- FFF procedure

FFF technique was chosen for this study in order to fabricate multi-metal parts. According to literatures, the raw materials in this method must be in the form of filaments, mixture of metallic powder and polymer (binder). The printed samples, after de-binding, need to be sintered at certain temperature and time to become a dense part. Each stage has some specific parameters that directly affect the degree of process success. Therefore, the equipment and methods used in this work are determinant, which described as follows:

3-1-1- Materials

It was decided to use two materials (metallic filaments) to fabricate multi-metal parts: a) stainless steel 316L, and b) high carbon iron. The used filaments were manufactured by The Virtual Foundry company, which called Filamet^{TM}. This type of filament is similar to PLA, but has extremely high metal powder content. The rolls of two Filamets^{TM} used in this work are shown in Figure 18. Also, the characteristics and some physical properties of each Filamet^{TM} are separately given in Table 1. The size (diameter) of each Filamet^{TM} is reported by tolerance of ± 0.05 mm.

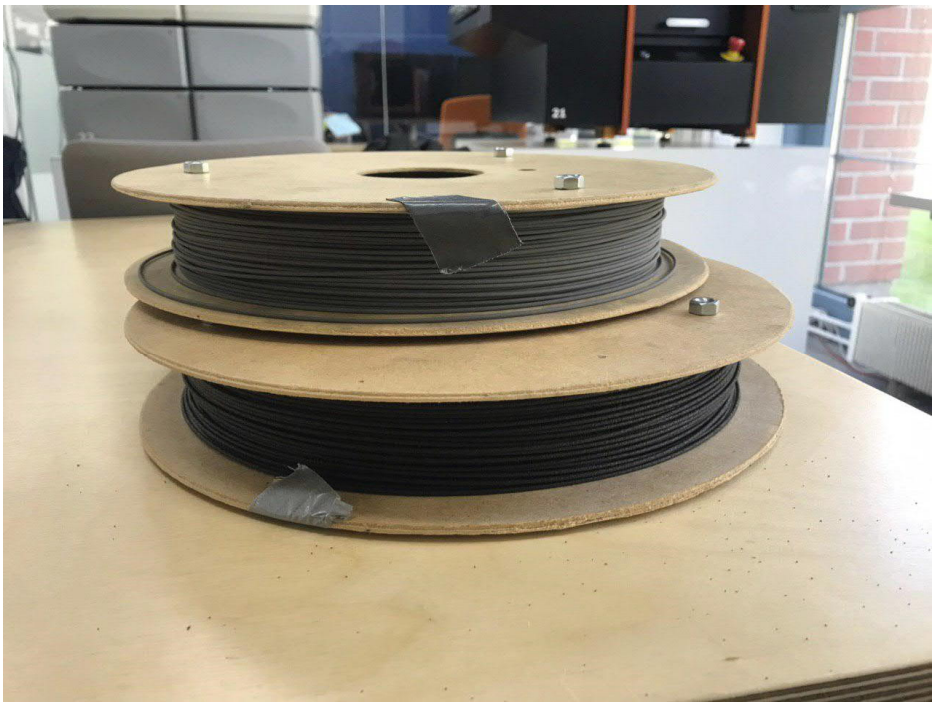

Figure 18: Stainless steel 316L (gray) and high carbon iron (black) Filamets^{TM} rolls.

Table 1. Characterization of used Filamets™ [63].

Filamets	Stainless steel 316L	High carbon iron
Density (g/cm^3)	3.50	2.75
Metal content (%-wt)	83.5	80
Diameter (mm)	1.75	1.75

3-1-2- Printing

3-1-2-1- Printer

The Crane Quad 3D printer was used in order to build the samples. This printer has been designed so that is able to take in four filaments. The Crane Quad can either print one filament at a time and quickly switch, allowing to use different materials on the same print, or it can combine filaments together to create multi materials in the same layer. Since two Filamets™ were used in this study, only two extruders occupied during printing. The extruded materials are combined in the nozzle chamber, and then the mixed materials printed on the platform. The image of Crane Quad printer alongside its components are separately shown in Figure 19.

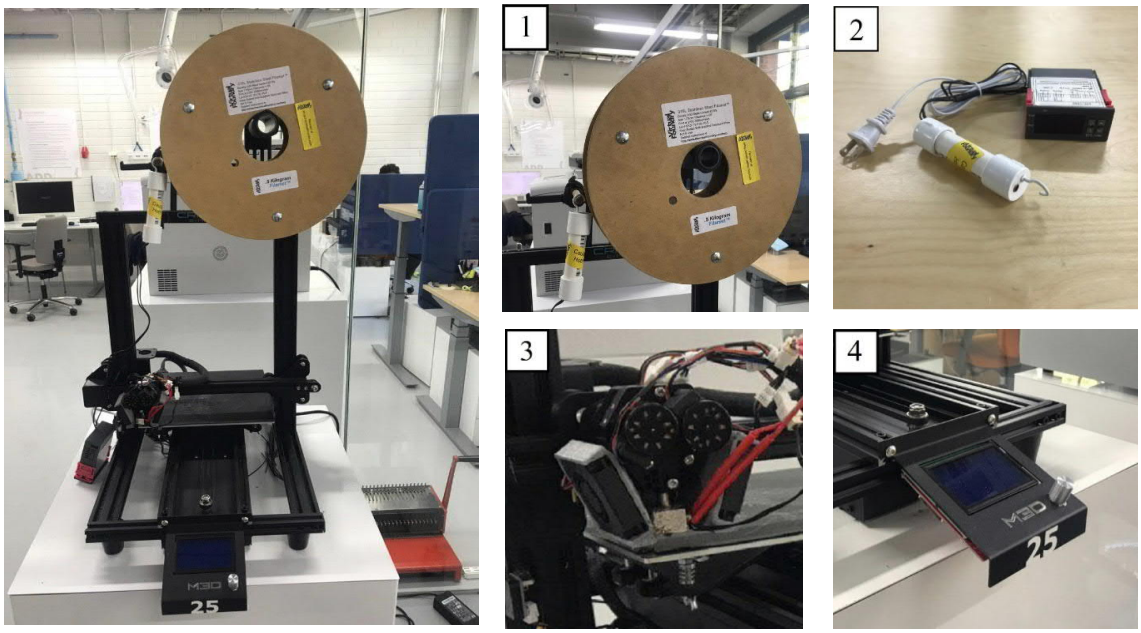

Figure 19: The images of Crane Quad 3D printer. 1) Filamet™ roll, 2) warmer, 3) nozzle setup, 4) setting controller.

The printer has several sections including: Filamet^{TM} roll, warmer, nozzle setup, and setting controller. A protrusion has been added at the top of printer to hold the roll in order to ease feeding the materials into the extruders. On the other side, since the used Filamets^{TM} are so brittle (because of high metal content), a warmer was used to make them flexible enough to prevent from breaking down inside the extruder box. Nozzle setup contains several items such as, **Extruders**: responsible for conveying Filamets^{TM} into the nozzle chamber; **Nozzle**: a standard hardened steel nozzle with 1 mm diameter deposits the materials onto the bed platform; **Heater**: responsible for increasing the nozzle temperature for better printing; **Cooling system**: three fans have been designed around the nozzle and heater to prevent damage to other parts, especially plastic structures. The last section of printer is a small monitor to manage the general printing settings including, initial position of nozzle based on x, y and z axes, speed of printing, temperature of nozzle and bed, feeding rate of materials for each extruder, etc. This section enables users to manually change the settings even during printing.

3-1-2-2- Design

Ultimaker Cura 4.4.1 software was used to design the 3D models. Since the main purpose of this project is to investigate the possibility of fabricating multi metal parts by FFF, a simple cube model with dimensions of 10×10×10 mm was chosen to be printed. Two types of samples that prepared for this study are: a) 100-100 (couple sample), b) 50-50 (mixed sample). Figure 20 indicates a schematic of these two samples for creating multi metal parts from stainless steel 316L and high carbon iron.

a) 100-100 (couple sample) b) 50-50 (mixed sample)

Figure 20: Two models of multi metal samples prepared for study.

As Ilies et al. [64] showed in their studies, the printing parameters have direct effect on the properties of final parts. Therefore, the proper values must be carefully chosen for these parameters to prevent presence of gap between the printed layers. Some of the most important parameters, which set for this work are given in Table 2. Most of these settings were chosen based on what Filamet^{TM} manufacturer recommended for stainless steel 316L and high iron carbon in [63].

Table 2: Print setting used for multi metal samples.

Nozzle temperature	210 °C
Bed temperature	60 °C
Infill density	100%
Wall line count	3
Printing speed	15 mm/s
Wall speed	12 mm/s
Diameter of deposited material	0.8 mm
Layer thickness	0.2 mm
First layer thickness	0.53 mm
Line width	0.7 mm

3-1-3- De-binding

After printing the samples, the binder should be completely removed from the samples to become prepared for the next stage (sintering). According to information from manufacturer, the binder is thermally decomposable at a certain temperature and time, which means no need any solvent for de-binding. In order to discover the appropriate temperature and time to completely remove the binder, thermogravimetric analysis (TGA) was carried out to monitor the weight changes of sample during heating process. Figure 21 shows a schematic and image of thermogravimetric test setup and equipment. The samples were suspended into a furnace (Heraeus) by a platinum wire to a digital balance (Mettler Toledo: AB104-S with accuracy of 0,1 mg), while argon used as protective gas. The mass changes determine the amount of removed binder in heating process. The temperature and time of de-binding process in the main tests were set based on the TGA results.

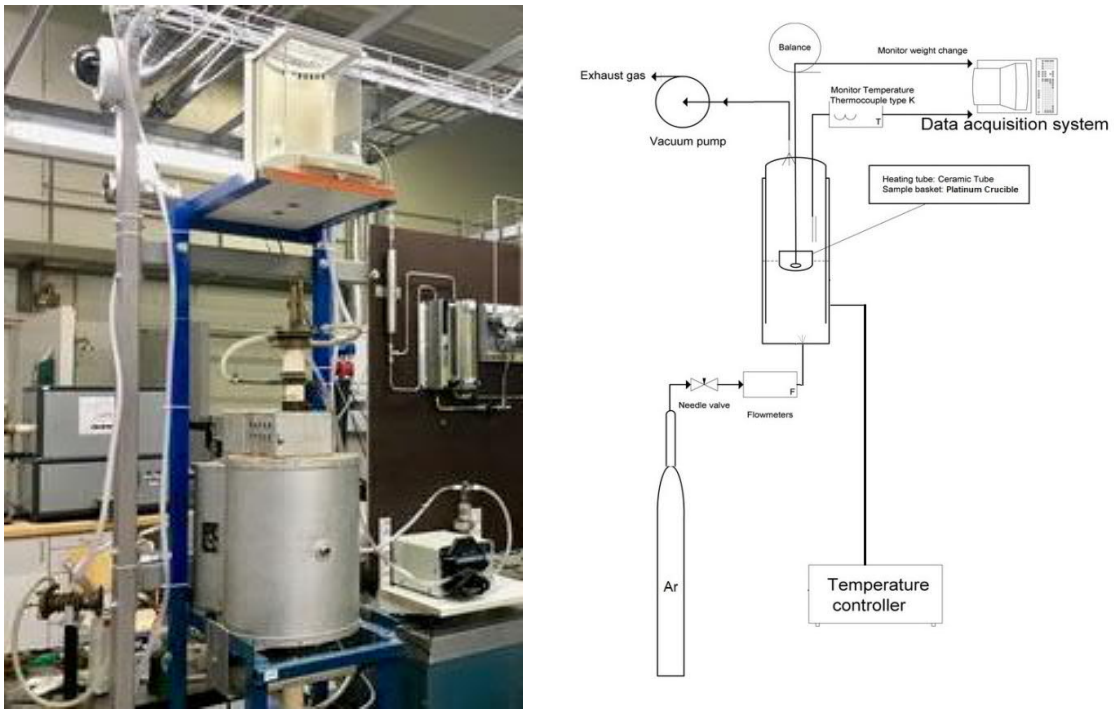

a) Image of TGA analyser b) A schematic of TGA analyser

Figure 21: The image and schematic of TGA equipment.

3-1-4- Sintering

Practically, both de-binding and sintering processes were carried out in the same furnace so that sintering followed by de-binding without any change in position of sample inside the furnace. Each sample was placed inside a cylindrical-shape magnesia (MgO) crucible, filled by alumina (Al_2O_3) powder so that all the print surfaces completely covered. The location of samples was chosen in the way that the distance from each crucible walls was the same. The crucible setup was placed in a molybdenum crucible holder and transferred into a vertical tube furnace (Lenton LTF 16/450). The inert gas used for both de-binding and sintering in this work was argon (purity of 99.997%) with the flow rate of 0.2 l/min in order to prevent oxidation. First, in de-binding process, the samples were heated according to heating program extracted from TGA results (see section 4-3). Thereafter, in sintering stage, the temperature increased from de-binding temperature to target temperatures with a certain heating rate and holding in different duration times (see section 4-4). Different sintering temperatures and times were studied in order to discover the optimum result. Then, the samples were slowly cooled down from target temperature inside the furnace with the rate of 30 °C/min.

a) Image of tube furnace

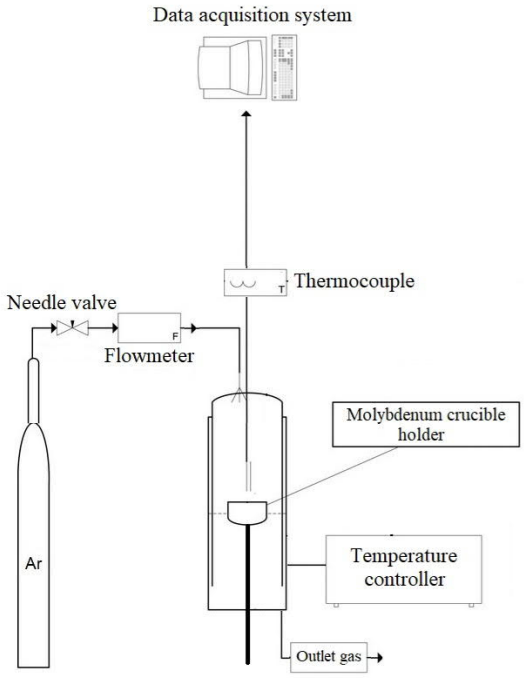

b) A schematic of tube furnace

c) Magnesia (MgO) crucible

d) Crucible holder

e) Alumina (Al_2O_3) powder

Figure 22: The setup furnace and equipment used for de-binding and sintering processes.

Figure 22 shows the setup of a vertical tube furnace and equipment used for de-binding and sintering processes. Although both de-binding and sintering were carried out in an inert atmosphere (argon gas), alumina powder (refractory) also used in order to protect the samples from oxidation. The actual temperature was measured by a thermocouple, which placed at the above of crucible setup, near the sample. Furthermore, a digital flowmeter was used to control the rate of argon gas flowing inside the furnace.

3-2- Characterization

The main aim of characterization of samples is analyzing a wide range of properties of final fabricated parts including physical properties and microstructural evolution. This can help to monitor the trend of evolution in properties with changes in production parameters. In this study, sintered density and shrinkage level were measured by standard methods that will be described later in next sections. On the other side, microstructural studies such as grain size, liquid phase formed at grain boundaries, microstructural evolution and gradient, and intermetallic compounds might be formed during sintering were carried out by various microscopes and laser equipment.

3-2-1- Sintered density

One of the most useful parameters can be measured is sintered density that represents the success rate of sintering process. There are few ways for measuring the density of sintered samples, but in this study, Archimedes method was used based on DIN ISO 3369 [65]. This method is considerably more precise than other techniques (e. g. calculating the dimensions), which makes this method reliable. According to standard, the sintered density is obtained by the following formula:

$$\rho_S = \left(\frac{M_1}{M_2 - M_3}\right)\rho_{water} \quad (1)$$

where, ρ_s is sintered density (g/cm^3), M_1 is the mass of sample measured in air (g), M_2 is mass of sample impregnated in the oil and then measured in air (g), M_3 is the mass of sample measured in water (g), and ρ_{water} is density of water (g/cm^3). Before immersing the samples into the water to measure M_3, the samples were impregnated in the oil in order to prevent water penetration into the porosity inside the samples. In order to investigation of success degree of sintering, another parameter was expressed as “relative density”, which represents the degree of sintering based on theoretical density. The “relative density” is given as follows:

$$\rho_r = \left(\frac{\rho_S}{\rho_{th}}\right) \times 100 \quad (2)$$

where, ρ_r is relative density (dimensionless), and ρ_{th} is theoretical density (g/cm^3) that acquired by:

$$\frac{1}{\rho_{th}} = \sum_{i}^{N} \frac{W_i}{\rho_i} \quad (3)$$

where, N is the number of components in mixture, W_i is the weight fraction of i component, and ρ_i is the theoretical density of i component (g/cm^3).

3-2-2- Shrinkage

Another important parameter that evaluates dimensional changes is shrinkage, which is effective in production procedure, especially in design step. Based on the nature of FFF technique, the polymer is removed from the sample in de-binding process leading to an initial shrinkage. On the other side, the secondary shrinkage happens with densification during sintering, where the porosity created by removing binder, is gradually disappeared and particles become more close to each other. The total shrinkage can be measured by comparing the dimensions of sintered sample with green sample (before de-binding), which expressed as following equation:

$$\text{Shrinkage } (\%) = \left(\frac{L_G - L_S}{L_G}\right) \times 100 \quad (4)$$

where, L_G and L_S are one of the main dimensions (in direction of x or y axis) of green and sintered samples, respectively. The dimensions of green sample (print) can be easily measured, while it is, to some extent, challenging for sintered samples due to their non-uniform shape. Therefore, another method must be used to measure the dimension for sintered sample. One of these methods is taking a photo from the sintered sample, and measuring the dimensions using a simple computer software. In fact, the dimensional changes profile can help to facilitate the shrinkage level measurement for each sample in various sintering conditions

For this purpose, the dimensional changes profiles were plotted by characterizing the dimensions of taken images using Screen Ruler 2D software. In this method, an image is taken from both green and sintered samples, where the green sample can be considered as a reference sample so that the scale is calibrated by this sample's dimensions. Thereafter, the dimensions of sintered sample are measured by a ruler in the software. Also, the investigation of dimensional changes profile is a useful way to characterize the apparent shape changes of samples during sintering process.

3-2-3- Microstructural studies

Microstructural evolution such as, grain and grain boundaries evolution, porosity shape and size, alloy elements distribution, etc., were precisely investigated using two types of microscopes. Optical microscope with medium magnification (e.g. 1000X) and electron microscope with high magnification (e.g. 20000X) are able to characterize the most critical aspects of samples' microstructures. The information about each type of microscope is expressed in below:

3-2-3-1- Optical microscope (OP)

First, the sintered samples were sectioned in parallel to z axis, polished with sand papers, and immersed in an etch solution (1g $CuCl_2.2H_2O$, 1ml HNO_3, 45ml HCL) for 10 seconds. Then, the microstructure of each sample was studied using an optical microscope (Olympus BH-2 Rami, Tokyo, Japan). Figure 23 shows the image of optical microscope that used in this work.

3-2-3-2- Scanning electron microscope (SEM)

A high-resolution analytical SEM (Tescan Mira3 – RAMI, Brno, Czech Republic) was used, in order to examination of microstructures in very high magnifications. Samples preparation is one of the most significant parts in using SEM to observe and take a high quality micrograph. Since the mechanism of microstructure observation in SEM is based on sample-electron interaction, the surface of the sample must be conductive. The materials used in this study are metals, which need no further preparation to make them conductive.

There are two types of detectors that receive the reflected electrons from the surface of the sample: 1) secondary electron (SE) detector, and 2) back-scattered electron (BSE) detector. Both of these detectors were used based on the required purposes. Another parameter that should be taken into account is the working distance (WD) that is a distance at which the beam is focused. The analytical WD used in taken micrographs was 20 mm.

Also the accelerating voltage was 5 kV. Figure 24 shows an image of SEM equipment that connected to a computer system. The polished samples that were prepared for optical microscope can be reused for SEM to take high-resolution micrographs with very high magnification. SEM is equipped by an energy-dispersive X-ray micro analyzer to characterize the alloy elements distribution that will be described in the next section.

Figure 23: The optical microscope (Olympus BH-2 Rami, Tokyo, Japan).

Figure 24: The scanning electron microscope (Tescan Mira3 – RAMI, Czech Republic).

3-2-4- X-ray analyses

X-ray analysis is a useful method to determine the elemental or compound composition, phase identification, and giving several information regarding crystalline of materials. Some of the most prominent X-ray analyses that used in this study are: 1) energy-dispersive X-ray (EDX), 2) X-ray diffraction (XRD), and 3) X-ray fluorescence (XRF). Further description of each analysis is given as follows:

3-2-4-1- Energy-dispersive X-ray (EDX)

Most of SEMs often equipped with a micro analyzer that determines the elemental composition of examined materials in micro-scale. EDX can be conducted in both point and line analysis, where the alloy element distribution can be easily identified. Other facilities that EDX has is showing a map based on each element in which the distribution of elements can be depicted in microstructure. The micro analysis can report the element distribution based on weight and atomic percentage that give some useful information about microstructural evolution. As it shown in Figure 24, the EDX equipment is located in right side of SEM chamber. It should be noted that the back-scattered electron (BSE) mode must be chosen as the detector, when micro analysis is need to be used.

3-2-4-2- X-ray diffraction (XRD)

Unlike EDX that is used to determine the element composition, XRD is used to identify bulk composition, type of phase, and some crystallographic characteristics such as, unit cell dimensions, the distance between atomic layers, and crystal structures. Similar to EDX (or other X-ray analysis), XRD is also based on sample-electron interaction and characterization of reflected X-rays from the sample's surface. The XRD (Malvern Panalytical X'Pert Pro MPD Powder, UK) machine used in this study that has Pixcel 1D detector and 2theta range of -6.7^0 – 155^0 is shown in Figure 25a. The raw materials, debinded sample, and sintered samples were analyzed by XRD, and the results discussed in section 4-4-4.

3-2-4-3- X-ray fluorescence (XRF)

XRF (Malvern Panalytical Axios mAX 3kW, UK) machine (Figure 25b) was used to determine the chemical composition of raw materials (elemental analysis from Beryllium (Be) to Uranium (U)). For this purpose, the Filamets^{TM} were first debinded for removing plastic, and then the remaining metallic powder was analyzed by XRF. The machine operates with 60 kV and 125 mA, X-ray source of Rh, and Scintillation detector.

a) XRD b) XRF

Figure 25: The images of a) XRD (Malvern Panalytical X'Pert Pro MPD Powder, UK), and b) XRF (Malvern Panalytical Axios mAX 3kW, UK) machines.

3-2-5- Particle size distribution analysis (PSD)

When powder particles are used as raw materials, one of the most significant parameters is particle size distribution. There are several methods to determine PSD, but laser diffraction/scattering is the most reliable and standard particle sizing technique due to rapid measurements, repeatability, high sample throughput, wide dynamic range, and no calibration is required. In this work, this technique was used based on ISO 31320 [66].

The principle of this technique is based on measuring the angular variation in intensity of light scattered, when a laser beam passes through a dispersed sample. The light is scattered at small and large angles for large and small particles, respectively. In this work, the machine (Malvern Mastersizer 3000, UK) uses Mie and Fraunhofer theory of light scattering to calculate the particle size distribution assuming a volume equivalent sphere model. The powders were used as dry type, where the measurable particle size range is 0.01-3500 μm. Figure 26 shows the used machine for PSD analysis.

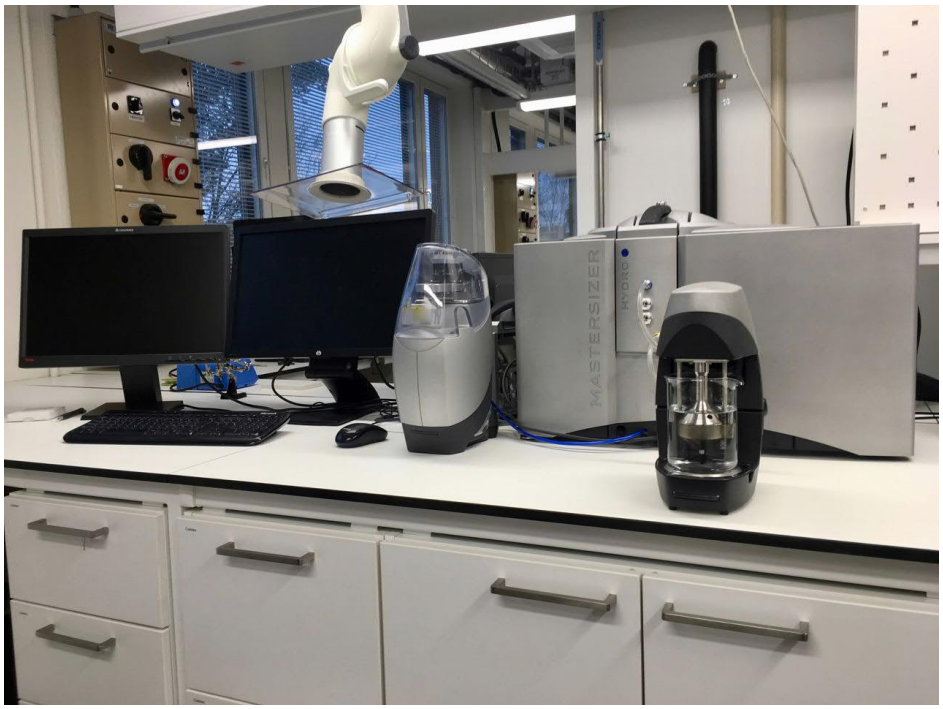

Figure 26: The image of particle size distribution analyzer (Malvern Mastersizer 3000, UK).

4- Results

In this section, the results obtained from the experiments and analyses will be represented with relevant images, graphs and tables. The comparison of these values in different experimental conditions can help for better understanding of the entire process and also facilitate their analysis in discussion section. In the following, the obtained results regarding materials characterization, processing parameters, and analyzing the final samples are given in more details.

4-1- Materials

Two filaments used in this work are: 1) stainless steel 316L, and b) high carbon iron. For better displaying of materials characteristics, the elemental composition, the micro-images using OM and SEM, and particle size distribution of each filament were studied and the results are given as follows:

4-1-1- Chemical composition

One of the most significant characteristics of each metallic alloy is chemical composition that directly affects production process. Since the raw materials are in the form of filaments (mixture of polymeric binder and metallic powder), the binder should be first removed, and then remaining powder must be gathered and analyzed to determine the elemental composition. Therefore, a certain amount of each filament (equivalent to volume of 1 cm^3) was debinded according to debinding process steps (see section 4-3), and the binder-free metallic powders were characterized by XRF analysis. Table 3 shows elemental composition of both stainless steel 316L and high carbon iron powders. In powders chemical compositions, the carbon content has the most role in selecting the proper temperature for sintering processing.

Table 3: Elemental composition of stainless steel 316L and high carbon iron powders.

Stainless steel 316L (%-wt)							
C	Cr	Ni	Mo	Mn	S	P	Fe
0.02	16.6	9.86	1.64	0.924	0.0285	0.0617	Balance
High carbon iron (%-wt)							
C	Si	Mn	Cr	Ni	S	P	Fe
1.21	0.281	0.107	0.246	0.193	0.0239	0.0314	Balance

4-1-2- Microscopy images

The images taken from cross-sectioned filaments by microscope can help to illustrate the distribution of metallic powders in polymeric binder (PLA) for each material. Figure 27 shows these micro-images using optical microscope (general image of filaments surface) and scanning electron microscope (images with higher magnification) to specify the distinction between the metallic powders and polymeric binder. Stainless steel 316L particles with spherical shape, and high carbon iron particles with irregular shape are clearly visible so that placed inside PLA structure.

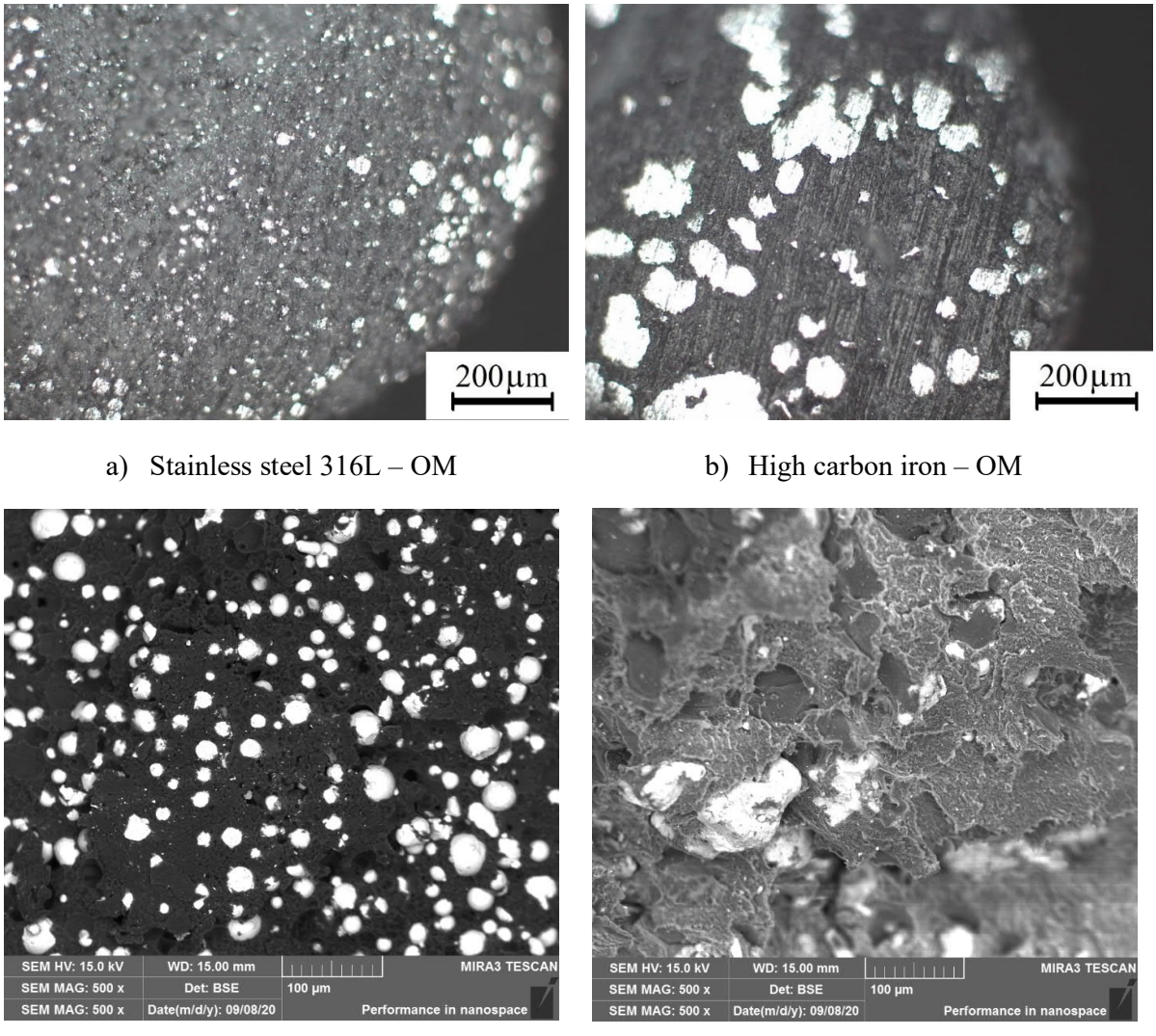

a) Stainless steel 316L – OM

b) High carbon iron – OM

c) Stainless steel 316L – SEM

d) High carbon iron – SEM

Figure 27: The images of polished cross-sectioned filaments taken using OM and unpolished by SEM.

4-1-3- Particle size distribution

Particle size distribution was investigated as another effective parameter in sintering process. The both stainless steel 316L and high carbon iron powders, which obtained from de-binding of single material samples, were characterized in the form of dry powder with pressure of 3.5 bar. The results of both powders based on frequency and cumulative values are given in Figure 28.

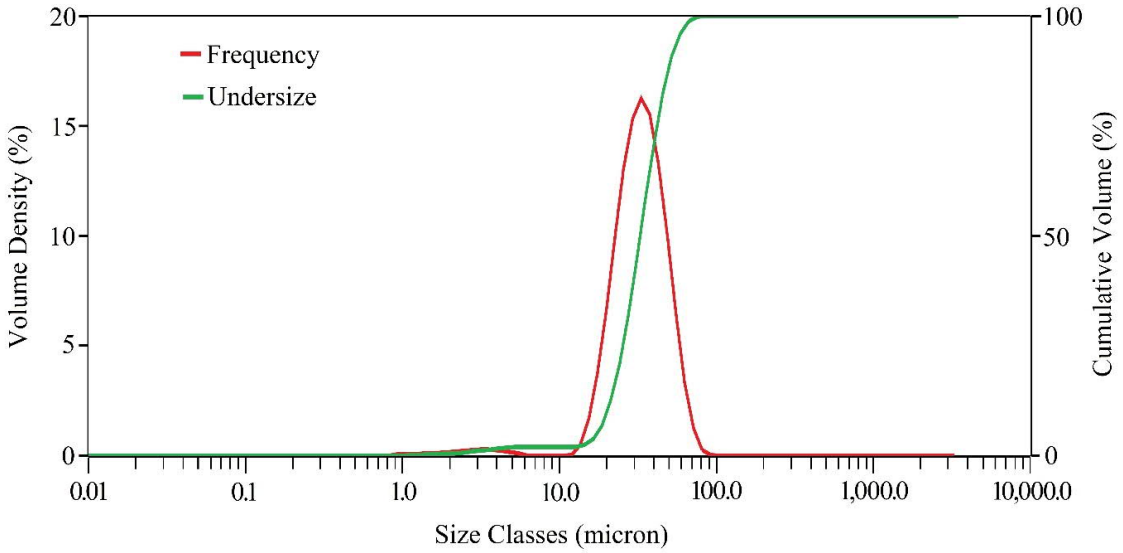

a) Stainless steel 316L

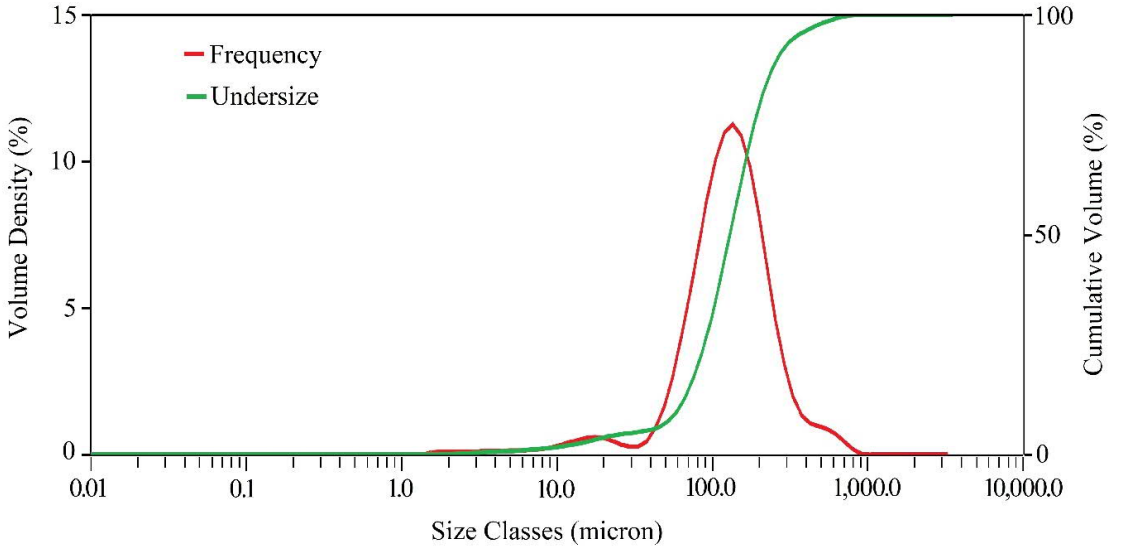

b) High carbon iron

Figure 28: Particle size distribution of stainless steel 316L and high carbon iron powders.

According to the results, the mean (D [4,3]) of stainless steel 316L is 34.2 µm, while this value for high carbon iron is 152 µm. Also, the median (D_{50}) for stainless steel 316L and high carbon iron is 32.7 µm and 129 µm, respectively. However, in most scientific literatures, the particle size distribution is referred as D_{90}, where this value is 51.2 µm and 261 µm for stainless steel 316L and high carbon iron, respectively. On the other side, the range of particle size for stainless steel 316L was measured 0.872-76 µm, while it was 1.45-756 µm for high carbon iron. These numbers clearly show that high carbon iron has larger particles than stainless steel 316L (as it can be seen in microscopy images in Figure 27).

4-2- Printing

Two types of prints including couple (100-100) and mixed (50-50) samples were designed to study the multi-metal parts. Each sample was printed based on printing parameters given in Table 2 with respect to type of samples so that the dimensions were 10.56×10.52×9.82 ± 0.05 mm. In the couple sample, the bottom half was printed by stainless steel 316L filament and the other half by high carbon iron. In the case of mixed sample, the entire layers have uniformly been printed with equal share of two materials (50-50). The latest case also can be assumed as alloying process (for metal filaments), in which the content of each metallic material (filament) can be shared based on the intended alloy composition. Figure 29 indicates each type of samples printed according to the mentioned parameters.

a) 100-100 (couple sample)

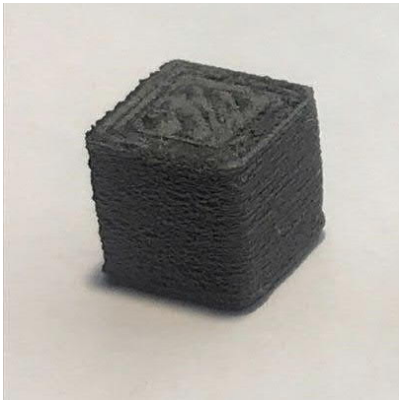

b) 50-50 (mixed sample)

Figure 29: Two types of printed samples.

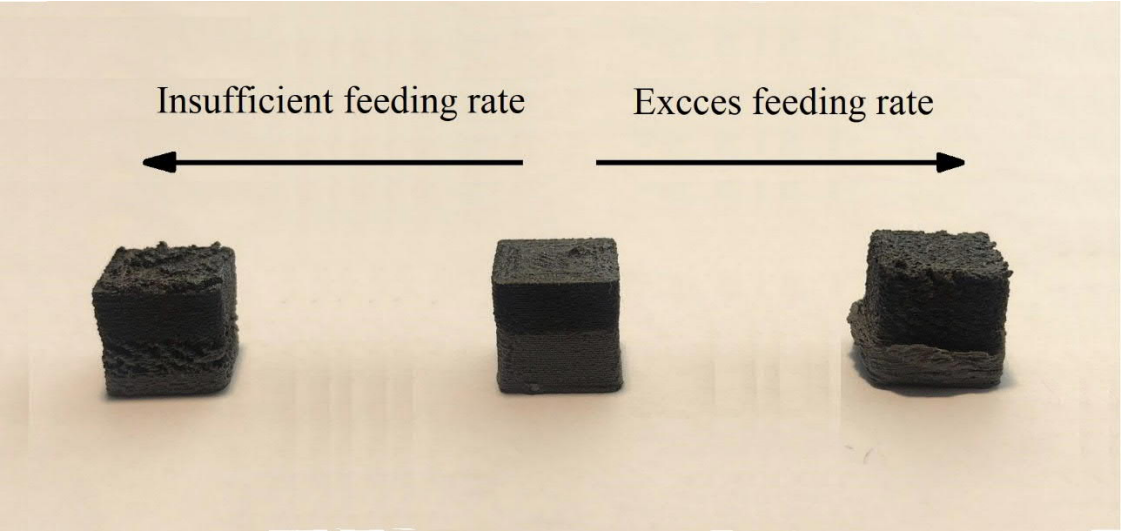

Figure 30: The effect of feeding rate on printed samples.

As it mentioned before, printing parameters have considerable role in production process so that directly affect the properties of final parts. One of these parameters, which is even more critical in the case of multi-material parts, is feeding rate of filaments. This parameter must be chosen in such a way that produces a defect-free print. Accordingly, excess feeding rate causes over deposition, while insufficient values may result in creating defects (porosity) in printed sample. Figure 30 shows the effect of different values of feeding rate on the printed samples. The proper feeding rate for the printer used in this work (Crane Quad 3D) was 200%. This value represents the sum of two filaments feeding rates, which might be different depending on the type of sample. For example, in the case of mixed sample, each filament is fed 100%-100%, while this proportion is 0%-200% for couple sample.

Moreover, the printed samples were investigated in micro scale to observe the success rate of mixing of two materials. The micro-images taken from cross-section of two types of prints by optical microscope are given in Figure 31. The dark areas in the images represent polymeric material (binder) and the light areas belong to metallic particles. As it previously shown in Figure 26, stainless steel 316L particles have spherical shape, while particle shape of high carbon iron is irregular. Furthermore, according to particle size distribution analysis results, the mean size of high carbon iron particles is greater than that of stainless steel 316L. Therefore, the particles of two materials are easily distinguishable in micro-images, which makes it easy to study the particles distribution based on the type of printing.

Figure 31a shows a micro-image of couple sample, in which the border between stainless steel 316L and high carbon iron particles is clearly visible. It should be noted that it is nearly impossible to obtain 100-100% sample in reality. In fact, the fed filaments are mixed in nozzle chamber, and then deposited onto the platform. It means that a share of filament A remains in the chamber and extruded with filament B. This, to some extent, can be seen in micro-image of couple sample. Practically, the high carbon iron particles content from bottom to top would be around from 0 to 90%, respectively. The micro-image of mixed sample is also shown in Figure 31b, which indicates the mixing of stainless steel 316L and high carbon iron particles (50-50%). It also shows that the mixing is successfully done, and the structure is generally homogenous.

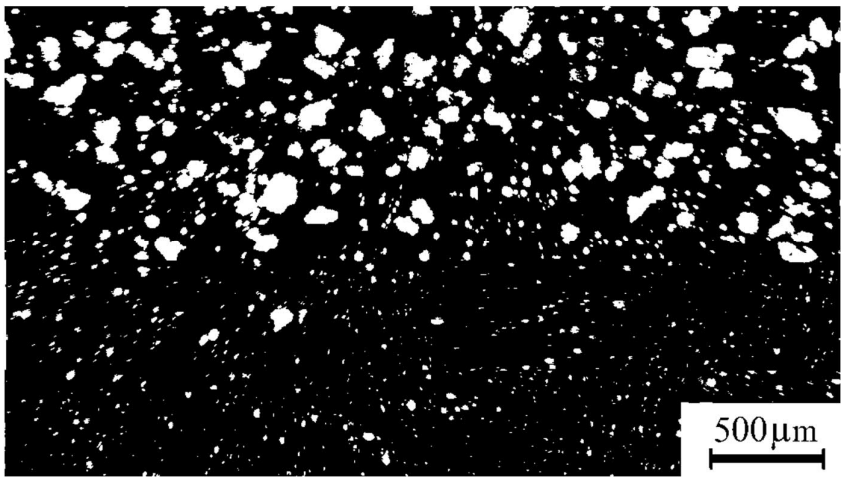

a) Couple sample

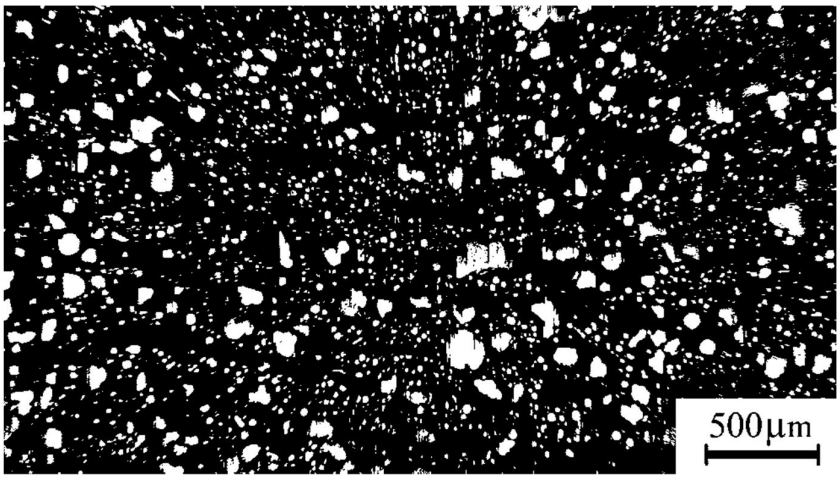

b) Mixed sample

Figure 31: The micro-images of two types of prints taken by optical microscope.

4-3- De-binding

TGA test was carried out to discover evaporation behavior of binder during de-binding process. Therefore, the mass changes of print was measured in a certain heating regime, with specific heating rates, and in Ar atmosphere. Based on what recommended by manufacturer [63], The print was heated from room temperature to 250 °C with the rate of 5 °C/min, and then from 250 °C to 400 °C with the rate of 1 °C/min. When the print reached at 400 °C, the temperature remained constant until no further mass changes observed or the graph becomes standstill. Mass loss represents the amount of removed (evaporated) binder, which can be expressed as below equation:

$$\text{Mass loss}\ (\%) = \left(\frac{\mathrm{dM}}{\mathrm{M}}\right) \times 100 \qquad (5)$$

where, dM is measured mass changes by TGA (g), and M is the mass of print before de-binding process (g). Figure 32 indicates the mass loss of prints with time during de-binding process obtained by TGA test. This graph illustrates that the highest level of removing binder is between 250 °C and 400°C. Furthermore, from this graph, it can be interpreted that the binder is completely removed when the graph tends to standstill, where no further mass changes is observed. According to information in Table 1, each print contains around 20 wt.% binder. It means that holding for 1 hour at 400°C would be enough to remove the whole binder (~20 wt.%) from the samples.

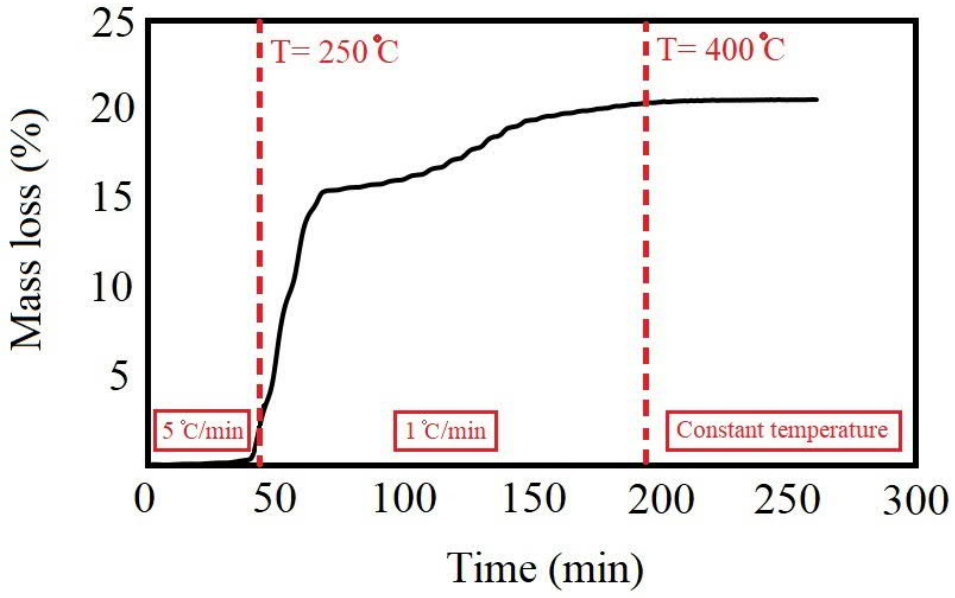

Figure 32: The mass changes of prints versus time during de-binding process.

4-4- Sintering

In order to obtain a dense part, sintering process is required to be carried out at adequate temperature and time in the following of de-binding. Sintering process was conducted in the same furnace immediately after de-binding to save the time and energy, and prevent destroying the flabby sample (after de-binding) due to transportation. According to TGA result, in de-binding stage, the sample is heated up to 400 °C by two different rates (5 °C/min and 1 °C/min) and hold for 1 h, based on the mentioned heating regime (see section 4-3).

Thereafter, in sintering stage, the temperature increases from 400 °C to target temperatures with the rate of 5 °C/min. The samples were isothermally sintered at different target temperatures in the range of 1310-1400 °C for 1h and 6h. Various sintering temperatures and times were chosen to discover the impact of these two parameters on the final results. Then, the sample was slowly cooled down to room temperature with the rate of 30 °C/min inside the furnace. During the whole process, argon gas is being used as protective atmosphere to prevent oxidation. Figure 33 indicates the temperature profile of the whole heating process.

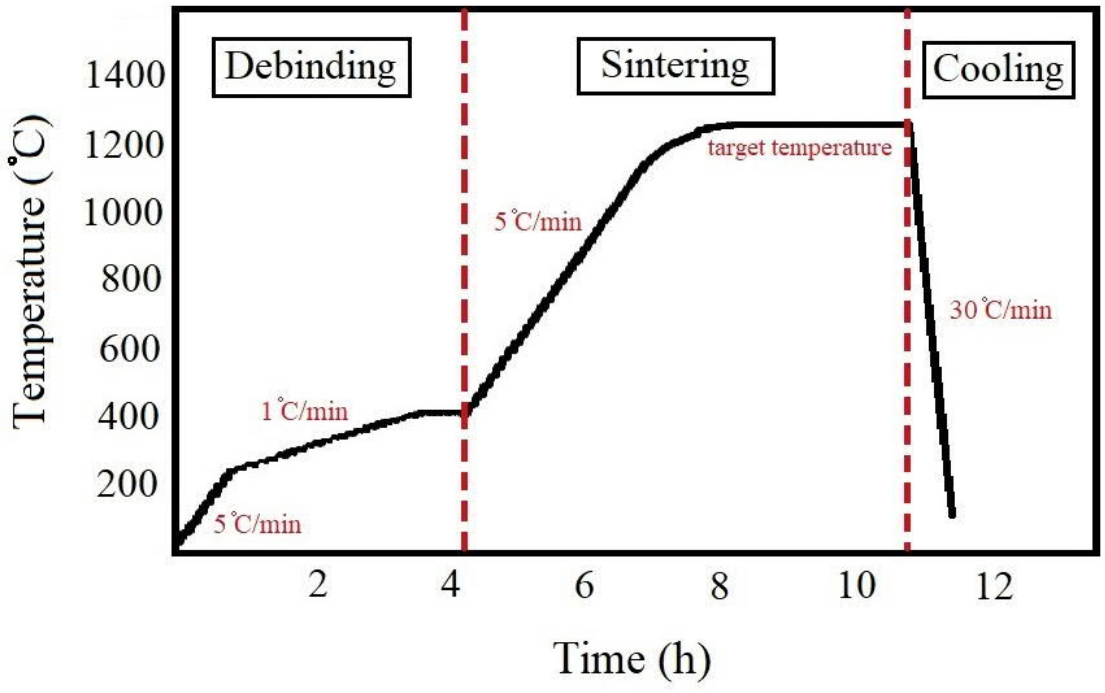

Figure 33: The temperature profile for de-binding, sintering, and cooling processes of couple and mixed samples in Ar atmosphere.

4-4-1- Sintered density

The sintered density for each sample was measured in different sintering conditions based on the Archimedes method (see section 3-2-1). Furthermore, theoretical density was obtained by equation 3 and also the information given in Table 3. Since each raw material was equally distributed in both couple and mixed samples (generally 50% stainless steel 316L and 50% high carbon iron), the theoretical density is the same for both types (7.695 g/cm^3). For the same reason, the mass of each green sample (both types), which measured before de-binding process, was 3.17±0.05g.

Table 4 gives the values of measured sintered density at various sintering temperatures and times. In the case of couple sample, all specimens were sintered at target temperatures (1330-1380 °C) for 6h because each side of sample has single material, and consequently, needs longer time to become densified. In contrast, the mixed sample was sintered at various temperatures for 1h and 6h in order to study the impact of sintering time on densification. Also, a wider range of temperature (1310-1400 °C) was investigated to discover the optimum condition for densification. Eventually, relative density was calculated for each specimen as an adequate criterion for densification level.

Table 4. The values of sintered, theoretical and relative densities of the samples (both types) at various sintering temperatures and times.

Sample	Temperature (°C)	Time (h)	Theoretical density (g/cm^3)	Sintered density (g/cm^3)	Relative density (%)
Couple	1330	6	7.695	5.31	69
	1360	6		5.94	77
	1370	6		6.45	84
	1380	6		5.65	73
mixed	1310	1		5.58	72
	1320	1		5.64	73
	1330	1		6.07	79
	1330	6		6.41	83
	1360	1		6.69	87
	1400	1		5.88	76

The relative density evolution of each sample at different sintering temperatures and times is separately shown in Figure 34. In both types, the density increases with increasing temperature, while it dramatically drops at very high temperatures. In the case of couple sample (Figure 34a), the highest density value was achieved at 1370 °C. A similar trend was observed in mixed sample, where the maximum density value obtained for the specimen that sintered at 1360 °C for 1h. The effect of sintering time on the density value is also shown in Figure 34b, where it improved with longer duration of sintering. However, it can be clearly seen that sintering temperature has more impact on the density than time.

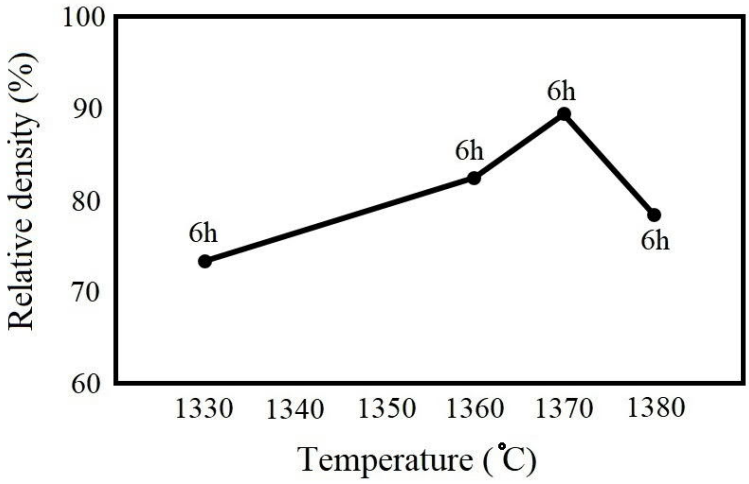

a) Couple sample

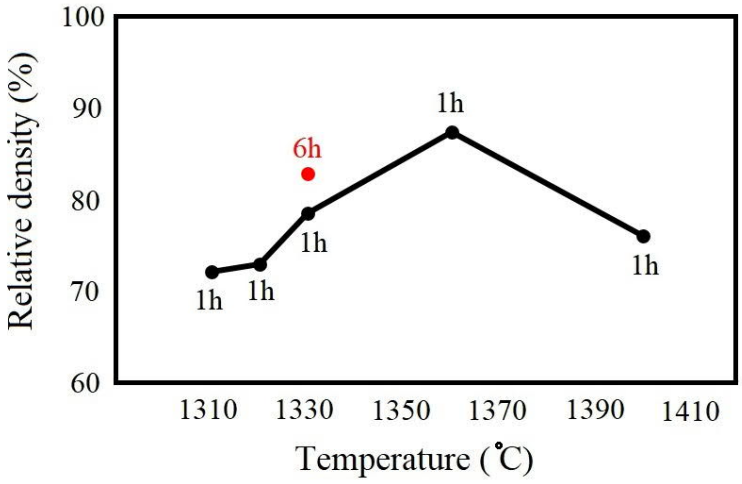

b) Mixed sample

Figure 34: The effect of sintering temperature and time on sintered density.

4-4-2- Dimensional changes

In order to investigation of shrinkage of samples during de-binding and sintering processes, the apparent shape evolution was studied by dimensional changes profile. The measured dimensions obtained from taken images were plotted for each type of samples in different sintering conditions. Figure 35 shows a dimensional profile of couple sample sintered at 1370 °C for 6h in Ar atmosphere in which the dotted line represents the dimensions of green sample (reference), while the solid line introduces the dimensions of sample after sintering. In this profile, H/H_0 and L/L_0 are the sintered/green ratios for height and dimension in x axis, respectively, where H_0 is the actual height (H_0 = 9.82 mm) and L_0 is a half of the actual length of green sample (L_0 = 5.28 mm). For example, $L/L_0 = 1$ represents the edge of sample, while $L/L_0 = 0$ implies the center of sample.

According to Figure 35, the dimensional changes in couple sample has two different behaviors. It can be clearly seen that the bottom area was expanded compared to green sample dimensions, while shrinkage observed in the upper section. Since the upper half of the sample belongs to high carbon iron and the bottom half is for stainless steel 316L, it can be concluded that the type of material is the agent of this difference. However, it seems that there is another area in the center of sample (intermediate area), which shows a transitional behavior so that has more shrinkage near to upper section (high carbon iron). This phenomenon could be due to a compositional gradient, which probably formed during sintering in center area. A similar behavior was observed for other temperatures (see appendices). Since the couple sample has asymmetric dimensional changes from top to bottom, the shrinkage of upper and bottom sections can be separately calculated and the sum of them reported as the total shrinkage value. Table 5 gives the shrinkage values for couple sample sintered at various temperatures for 6h and in different areas.

Table 5. The shrinkage values (%) of couple sample sintered at various temperatures for 6h.

Temperature (°C)	Top (%)	Center (%)	Bottom (%)	Total (%)
1330	22	7	-5.5*	7.8
1360	22.6	9	-3.5*	9.4
1370	25.3	16	1	14
1380	13	3	-9*	2.3

* The negative values represent expansion.

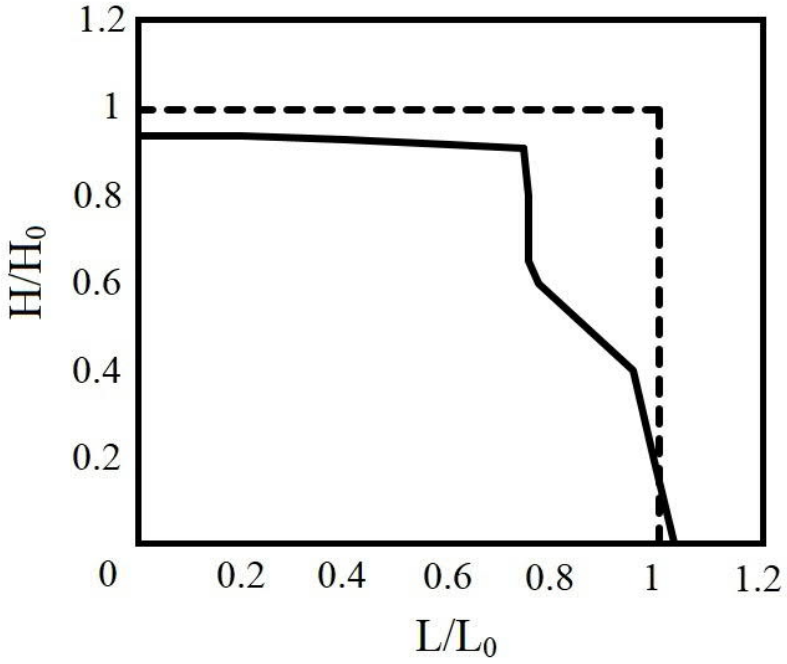

Figure 35: The dimensional profile of couple sample before (dotted line) and after (solid line) sintered at 1370 °C for 6h.

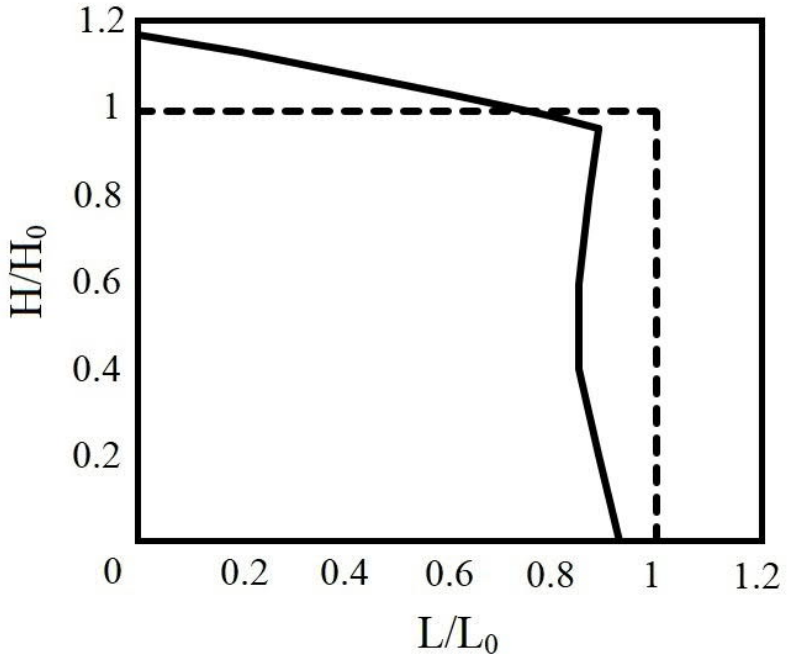

Figure 36: The dimensional profile of mixed sample before (dotted line) and after (solid line) sintered at 1360 °C for 1h.

According to Table 5 and Figure 35, in couple samples, the upper zone has the highest shrinkage values, where represents high carbon iron section. In contrast, in stainless steel 316L side (bottom zone), mostly expansion was observed. The impact of temperature on shrinkage is the other aspect that can be obtained from Table 5 so that the values increase with an increase in temperature up to 1370 °C, and considerably drop at 1380 °C. In total, the couple sample recorded the highest shrinkage at 1370 °C, which is in a good agreement with the density results in Figure 33.

Unlike couple sample, the dimensional changes in mixed samples were more symmetric from top to bottom, due to uniform deposition of two materials in each layer. Figure 36 shows a dimensional profile of mixed sample sintered at 1360 °C for 1h. A unique feature shown in this profile is a "curved-shaped" roof that appeared at the top of mixed samples after sintering. This part of sample, however, can be removed in post-processing stage, and not considered in shrinkage calculations. Table 6 shows the shrinkage values of mixed samples sintered at different temperatures for 1h and 6h. Similar to couple sample, temperature has direct effect on shrinkage, where the values increase with temperature up to 1360 °C, and drop at very high temperatures (1400 °C). As well as this, sintering time can be also effective in increase of shrinkage value, where a slightly increase was observed in the sample sintered at 1330 °C with longer exposure (6h).

Figure 37 shows both sample types before and after sintering, and also schematically indicates the total apparent shape of both samples, where the dotted line is the dimensions of green sample and the solid line belongs to sintered samples' dimensions. From apparent shape point of view, the type of distortion is different for each sample. The couple sample has a "stair-shaped" distortion after sintering due to the difference in amount of shrinkage for each material. In contrast, "X-shaped" distortion was observed in mixed samples, where shrinkage in center was more than that in top and bottom edge of sample. This type of distortion ("X-shaped") is a common phenomenon that has also been reported for other alloys such as bronze, brass, stainless steel, etc. [67,68].

Table 6. The shrinkage values of mixed sample sintered at various temperatures for 1h and 6h.

Temperature (°C)	1310	1320	1330	1330	1360	1400
Time (h)	1	1	1	6	1	1
Shrinkage (%)	4.6	7.3	8.3	9	11	7.6

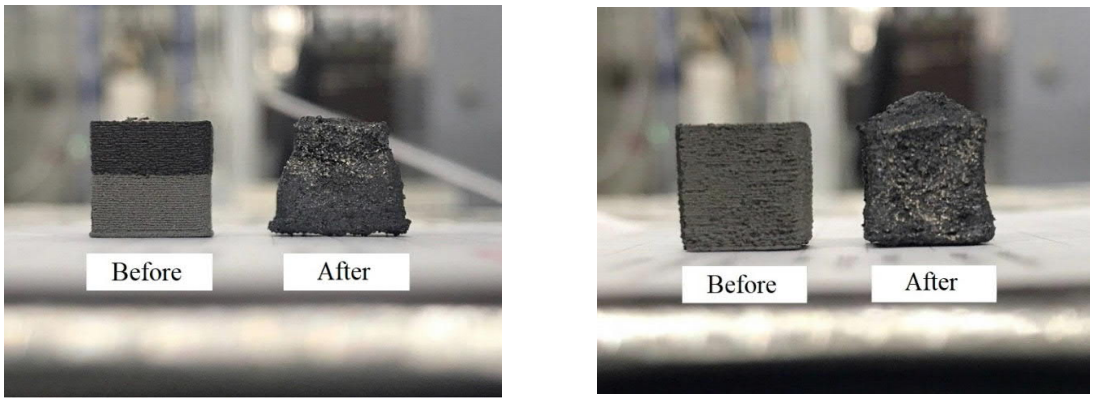

a) Couple sample b) Mixed sample

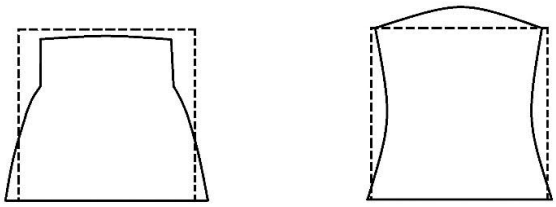

Couple sample Mixed sample

c) Distortion mode

Figure 37: The images of samples before and after sintering.

4-4-3- Microstructural studies

In order to investigation of samples evolution in micro scale, microstructural images were studied. Figure 38 illustrates the microstructures of couple sample sintered at different temperatures for 6h. Since the couple sample has two sections with different materials, both top and bottom areas of sample were investigated to discover the impact of temperature on microstructural evolution (such as porosity shape and size, and also grain size changes) in each material. According to obtained images, in stainless steel 316L side, the structure of porosity has changed from irregular to rounded shape with increasing in temperature. Furthermore, the reduction of porosity is observed in both top (high carbon iron) and bottom (stainless steel 316L) of sample at higher temperatures (1370 °C). This fact is in a good agreement with the measured density results given in Table 4. Another evident phenomenon induced by temperature is “pores closure”, where open pores gradually become closed at higher temperatures. This process is clearly visible in both materials, especially stainless steel 316L. From grain size point of view, grain growth is dominant phenomenon with increasing temperature, where larger grains at higher temperatures can be seen in both materials.

By comparing the two materials microstructures, it is recognizable that the pores size in high carbon iron area is larger, while the number is to some extent less than that in stainless steel 316L zone. On the other side, stainless steel 316L section has smaller grains compared to high carbon iron area, which shows the different behavior of these two materials at the same heating conditions.

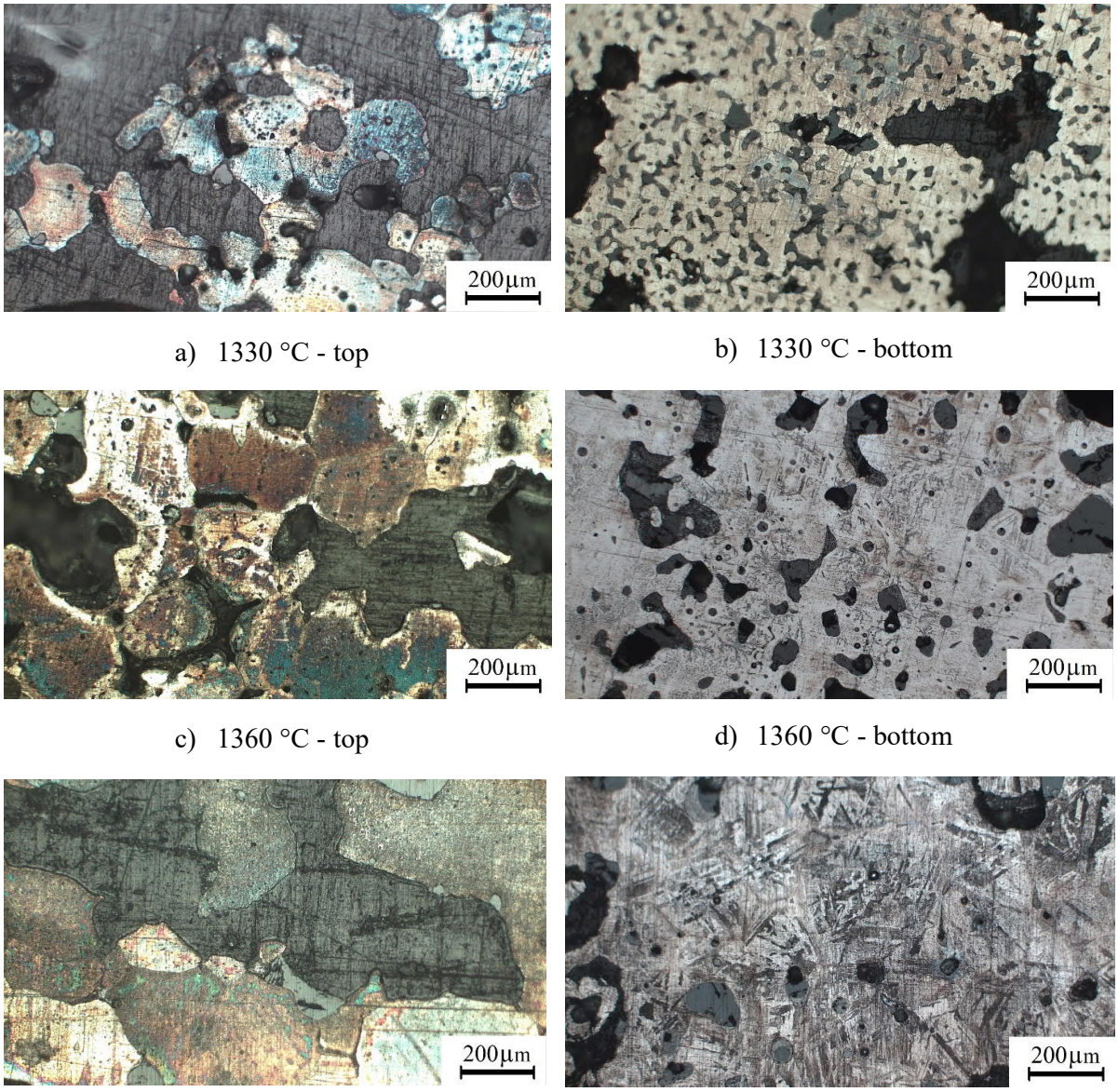

a) 1330 °C - top

b) 1330 °C - bottom

c) 1360 °C - top

d) 1360 °C - bottom

e) 1370 °C - top

f) 1370 °C - bottom

Figure 38: Microstructure of couple sample sintered at different temperatures for 6h. Top and bottom of samples at a distance of 0.8H and 0.2H. H is the height of sample.

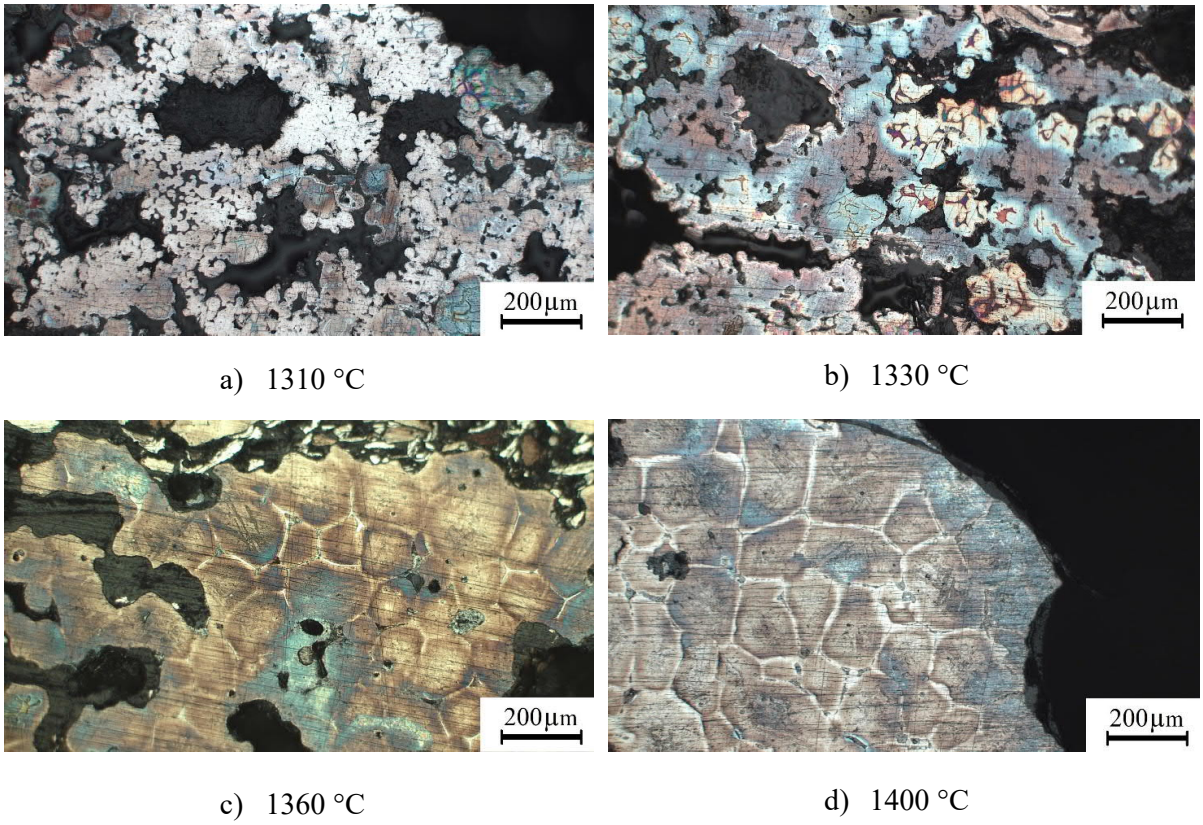

a) 1310 °C b) 1330 °C

c) 1360 °C d) 1400 °C

Figure 39: Microstructure of mixed sample sintered at different temperatures for 1h.

The microstructures of mixed samples sintered at different temperatures for 1h are shown in Figure 39. As it can be seen, the sintering process has not been completely conducted at low temperature (1310 °C), and the connection between the particles is too weak so that the particles maintained their initial shape. With increasing temperature, however, sintering process is gradually completed, and the pores disappeared.

Similar to couple sample, the pores in mixed sample have irregular shape at low temperatures, while they become rounded at higher sintering temperatures. Although the pores size at low temperatures (1310-1330 °C) is relatively small, the pores density is considerably high, which results in reduction of sample density (see Table 4). On the other side, the number of pores reduces with sintering temperature, however the size enlargement is observed. As a consequence of this, a dense sample with several big pores is obtained at very high temperature (1400 °C: Figure 39d).

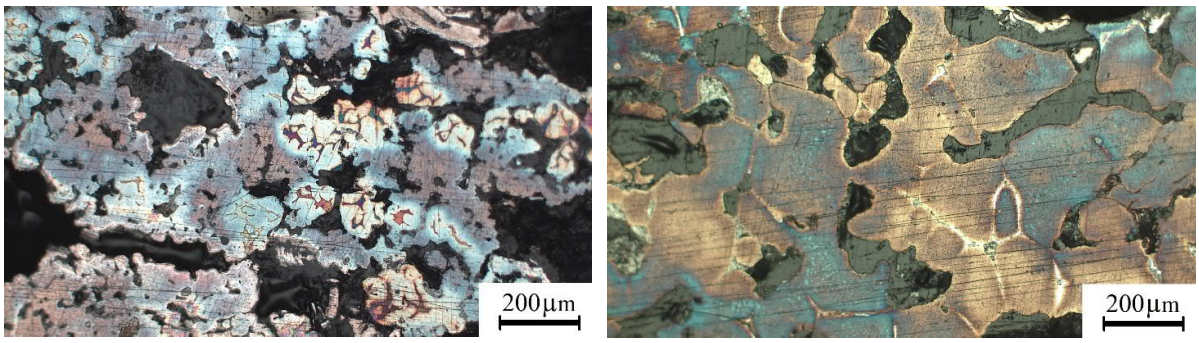

a) 1 hour b) 6 hours

Figure 40: Microstructure of mixed sample sintered at 1330 °C for different sintering time.

Regarding the grain size, the samples with higher sintering temperatures have larger grains compared to those sintered at lower temperatures. Another phenomenon that occurs at high temperatures is forming liquid phase at grain boundaries. Based on Fe-C phase diagram [69], both liquid and solid phases are appeared in the microstructure of high carbon iron at temperatures higher than 1360 °C, while stainless steel 316L still remains in solid form. The formed liquid phase of high carbon iron can move through the solid structure and fill the porosity between the particles and at grain boundaries, which resulting in improvement of density.

Another important parameter, which studied in this work was sintering time to discover its impact on microstructure of mixed sample. Figure 40 shows the microstructures of mixed samples sintered at 1330 °C for 1h and 6h. It can be clearly seen that the pores density has reduced with longer exposure time. Moreover, “pores closure” is observed in the microstructure with duration, where smaller pores disappeared (Figure 40b). Also, it is predictable that grain growth occurs with longer times so that grain size in the sample with duration of 6h is considerably larger than that in 1h.

4-4-4- X-ray characterization

In order to study of compounds and phases that might be formed in the samples during sintering, XRD analysis was carried out for both couple and mixed samples sintered at different temperatures and times, and compared with raw powder, which obtained from de-binding the sample. Figure 41 gives the XRD patterns for each condition in which each peak has been identified based on diffraction angle (2θ) and Bragg’s law ($n\lambda=2d\sin\theta$).

.

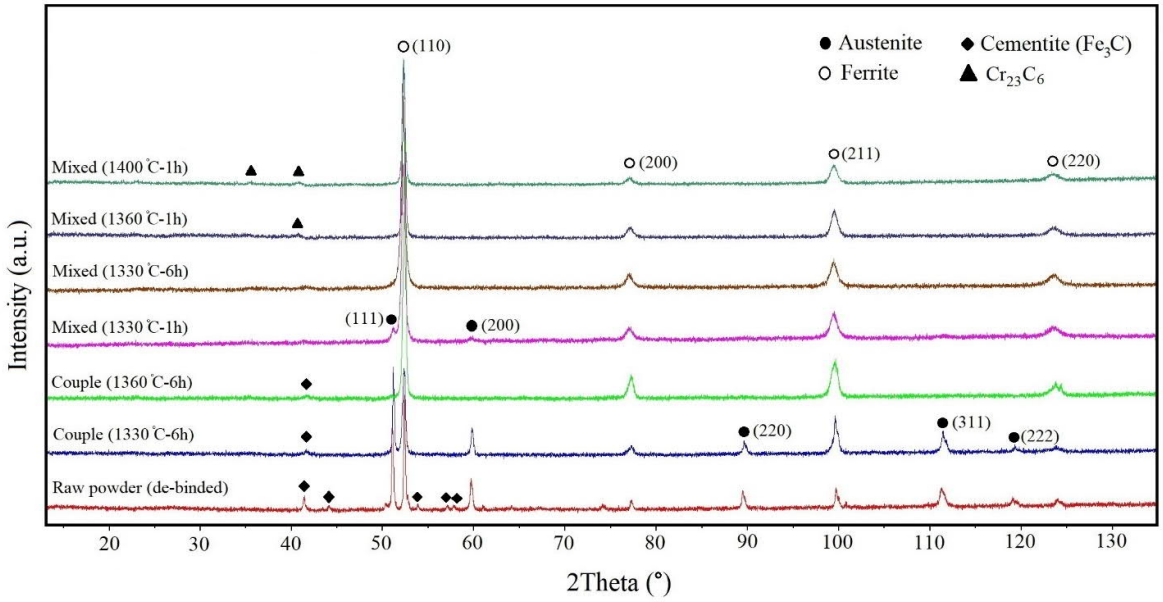

Figure 41: The XRD patterns of raw powder (de-binded material) couple and mixed samples sintered at different temperatures and times.

Based on the XRD patterns, austenite and ferrite phases beside cementite (Fe_3C) were identified in raw powder. The raw powder, which was obtained from de-binding the printed sample is included both stainless steel 316L and high carbon iron particles. At room temperature, austenite (γ) is the dominant phase in stainless steel 316L with face centered cubic (FCC) lattice, while high carbon iron has a structure containing ferrite (α) with body centered cubic (BCC) lattice and cementite.

According to Fe-C phase diagram, both stainless steel 316L and high carbon iron structures are placed in single phase zone, and turned into austenite at high temperatures (during sintering). In fact, in high carbon iron, cementite is dissolved in matrix solid solution and appears as austenite. Once the samples are cooled down to room temperature in the furnace (i.e. slowly), the austenite starts transforming to ferrite, while cementite is precipitated at grain boundaries. In contrast, in stainless steel 316L, the austenite remains unchanged in the structure after cooling down. The XRD pattern for the “Couple: 1330°C-6h” sample shows these transformations, where austenite, ferrite and cementite peaks are identified after sintering. With increasing in temperature, in “Couple: 1360°C-6h” sample, austenite peaks are disappeared, and instead ferrite peaks become more intense, which represents increase in ferrite concentration.

Similarly, ferrite is the phase that identified in “Mixed: 1330°C-6h”, “Mixed: 1360°C-1h” and “Mixed: 1400°C-1h” samples. In “Mixed: 1330°C-1h” sample, two austenite peaks with very low intensity at around 51° and 59° show that there is a small amount of austenite in the structure. It seems that stainless steel 316L at very high temperatures and long durations makes an alloy with high carbon iron (based on diffusion mechanisms) so that loses its austenite structure. In fact, the agents that make austenite stable in stainless steel 316L weaken or disappear as diffusion occurs between stainless steel and high carbon iron. Regarding the “Couple: 1330°C-6h” and “Mixed: 1330°C-1h” samples, temperature and duration are not sufficient to active diffusion mechanism for making alloy, respectively. According to microstructure images (Figure 38d), the stainless steel 316L side (bottom area) has fingerprint structure (pearlite phase), which is a mixture between ferrite and cementite. This microstructure is in a good agreement with the results obtained in XRD pattern.

In order to investigation of elemental distribution of components in different sintering conditions, EDS analysis including mapping and point analysis was carried out for both couple and mixed samples. This analysis can give a good evidence to prove that homogenization and alloying are successfully conducted, especially for mixed sample. The microanalysis of each sample is given in more details in appendices.

Figure 42 shows the EDS mappings of the main elements including Fe, Cr, Ni, Mo and Mn in the mixed samples sintered at different temperatures. At low temperature (1310°C), where the sample is not successfully sintered, the areas with more chromium and molybdenum represent stainless steel 316L particles. These areas are specified in Figure 42a, where high carbon iron particles with larger size are distinct. At very high temperature (1400°C), when liquid phase is formed at grain boundaries, Cr and Mo are segregated into the grain boundaries so that necklace structure is visible. With increasing in temperature, based on diffusion mechanism, Cr and Mo are more homogenously distributed through the whole structure (“Mixed: 1330°C-1h” sample), while accumulated to a certain area with more exposure time (“Mixed: 1330°C-6h” sample). According to the point analysis (see appendices) and XRD patterns, chromium carbide with the composition of $Cr_{23}C_6$ was observed at grain boundaries. In fact, the chromium in the structure reacts with carbon and precipitated as carbide at the grain boundaries. In the case of couple samples, a concentration gradient of elements is observed in the interface between the high carbon iron and stainless steel 316L sections so that increasing in temperature intensifies the diffusion in this zone.

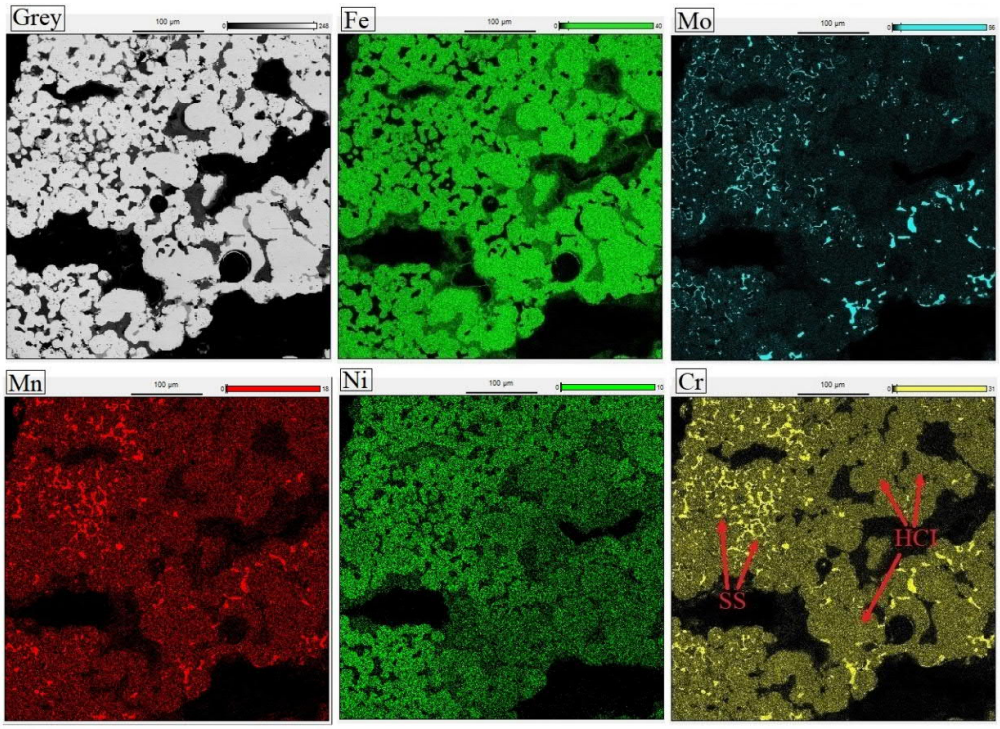

a) 1310 °C – 1h

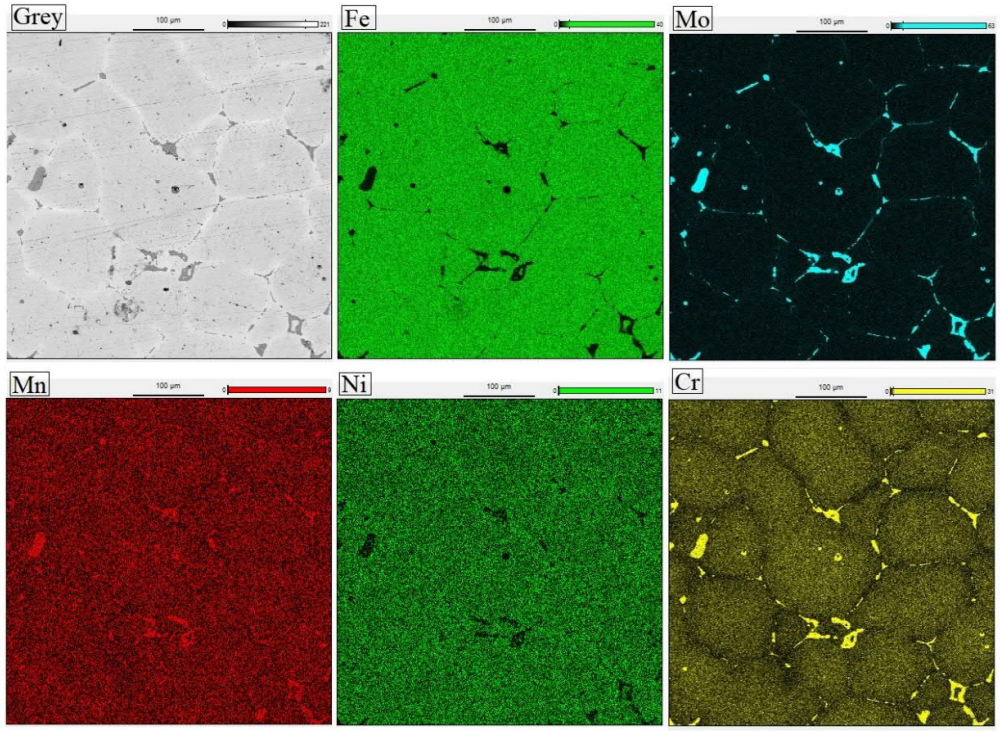

b) 1400 °C – 1h

Figure 42: The EDS elemental mappings for mixed samples sintered at different temperatures.

5- Discussion and conclusion

Each stage of FFF technique has specific influence on the properties of final part. Therefore, investigation of these stages and effective parameters on them is essential to obtain the best possible results. The first stage in this process is printing, where the green sample is built up from a 3D model. Undoubtedly, to print a multi-metal part, the most challenging issue is building a homogenous sample with least defect (e.g. vacancy) in the structure, and correct geometry. Although the used printing parameters in this work, based on what the Filamets^{TM} manufacturer recommended, were appropriate and gave favorable results, the other values for each parameter can also be used to find out the optimum conditions. Since concentrating on printing parameters and study on their effects would have created too many experiments, the samples were printed by the same parameters that the manufacturer suggested. However, more investigations on printing parameters can be done in other works.

The next stage is de-binding process that should be done in order to removing the binder (PLA) from the print so that the shape of sample remains unchanged. Since PLA can be completely evaporated by thermal decomposition, no solvent was used for de-binding process. Based on literatures, the heating program, specially heating rate (when the binder starts evaporation) is the most significant parameter in de-binding. According to TGA results, most of PLA is evaporated from the sample between 250 °C and 400 °C. The heating rate in this range of temperature was chosen 1 °C/min, which is slow enough to present reasonable results. However, based on the research done by Thompson et al. [70], very low heating rates (around 0.3 °C/min) might provide even more adorable results when the other conditions are the same. This very low heating rate suggested by Thompson can prevent from creation of large gaps between the particles during de-binding process, which results in production of a part with high densities close to theoretical density. Also, there is a possibility that very low heating rate in de-binding process can prevent from formation of the “curved-shaped” roof, which is appeared at the top of mixed samples after sintering. Since such very low heating rate makes the whole process too long (practically over 24 hours) and also the argon gas as protective atmosphere is too expensive, in this thesis, it was chosen to use the normal low rate (1 °C/min). Of course, the effect of heating rate in de-binding process on the physical and mechanical properties of the final part can be investigated in next works.

The next stage, or probably the most challenging one, is sintering process in order to achieve a dense part. The most two important parameters in sintering are temperature and time, and finding an appropriate balance between them can help to achieve a part with more desirable properties. According to obtained results, in both couple and mixed samples, the density improved with temperature, while it dropped at very high temperatures. Moreover, time has positive effect on the density, however, it can cause grain growth in microstructure, which results in reduction of mechanical properties.

In the case of apparent shape, a specific shape type was observed after sintering in each sample. According to taken images from the specimens, the couple sample has “stair-shaped” type, while “X-shaped” is distortion type in the mixed sample. On the other side, the surface quality of both samples was not favorable enough to be directly used as the final part. Therefore, further operations or “post-processing” stage, such as filing, sanding, or even machining, seem to be inevitable. Since the bottom area of couple sample is larger than the top (due to different amount of shrinkage for each material), it can be machined to make an equal dimension for the whole part from top to bottom. The other option, however, is changing the 3D model dimension for bottom zone (in printing stage) based on the difference between the amount of measured shrinkage at mentioned areas. In the case of mixed sample, the “curved-shaped” roof at the top of sample must be first removed by machining (or filing), and then each surface should be machined so that the concavity surface disappeared and becomes level.

The shrinkage phenomenon caused by evaporation of the binder and densification during sintering, results in changes in the samples’ dimensions. In each sample type, the shrinkage values were different based on the type of materials and also sintering conditions. The possible two ways that can be considered for evaluation of shrinkage values are calculation of samples: 1) after sintering (intact state), and 2) after machining (processed state). Table 5 and Table 6 give the shrinkage values (%) of couple and mixed samples, respectively, which were evaluated in first way (intact state). In this type of calculation, the couple sample has shrinkage in the range of 2-14%, while it is around 5-11% for mixed sample. However, the second way (processed state) calculation shows higher shrinkage values after machining. In this type, the average shrinkage values for couple and mixed samples are around 23% and 12%, respectively. In both ways, the shrinkage in couple sample is more than that in mixed sample, which represents less dimensional changes in homogenous samples.

The presence of two metallic materials with different characteristics in the samples not only affects dimensional changes, but also some unique microstructural phenomena can be observed during sintering. Due to the difference in melting points of used materials, liquid phase might be formed in microstructure of samples, which results in better densification by filling the porosities. Since one of the used materials in this study (high carbon iron) is a metallic alloy, there is a range of temperature in which a mixture of solid and liquid phases is available in the microstructure. This biphasic region is placed at lower temperatures than stainless steel 316L melting point. Therefore, stainless steel 316L remains in solid form, while high carbon iron is partially melted. The liquid volume fraction formed in this condition, which is called Supersolidus Liquid Phase Sintering (SLPS), depends on the sintering temperature used in experiments. For example, after sintering the mixed sample at 1400 °C, the microstructure has 50% stainless steel 316L solid, 35% high carbon iron solid, and 15% high carbon iron liquid. In fact, this 15% of liquid phase is homogenously spread in the whole mixed sample, while it is accumulated at the top of the couple sample. This could be the main reason that the couple sample does not have uniform changes in shape compared to mixed sample.

According to what mentioned about formation of liquid phase, the type of materials should be carefully chosen. This actually limits the materials selection for multi-metal parts, where those metals or alloys that have close melting points are suitable to be used. In the case of couple sample, it is almost impossible to use two materials with a huge difference in melting points. The reason is one side of sample (the material with lower melting point) is completely melted, while the other side is not even densified. A simple example could be Al and Ni with melting points of 660 °C and 1455 °C, respectively. If Al-Ni couple is sintered at a temperature lower than 660 °C (which is suitable for sintering of pure Al), the Ni particles in the other side of couple will not be sintered and remain in powder form. In contrast, sintering at higher temperatures causes to melt Al side and loose its shape. This is the main reason why two ferrous alloys (stainless steel 316L and high carbon iron) were chosen for this work. This limitation, to a large extent, is not observed in mixed samples, where the materials are homogenously distributed in the sample, and the formed liquid phase can result in more densification. However, the amount of material with lower melting point must be carefully chosen in the way that prevents formation of extra liquid phase. In fact, high liquid volume fraction causes intense distortion in the sample, which is not desirable.

The other effective parameters that were not studied in this work are including the heating rate in de-binding process (discussed earlier in this section), the used atmosphere in de-binding and sintering processes, the particle size distribution of used materials, and also the cooling rate after sintering process. Although argon gas is one of the most appropriate atmospheres for sintering, its high price causes to consider other options such as vacuum atmosphere, especially as the process becomes too long. The effects of vacuum on the porosity and density of multi metal parts are good topics that can be investigated in next works. The other significant parameter is particle size distribution, which plays a key role in densification, and consequently dimensional changes after sintering. The powder with large size increases the empty space between the particles in the sample, which results in increasing the initial porosity. This large space between the particles can improve the densification and prevent from expansion in the same sintering conditions. This phenomenon was observed in this work, where more shrinkage recorded for high carbon iron with larger particles, and expansion occurred in stainless steel 316L with fine particles. However, the type of material is effective for making this difference as well. Another parameter is cooling rate from sintering to ambient temperature, which affects the microstructure and mechanical properties of the final part. Slow cooling rate, which was used in this study, results in formation of ferrite or pearlite phases at room temperature so that the part is ductile. In fast cooling rate (quenching the sample in water), the final phase will be martensite in which the part is brittle but has high strength.

In comparison with other AM techniques, FFF has some benefits and challenges in fabrication of multi metal parts. FFF is much cheaper than the other methods, especially powder bed fusion technologies (e.g. SLM, DMLS, EBM, etc.), which makes multi metal parts more accessible to fabricate by simple home printers. On the other side, the fabrication process of a multi metal part by FFF is much easier than other technologies. In fact, it is too easy to combine different metals (filaments) as a homogenous part or a discrete part in printing stage, compared to other methods particularly PBF, VAT, and LOM, which using different materials in one layer is difficult, if not impossible. In contrast, FFF is a quite long process due to de-binding and sintering stages, compared to VAT, PBF, DED, and even LOM, which is a serious challenge when the production time is important. As well as this, the surface quality of the part fabricated by FFF is not comparable with PBF at all, and post-processing such as machining, sanding or filing is required, which makes the process even longer.

In total, the multi metal parts were successfully fabricated by FFF technique from stainless steel 316L and high carbon iron metal filaments. The mixed and couple samples printed by Crane Quad 3D printer were sintered at different conditions, where become dense up to 87% and 84% of theoretical density, respectively. The couple sample shows different shrinkage in each side due to the difference in type of materials, and has “stair-shaped” distortion while a more symmetric behavior was observed in dimensional changes of mixed sample so that “X-shaped” distortion was evident after sintering. In this condition, a post-processing (machining, filing, etc.) is required to prepare the surface of multi metal part as high quality as it is acceptable. Since couple sample has more shrinkage in high carbon iron part, the total dimensional changes in this sample are larger than that in mixed sample. After post-processing, the shrinkage values were measured around 23% for couple sample and 12% for mixed sample. Based on microstructural images and XRD results, in mixed sample, alloying between stainless steel 316L and high carbon iron was successfully done after sintering. This proves that FFF technique can be used as an alternative method for conventional powder metallurgy methods to make metallic alloys.

References

1- Bandyopadhyay A, Bose S. Additive manufacturing. 2019.

2- Zhang J, Yeon-Gil J. Additive manufacturing: materials, processes, quantifications and applications. Butterworth-Heinemann, 2018.

3- Tuomi J, Paloheimo KS, Björkstrand R, Salmi M, Paloheimo M, Mäkitie AA. 4th International Conference on Advanced Research in Virtual and Rapid Prototyping. TAYLOR & FRANCIS LTD, 2010.

4- Lyons B. Additive manufacturing in aerospace: Examples and research outlook. The Bridge, 2014; 44(3).

5- Juechter V, Franke MM, Merenda T, Stich A, Körner C, Singer RF. Additive manufacturing of Ti-45Al-4Nb-C by selective electron beam melting for automotive applications. Addit. Manuf., 2018; 22: 118-126.

6- Kodama, H. Automatic method for fabricating a three-dimensional plastic model with photo-hardening polymer. Review of scientific instruments, 1981; 52(11): 1770-1773.

7- Tuomi J, Chekurov S, Partanen J. 3d printing, intellectual property and innovation. Wolters Kluwer, 2017.

8- Akmal JS, Salmi M, Mäkitie A, Björkstrand R, Partanen J. Implementation of industrial additive manufacturing: intelligent implants and drug delivery systems. J. funct. Biomater., 2018; 9(3): 41.

9- Salmi M, Akmal JS, Pei E, Wolff J, Jaribion A, Khajavi SH. 3D Printing in COVID-19: Productivity Estimation of the Most Promising Open Source Solutions in Emergency Situations. Appl. Sci., 2020; 10(11): 4004.

10- Huotilainen E, Salmi M, Lindahl J. Three-dimensional printed surgical templates for fresh cadaveric osteochondral allograft surgery with dimension verification by multivariate computed tomography analysis. The Knee, 2019; 26(4): 923-932.

11- Guo N, Leu MC. Additive manufacturing: technology, applications and research needs. Front Mech Eng, 2013; 8(3): 215-243.

12- Campbell I, Bourell D, Gibson I. Additive manufacturing: rapid prototyping comes of age. Rapid Prototyp J, 2012; 18(4): 255-258.

13- Gibson I, Rosen DW, Stucker B. Additive manufacturing technologies: 3d printing, rapid prototyping, and direct digital manufacturing. New York: Springer, 2014.

14- Kretzschmar N, Chekurov S, Salmi M, Tuomi J. Evaluating the readiness level of additively manufactured digital spare parts: an industrial perspective. Appl. Sci., 2018; 8(10): 1837.

15- Redwood B, Schffer F, Garret B. The 3D printing handbook: technologies, design and applications. 3D Hubs. 2017.

16- Huang S H, Liu P, Mokasdar A, Hou L. Additive manufacturing and its societal impact: a literature review. Int J Adv Manuf Technol, 2013; 67: 1191-1203.

17- Wong K V, Hernandez A. A review of additive manufacturing. International Scholarly Research Network, 2012: 1-10.

18- Frazier W E. Metal additive manufacturing: a review. J Mater Eng Perform, 2014; 23(6): 1917-1928.

19- Noorani R. 3D Printing: Technology, Applications, and Selection. CRC Press, 2017.

20- Gonzalez-Gutierrez J, Cano S, Schuschnigg S, Kukla C, Sapkota J, Holzer C. Additive manufacturing of metallic and ceramic components by the material extrusion of highly filled polymers: A review and future perspectives. Materials, 2018; 11(5): 840.

21- Cuan-Urquizo E, Barocio E, Tejada-Ortigoza V, Pipes R B, Rodriguez C A, Roman-Flores A. Characterization of the mechanical properties of FFF structures and materials: A review on the experimental, computational and theoretical approaches. Materials, 2019; 12(6): 895.

22- Chua C K, Kah F L. 3D Printing and Additive Manufacturing: Principles and Applications (with Companion Media Pack) of Rapid Prototyping Fourth Edition. World Scientific Publishing Company, 2014.

23- DIN, E. ISO/ASTM 52900: 2017-06. Additive Manufacturing - General Principles - Terminology (ISO/ASTM 52900: 2015). German version EN ISO/ASTM, 52900, 2017.

24- Gardan J. Additive manufacturing technologies: state of the art and trends. International Journal of Production Research, 2016; 54(10): 3118-3132.

25- Salmi M, Ituarte IF, Chekurov S, Huotilainen E. Effect of build orientation in 3D printing production for material extrusion, material jetting, binder jetting, sheet object lamination, vat photopolymerisation, and powder bed fusion. Int. J. Collab. Enterp., 2016; 5(3-4): 218-231.

26- Medellin A, Du W, Miao G, Zou J, Pei Z, Ma C. Vat Photopolymerization 3D Printing of Nanocomposites: A Literature Review. Journal of Micro and Nano-Manufacturing, 2019; 7(3).

27- Ngo T D, Kashani A, Imbalzano G, Nguyen K T, Hui D. Additive manufacturing (3D printing): A review of materials, methods, applications and challenges. Compos. B. Eng., 2018; 143: 172-196.

28- Vaezi M, Chianrabutra S, Mellor B, Yang S. Multiple material additive manufacturing–Part 1: a review. Virtual Phys. Prototyp., 2013; 8(1): 19-50.

29- Yang L, Hsu K, Baughman B, Godfrey D, Medina F, Menon M, Wiener S. Additive manufacturing of metals: the technology, materials, design and production. Schwitzerland: Springer, 2017.

30- Bertrand P, Bayle F, Combe C, Gœuriot P, Smurov I. Ceramic components manufacturing by selective laser sintering. Appl. Surf. Sci. 2007; 254(4): 989-992.

31- Qian B, Shen Z. Laser sintering of ceramics. J. Asian Ceram. Soc. 2013; 1(4): 315-321.

32- Yadroitsev I, Gusarov A, Yadroitsava I, Smurov I. Single track formation in selective laser melting of metal powders. J. Mater. Process. Technol. 2010; 210(12): 1624-1631.

33- Calle MA, Salmi M, Mazzariol LM, Alves M, Kujala P. Additive manufacturing of miniature marine structures for crashworthiness verification: Scaling technique and experimental tests. Mar. Struct., 2020; 72: 102764.

34- Calle MA, Salmi M, Mazzariol LM, Kujala P. Miniature reproduction of raking tests on marine structure: Similarity technique and experiment. Eng. Struct., 2020; 212: 110527.

35- Louvis E, Fox P, Sutcliffe C J. Selective laser melting of aluminium components. J. Mater. Process. Technol. 2011; 211(2): 275-284.

36- Sames W J, List F A, Pannala S, Dehoff R R, Babu S S. The metallurgy and processing science of metal additive manufacturing. Int. Mater. Rev. 2016; 61(5): 315-360.

37- Salmi M, Partanen J, Tuomi J, Chekurov S, Björkstrand R, Huotilainen E, Kukko K, Kretzschmar N, Akmal J, Jalava K, Koivisto S, 2018; Digital spare parts.

38- Zhang Y, Wu L, Guo X, Kane S, Deng Y, Jung Y G, Zhang J. Additive manufacturing of metallic materials: a review. J. Mater. Eng. Perform. 2018; 27(1): 1-13.

39- Turner B N, Gold S A. A review of melt extrusion additive manufacturing processes: II. Materials, dimensional accuracy, and surface roughness. Rapid. Prototyp. J. 2015; 21(3): 250-261.

40- Wang X, Jiang M, Zhou Z, Gou J, Hui D. 3D printing of polymer matrix composites: A review and prospective. Compos. B. Eng. 2017; 110: 442-458.

41- Nuñez P J, Rivas A, García-Plaza E, Beamud E, Sanz-Lobera A. Dimensional and surface texture characterization in Fused Deposition Modelling (FDM) with ABS plus. Procedia. Eng. 2015; 132: 856-863.

42- Dul S, Fambri L, Pegoretti A. Fused deposition modelling with ABS–graphene nanocomposites. Compos. Part A Appl. Sci. Manuf. 2016; 85: 181-191.

43- Liu Z, Wang Y, Wu B, Cui C, Guo Y, Yan C. A critical review of fused deposition modeling 3D printing technology in manufacturing polylactic acid parts. Int. J. Adv. Manuf. Tech. 2019; 102(9-12): 2877-2889.

44- Farah S, Anderson D G, Langer R. Physical and mechanical properties of PLA, and their functions in widespread applications - A comprehensive review. Adv. Drug Deliv. Rev. 2016; 107: 367-392.

45- Giberti H, Strano M, Annoni M. An innovative machine for Fused Deposition Modeling of metals and advanced ceramics. In MATEC web of conferences. EDP Sciences. 2016; Vol. 43: p. 03003.

46- Novakova-Marcincinova L, Novak-Marcincin J, Barna J, Torok J. Special materials used in FDM rapid prototyping technology application. In 2012 IEEE 16th International Conference on Intelligent Engineering Systems (INES). 2012: 73-76.

47- Onagoruwa S, Bose S, Bandyopadhyay A. Fused deposition of ceramics (FDC) and composites. In 2001 International Solid Freeform Fabrication Symposium. 2001.

48- Bandyopadhyay A, Heer B. Additive manufacturing of multi-material structures. Mater. Sci. Eng. R Rep. 2018; 129: 1-16.

49- Sugavaneswaran M, Arumaikkannu G. Modelling for randomly oriented multi material additive manufacturing component and its fabrication. Mater. Des. 2014; 54: 779-785.

50- Mognol P, Muller P, Hascoet J Y. A novel approach to produce functionally graded materials for additive manufacturing. In Proceedings of the Conference on Advanced Research in Virtual and Rapid Prototyping. 2011; 473-478.

51- Choi J W, Kim H C, Wicker R. Multi-material stereolithography. J. Mater. Process Technol. 2011; 211(3): 318-328.

52- Tibbits S. 4D printing: multi-material shape change. Archit. Des. 2014; 84(1): 116-121.

53- Pedersen D B. Additive Manufacturing: Multi Material Processing and Part Quality Control. Kgs.Lyngby: Technical University of Denmark, 2013.

54- Lu L, Fuh J Y H, Nee A Y C, Kang E T, Miyazawa T, Cheah C M. Origin of shrinkage, distortion and fracture of photopolymerized material. Mater. Res. Bull. 1995; 30(12): 1561-1569.

55- Spackman C C, Picha K C, Gross G J, Nowak J F, Smith P J, Zheng J, Samuel J, Mishra S. A novel multimaterial additive manufacturing technique for fabricating laminated polymer nanocomposite structures. J. Micro Nano Manufact. 2015; 3(1): 11008.

56- Ding D, Pan Z, Cuiuri D, Li H. Wire-feed additive manufacturing of metal components: technologies, developments and future interests. Int. J. Adv. Manuf. Technol. 2015; 81: 465-481.

57- Hofmann D C, Kolodziejska J, Roberts S, Otis R, Dillon R P, Suh J O, Liu Z K. Borgonia J P. Compositionally graded metals: A new frontier of additive manufacturing. J. Mater. Res. 2014; 29(17): 1899-1910.

58- Pavlov M, Novichenko D, Doubenskaia M. Optical diagnostics of deposition of metal matrix composites by laser cladding. Phys. Procedia. 2011; 12: 674-682.

59- Bandyopadhyay A, Dittrick S, Gualtieri T, Wu J, Bose S. Calcium phosphate–titanium composites for articulating surfaces of load-bearing implants. J. Mech. Behav. Biomed. 2016; 57: 280-288.

60- Roy M, Krishna B V, Bandyopadhyay A, Bose S. Laser processing of bioactive tricalcium phosphate coating on titanium for load-bearing implants. Acta Biomater. 2008; 4(2): 324-333.

61- Regenfuss P, Streek A, Hartwig L, Klötzer S, Brabant T, Horn M, Ebert R, Exner H. Principles of laser micro sintering. Rapid Prototyp. J. 2007: 740-753.

62- Hu Y, Cong W. A review on laser deposition-additive manufacturing of ceramics and ceramic reinforced metal matrix composites. Ceram Int. 2018; 44(17): 20599-20612.

63- https://shop.thevirtualfoundry.com/collections/metal-filaments/products.

64- Ilies A, Kretzschmar N, Chekurov S, Salmi M, Rech J. "Design-dependent shrinkage compensation modeling and mechanical property targeting of metal FFF." Prog. Adv. Manuf. 2020; 1-7.

65- DIN, E. 3369: 2010-08, Impermeable sintered metal materials and hardmetals–determination of density (ISO 3369: 2006); German version EN ISO 3369: 2010.

66- Standardization, TIOf: 2009, Particle Size Analysis - Laser Diffraction Methods (ISO 13320); 2009.

67- Mousapour M, Azadbeh M, Danninger H. Effect of compacting pressure on shape retention during supersolidus liquid phase sintering of Cu base alloys. Powder Metall. 2017; 60(5): 393-403.

68- Ghasemi S, Azadbeh M, Mousapour M, Mohammadzadeh A, Danninger H, Salimi N. The role of pore evolution during supersolidus liquid phase sintering of prealloyed brass powder. Powder Metall. 2020; 63(3): 187-196.

69- Baker H, Okamoto H. ASM Handbook. Vol. 3. Alloy Phase Diagrams. ASM International, Materials Park, Ohio, USA, 1992: 527.

70- Thompson Y, Gonzalez-Gutierrez J, Kukla C, Felfer P. Fused filament fabrication, debinding and sintering as a low cost additive manufacturing method of 316L stainless steel. Additive Manufacturing, 2019; 30: 100861.

Appendices

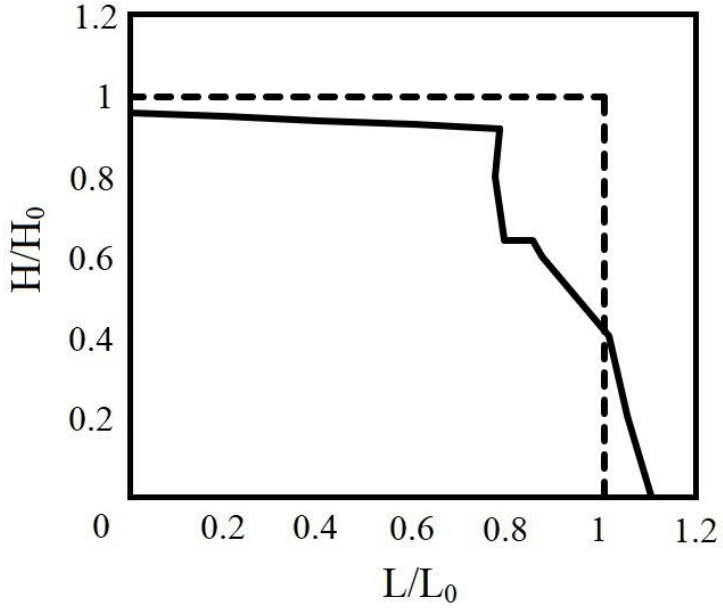

A1: The dimensional profile of couple sample before (dotted line) and after (solid line) sintered at 1330 °C for 6h.

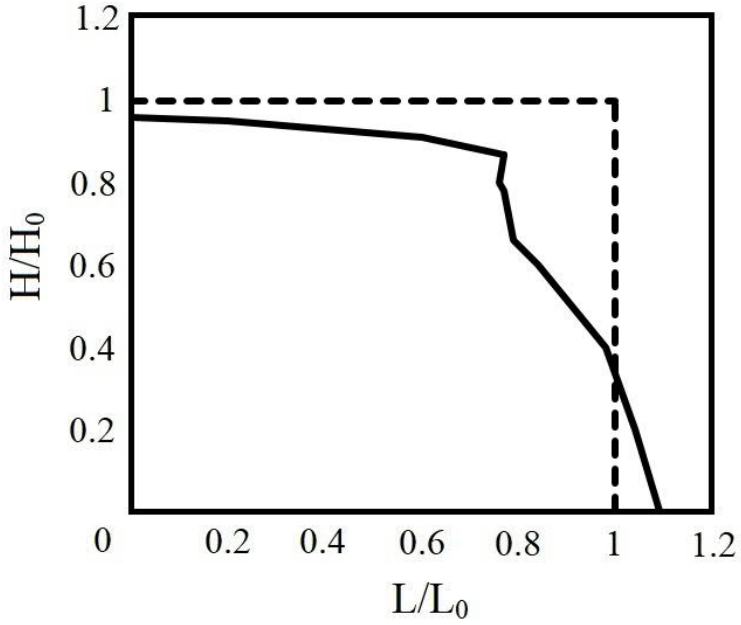

A2: The dimensional profile of couple sample before (dotted line) and after (solid line) sintered at 1360 °C for 6h.

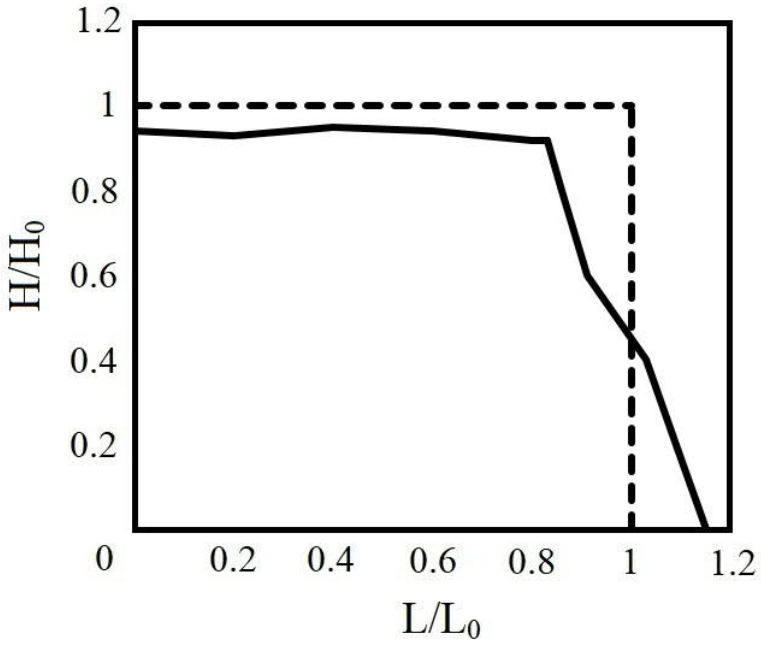

A3: The dimensional profile of couple sample before (dotted line) and after (solid line) sintered at 1380 °C for 6h.

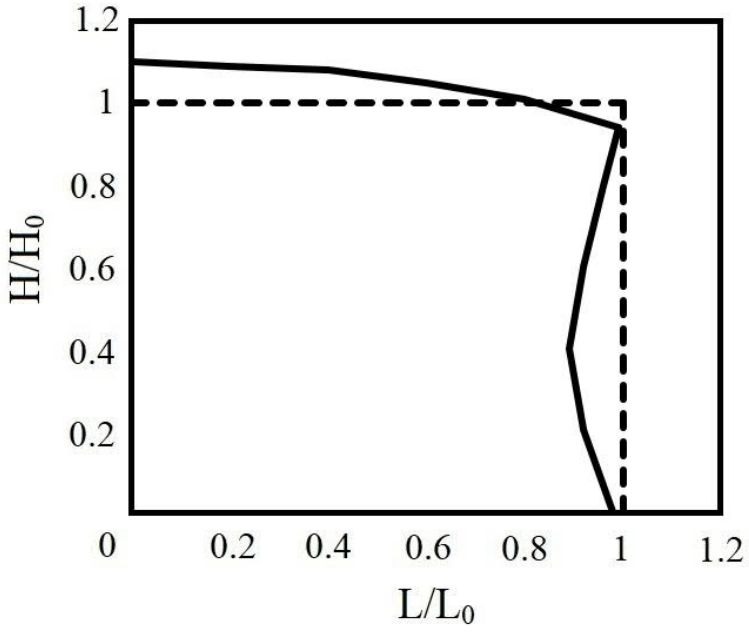

A4: The dimensional profile of mixed sample before (dotted line) and after (solid line) sintered at 1310 °C for 1h.

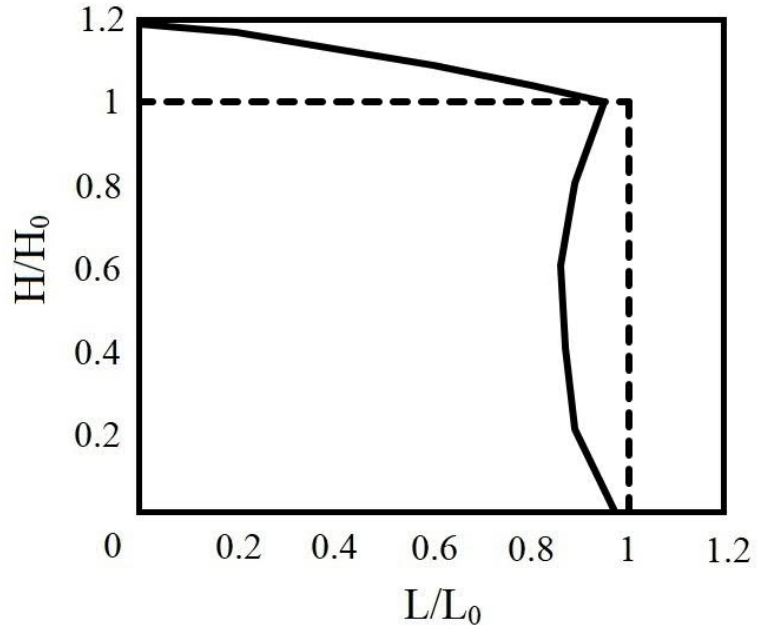

A5: The dimensional profile of mixed sample before (dotted line) and after (solid line) sintered at 1320 °C for 1h.

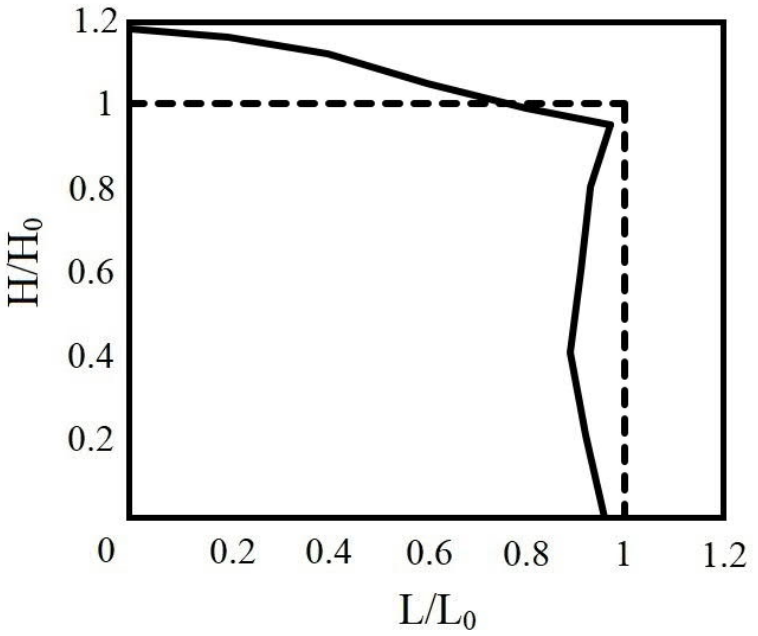

A6: The dimensional profile of mixed sample before (dotted line) and after (solid line) sintered at 1330 °C for 1h.

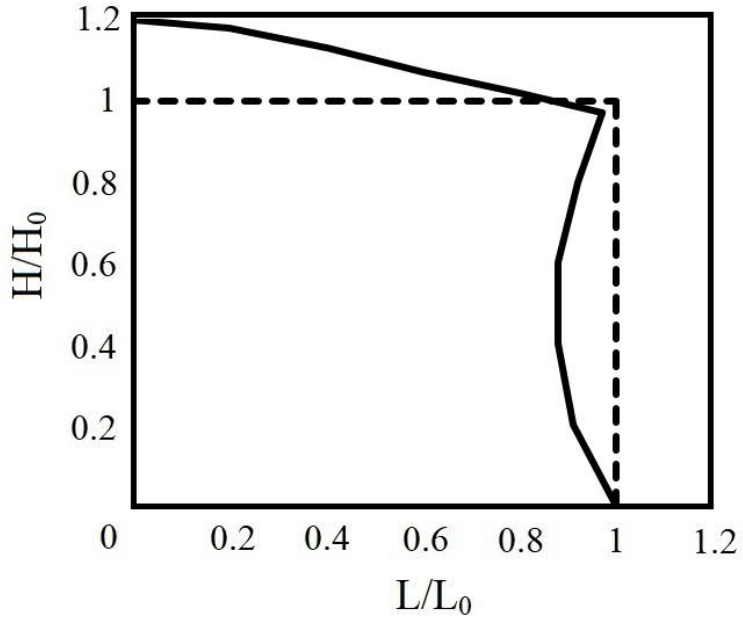

A7: The dimensional profile of mixed sample before (dotted line) and after (solid line) sintered at 1330 °C for 6h.

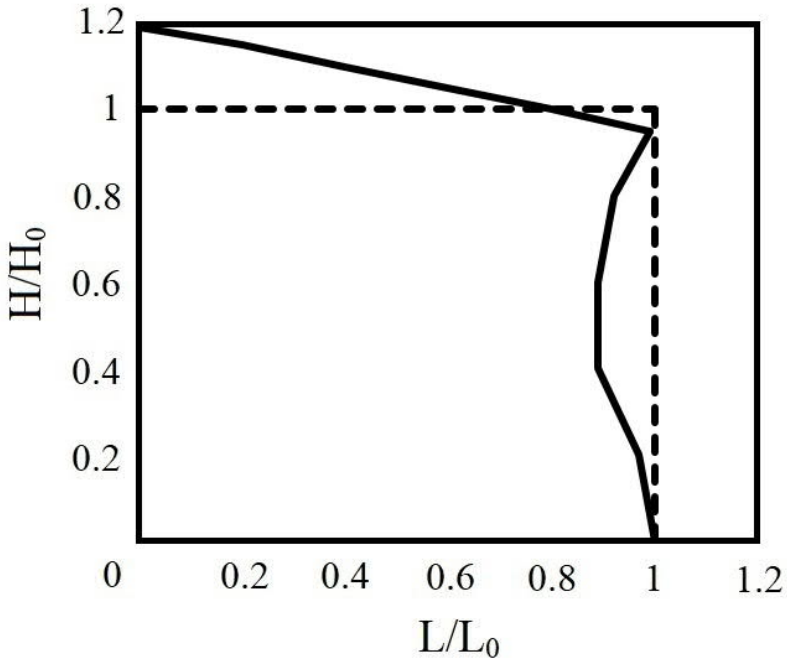

A8: The dimensional profile of mixed sample before (dotted line) and after (solid line) sintered at 1400 °C for 1h.

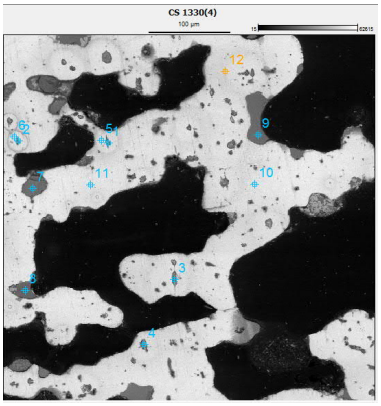

a) Top (high carbon iron)

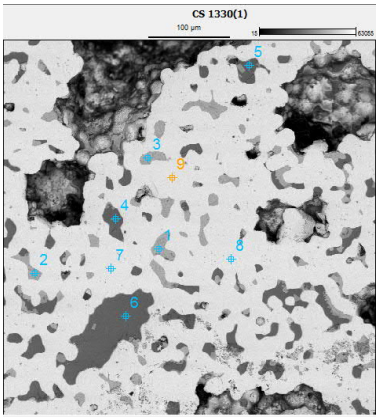

b) Bottom (stainless steel 316L)

Top		1	2	3	4	5	6	7	8	9	10	11	12
C	wt-%	5.81	6.61	5.66	5.56	2.33	2.2	2.45	3.16	2.66	2.18	2.39	2.87
	atm-%	18.51	19.73	20.96	19.32	9.63	9.36	10.67	10.38	9.88	9.31	9.65	9.6
O	wt-%	18.67	15.63	8.6	4.7	-	-	15.92	17.98	19.59	-	-	-
	atm-%	14.3	14.89	14.37	12.25	-	-	21.65	23.53	26.25	-	-	-
Al	wt-%	-	-	-	-	-	-	0.8	1.47	1.13	-	-	-
	atm-%	-	-	-	-	-	-	0.65	1.14	0.89	-	-	-
Si	wt-%	4.41	3.84	2.37	2.55	0.71	0.64	48.49	50.15	48.94	0.7	1	0.98
	atm-%	4.08	3.9	3.04	3.78	0.92	0.84	45.95	46.21	52.91	0.91	1.3	1.26
Ca	wt-%	-	-	-	-	-	-	2.72	2.86	3.85	-	-	-
	atm-%	-	-	-	-	-	-	1.47	1.49	2.06	-	-	-
Cr	wt-%	0.43	0.15	0.12	0.14	0.1	0.11	0.93	0.23	0.2	0.07	0.02	0.09
	atm-%	0.21	0.08	0.08	0.11	0.07	0.08	0.39	0.09	0.08	0.05	0.01	0.06
Mn	wt-%	0.02	0.1	0.11	0.17	0.14	0.09	3.96	2.89	4.77	0.02	0.1	0.12
	atm-%	0.01	0.05	0.07	0.13	0.09	0.06	1.57	1.1	1.86	0.01	0.07	0.08
Fe	wt-%	66.84	70.68	80.08	82.64	93.78	94.27	23.69	20.26	18.43	94.19	93.69	93.34
	atm-%	61.5	60.04	59.72	61.73	87.56	88.05	17.28	15.72	15.92	88	87.29	86.48
Ni	wt-%	2.08	2.2	2.52	3	2.47	2.38	0.91	0.85	0.28	2.61	2.56	2.28
	atm-%	0.92	1.07	1.55	2.13	1.54	1.49	0.34	0.3	0.1	1.63	1.59	1.4
Mo	wt-%	1.74	0.79	0.54	1.24	0.47	0.31	0.13	0.14	0.15	0.24	0.25	0.33
	atm-%	0.47	0.23	0.2	0.54	0.18	0.12	0.03	0.03	0.03	0.09	0.1	0.12

Bottom		1	2	3	4	5	6	7	8	9
C	wt-%	2.07	2.48	2.21	3.05	1.85	2.24	0.46	1.08	0.76
	atm-%	8.97	9.79	7.11	5.26	4.27	4.11	7.79	9.21	6.16
O	wt-%	-	-	-	33	43.17	42.74	-	-	-
	atm-%	-	-	-	47.42	59.55	59.33	-	-	-
Al	wt-%	0.14	0.13	-	2.22	2.01	1.81	-	-	-
	atm-%	0.24	0.2	-	1.85	1.59	1.44	-	-	-
Si	wt-%	2.42	0.39	0.52	25.91	22.87	21.84	0.21	0.18	0.21
	atm-%	3.99	0.58	0.89	27.2	20.09	20.41	0.29	0.25	0.29
Ca	wt-%	3.84	0.08	-	21.6	18.18	16.55	-	-	-
	atm-%	4.44	0.08	-	12.16	9.67	8.87	-	-	-
Cr	wt-%	41.23	47.34	40.94	11.85	9.65	11.42	10.17	10.11	10.19
	atm-%	48.28	53.88	54.4	5.14	3.96	4.72	7.75	7.57	7.91
Mn	wt-%	1.21	12.84	0.8	1.44	1.28	1.58	-	-	-
	atm-%	1.02	9.73	0.71	0.59	0.5	0.62	-	-	-
Fe	wt-%	0.89	4.92	1.06	0.93	0.95	0.64	72.28	71.7	71.53
	atm-%	0.74	3.67	0.92	0.37	0.36	0.25	73.46	72.36	74.47
Ni	wt-%	-	0.03	-	-	-	-	14.31	14.46	14.55
	atm-%	-	0.02	-	-	-	-	9.65	9.6	10
Mo	wt-%	48.21	31.79	54.48	-	0.03	1.19	2.57	2.46	2.76
	atm-%	32.32	22.05	35.98	-	0.01	.27	1.06	1	1.16

A9: The point analysis of couple sample sintered at 1330 °C for 6h.

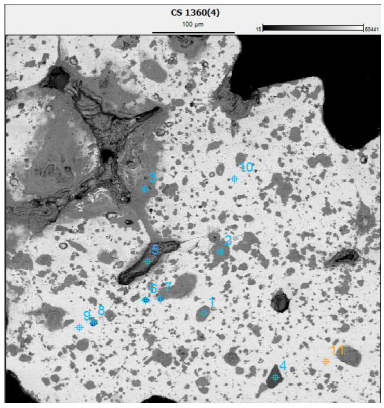

a) Top (high carbon iron)

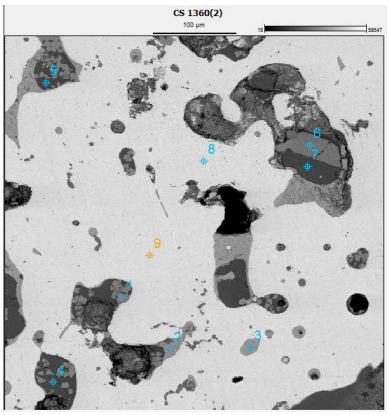

b) Bottom (stainless steel 316L)

Top		1	2	3	4	5	6	7	8	9	10	11
C	wt-%	6.22	5.97	5.19	5.2	4.68	5.12	6.25	4.5	2.12	1.98	1.95
	atm-%	22.23	21.74	21.07	6.32	8.76	19.78	17.98	6	9.85	10.08	10.18
O	wt-%	16.96	17.13	15.32	37.56	35.79	10.44	15.57	20.4	-	-	-
	atm-%	11.03	11.47	15.31	52.32	54.73	18.93	33.6	42.29	-	-	-
Al	wt-%	-	0.11	0.09	0.75	0.02	0.08	0.03	0.17	-	-	-
	atm-%	-	0.12	0.01	0.58	0.01	0.08	0.03	0.17	-	-	-
Si	wt-%	0.42	0.32	0.26	35.48	0.4	0.61	0.2	1.23	-	-	-
	atm-%	0.44	0.34	0.28	32.57	0.35	0.63	0.24	1.17	-	-	-
Ca	wt-%	0.36	0.01	0.04	2.13	0.02	0.26	0.55	0.8	-	-	-
	atm-%	0.26	0.01	0.03	1.1	0.01	0.19	0.47	0.53	-	-	-
Cr	wt-%	0.05	0.06	0.06	2.12	0.06	0.04	0.05	0.1	0.06	0.09	0.25
	atm-%	0.03	0.04	0.03	0.85	0.03	0.02	0.04	0.05	0.05	0.07	0.2
Mn	wt-%	0.03	0.13	0.16	5.38	0.09	0.08	0.16	0.18	0.23	0.17	0.15
	atm-%	0.02	0.07	0.09	2.04	0.04	0.04	0.1	0.09	0.17	0.12	0.11
Fe	wt-%	73.18	73.01	75.13	11.2	56.46	79.8	73.79	69.85	94.66	94.83	92.86
	atm-%	64.69	64.74	61.35	4.17	35.11	58.7	45.63	48.54	87.87	87.73	86.71
Ni	wt-%	2.39	2.47	2.63	0.09	1.97	2.86	2.98	2.27	2.77	2.74	2.7
	atm-%	1.19	1.24	1.37	0.03	0.82	1.41	1.76	1.03	1.98	1.91	1.9
Mo	wt-%	0.39	0.78	1.11	0.1	0.52	0.72	0.41	0.51	0.16	0.2	2.09
	atm-%	0.12	0.24	0.35	0.02	0.13	0.22	0.15	0.14	0.07	0.08	0.9

Bottom		1	2	3	4	5	6	7	8	9
C	wt-%	2.41	2.71	2.53	2.46	2.14	2.61	2.46	0.69	0.97
	atm-%	9.33	9.11	10.17	4.91	5	9.26	7.98	9.58	9.19
O	wt-%	29.22	3.37	6.54	38.43	37.85	26.18	26.45	-	-
	atm-%	46.93	9.61	17.37	50.13	49.15	46.02	35.92	-	-
Al	wt-%	0.5	0.08	0.11	1.43	1.55	0.52	1.27	-	-
	atm-%	0.51	0.14	0.17	1.1	1.19	0.53	1.02	-	-
Si	wt-%	0.37	0.37	0.26	30.12	30.98	0.16	37.3	0.2	0.21
	atm-%	0.36	0.61	0.39	30.7	31.52	0.16	38.8	0.27	0.28
Ca	wt-%	-	-	-	17.83	18.56	0.06	22.19	-	-
	atm-%	-	-	-	9.28	9.62	0.04	12.03	-	-
Cr	wt-%	44.86	40.74	41.72	8.41	7.33	70.28	7.96	6.75	6.53
	atm-%	31.68	54.51	49.2	3.37	2.93	43.91	3.33	4.99	4.79
Mn	wt-%	10.24	0.47	0.8	0.76	0.92	-	1.54	-	-
	atm-%	5.14	0.39	0.62	0.29	0.35	-	0.61	-	-
Fe	wt-%	10.81	2.15	2.51	0.54	0.59	0.06	0.77	75.6	76.32
	atm-%	5.34	1.76	1.91	0.2	0.22	0.03	0.3	74.75	75.94
Ni	wt-%	1.36	0.08	0.02	0.01	0.08	0.07	-	14.54	13.68
	atm-%	0.64	0.06	0.01	-	0.03	0.03	-	9.51	8.89
Mo	wt-%	0.23	50.03	45.52	0.02	-	0.05	0.06	2.22	2.3
	atm-%	0.07	23.81	20.16	-	-	0.02	0.01	0.89	0.91

A10: The point analysis of couple sample sintered at 1360 °C for 6h.

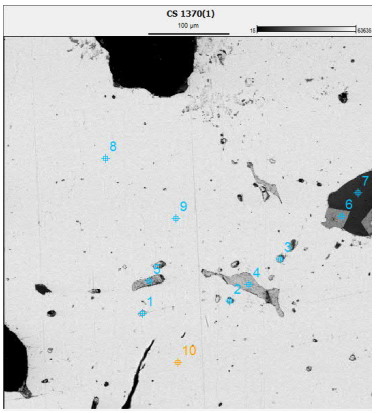

a) Top (high carbon iron)

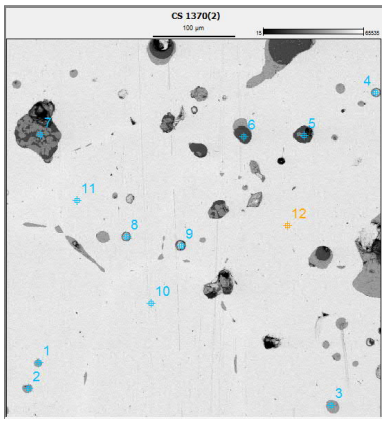

b) Bottom (stainless steel 316L)

Top		1	2	3	4	5	6	7	8	9	10
C	wt-%	2.32	2.94	2.44	1.85	1.79	1.67	1.85	2.11	2.44	2.64
	atm-%	8.82	9.91	8.72	4.69	3.76	3.74	4.93	9.14	7.26	7.89
O	wt-%	1.31	2.3	2.12	1.9	2.89	31.19	37.15	-	-	-
	atm-%	3.41	5.78	5.41	5.59	8.32	59.45	50.39	-	-	-
Al	wt-%	0.06	-	0.05	0.09	0.12	0.12	2.14	-	-	-
	atm-%	0.09	-	0.07	0.16	0.2	0.13	1.64	-	-	-
Si	wt-%	0.86	0.85	0.83	0.53	0.58	0.27	43.29	-	-	-
	atm-%	1.28	1.22	1.21	0.89	0.95	0.27	36.55	-	-	-
Ca	wt-%	-	0.09	0.11	-	0.03	0.07	4.54	-	-	-
	atm-%	-	0.09	0.11	-	0.03	0.05	2.35	-	-	-
Cr	wt-%	0.19	0.11	0.14	0.57	0.61	41.7	0.97	0.11	0.19	0.26
	atm-%	0.15	0.08	0.11	0.51	0.54	23.33	0.39	0.09	0.16	0.23
Mn	wt-%	0.15	0.16	0.11	0.48	0.34	4.08	2.45	0.21	0.13	0.08
	atm-%	0.11	0.12	0.08	0.41	0.28	2.16	0.92	0.16	0.1	0.07
Fe	wt-%	91.45	90.23	91.25	44.66	43.03	20.01	7.61	94.09	94.13	93.4
	atm-%	83.67	80.61	82.36	49.29	48.07	10.42	2.83	88.1	90.23	89.12
Ni	wt-%	3.22	3.02	2.48	1.41	1.37	0.89	-	3.27	2.8	3.32
	atm-%	2.28	2.06	1.72	1.13	1.07	0.44	-	2.41	2.1	2.55
Mo	wt-%	0.44	0.31	0.48	48.52	49.25	-	-	0.21	0.31	0.3
	atm-%	0.19	0.13	0.2	37.34	36.76	-	-	0.1	0.14	0.14

Top		1	2	3	4	5	6	7	8	9	10	11	12
C	wt-%	1.32	1.89	1.76	1.46	1.78	1.31	1.81	1.21	1.2	0.87	0.71	0.51
	atm-%	5.8	4	4.81	6.38	4.17	4.52	5.3	4.71	4.08	9.29	9.89	9.13
Si	wt-%	-	1	0.41	0.47	21.56	24.46	0.7	2.86	0.35	-	-	-
	atm-%	-	1.74	0.75	0.74	16.18	19.27	0.77	2.93	0.61	-	-	-
Cr	wt-%	39.71	40.08	40.3	6.36	6.23	8.22	56.92	3.79	4.85	6.13	6.09	6.32
	atm-%	51.83	52.82	53.46	5.39	2.52	3.5	46.35	2.09	4.58	4.82	4.81	5.09
Mn	wt-%	1.16	1.08	1.58	-	0.89	0.92	13.14	0.09	0.12	-	-	0.01
	atm-%	1.1	0.95	1.46	-	0.34	0.37	7.41	0.05	0.11	-	-	0.01
Fe	wt-%	2.32	3.08	2.38	74.76	0.71	0.78	8.25	58.23	77.25	75.41	75.92	75.53
	atm-%	2.17	2.68	2.16	75.26	0.27	0.31	4.58	44.78	75.17	74.23	73.83	73.85
Ni	wt-%	0.04	-	0.2	15.23	-	-	0.26	11.33	14.5	15.42	15.03	15.33
	atm-%	0.04	-	0.17	11.43	-	-	0.14	5.54	12.13	10.73	10.51	10.93
Mo	wt-%	55.45	52.87	53.37	1.73	-	0.02	0.16	1.79	0.59	2.17	2.25	2.3
	atm-%	39.06	37.8	37.19	0.79	-	-	0.05	0.54	0.3	0.93	0.96	1
O	wt-%	-	-	-	-	45.06	37.02	17.59	16.94	0.78	-	-	-
	atm-%	-	-	-	-	60.46	52.36	34.19	35.42	2.4	-	-	-
Al	wt-%	-	-	-	-	2.37	2.65	0.8	3.66	0.29	-	-	-
	atm-%	-	-	-	-	1.85	2.18	0.92	3.89	0.53	-	-	-
Ca	wt-%	-	-	-	-	21.39	24.63	0.37	0.08	0.07	-	-	-
	atm-%	-	-	-	-	14.2	17.49	0.29	0.06	0.09	-	-	-

A11: The point analysis of couple sample sintered at 1370 °C for 6h.

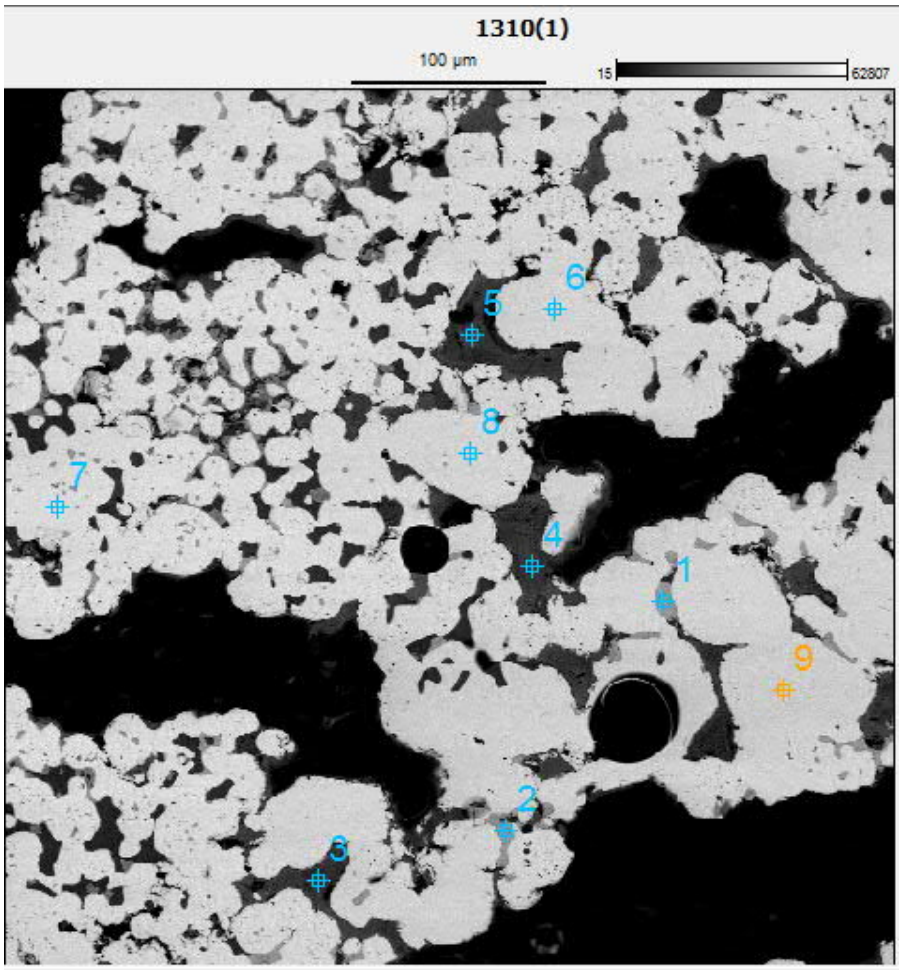

Elements		1	2	3	4	5	6	7	8	9
C	wt-%	1.25	1.42	1.26	2.03	2.63	2.41	2.13	2.23	2.52
	atm-%	4.03	4.64	8.87	8.18	9.35	9.55	9.9	9.43	9.16
Si	wt-%	-	-	0.44	1.03	0.87	0.12	0.27	0.17	0.15
	atm-%	-	-	0.43	0.96	0.86	0.18	0.4	0.26	0.22
Cr	wt-%	30.84	32.72	0.87	0.96	1.03	7.97	9.05	8.71	8.71
	atm-%	38.9	38.68	0.45	0.48	0.55	6.37	7.3	7.2	7.12
Mn	wt-%	11.25	8.91	0.19	0.08	0.09	0.1	0.07	0.05	0.03
	atm-%	11.03	8.7	0.1	0.04	0.04	0.07	0.05	0.04	0.02
Fe	wt-%	2.21	2.03	60.9	64.7	68.96	81.44	77.42	80.21	82.38
	atm-%	2.14	1.95	37.66	43.61	49.46	78.37	74.89	77.07	79.13
Ni	wt-%	0.01	-	5.67	2.97	4.47	7.33	9.47	7.53	5.69
	atm-%	0.01	-	2.62	1.32	2.12	5.19	6.76	5.51	4.12
Mo	wt-%	54.44	54.92	0.36	0.33	0.27	0.63	1.6	1.09	0.51
	atm-%	43.9	48.02	0.1	0.09	0.08	0.27	0.7	0.49	0.23
O	wt-%	-	-	28.72	27.5	21.35	-	-	-	-
	atm-%	-	-	48.63	44.94	37.24	-	-	-	-
Al	wt-%	-	-	0.25	0.32	0.18	-	-	-	-
	atm-%	-	-	0.25	0.31	0.19	-	-	-	-
Ca	wt-%	-	-	1.33	0.09	0.14	-	-	-	-
	atm-%	-	-	0.9	0.06	0.1	-	-	-	-

A12: The point analysis of mixed sample sintered at 1310 °C for 1h.

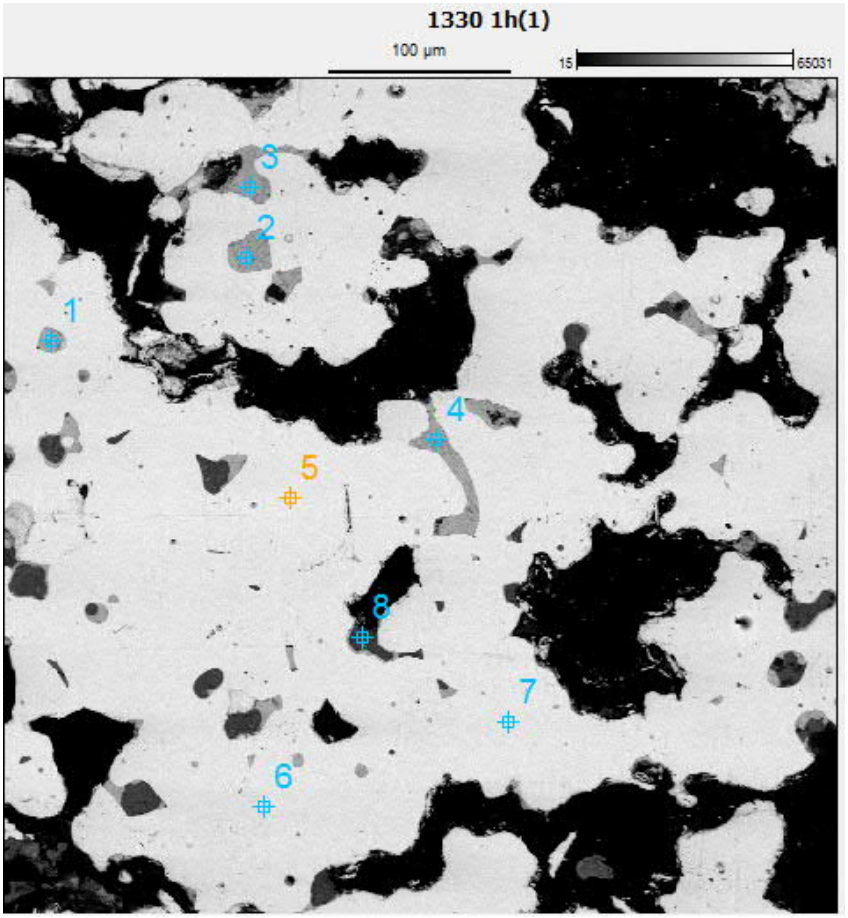

Elements		1	2	3	4	5	6	7	8
C	wt-%	0.74	0.7	0.17	1.5	2.71	2.79	2.63	2.54
	atm-%	6.71	6.58	6.71	6.23	9.87	9.09	9.66	6.9
Cr	wt-%	34.08	22.18	34.73	35.72	8.37	8.48	8.45	8.12
	atm-%	47.65	45.71	46.9	47.25	6.86	6.93	6.93	3.37
Mn	wt-%	9.65	11.91	9.85	8.45	0.1	0.02	0.14	3.37
	atm-%	9.31	11.49	9.67	8.38	0.08	0.02	0.11	1.32
Fe	wt-%	1.91	2.06	1.85	1.33	75.8	75.86	75.9	1.5
	atm-%	1.81	1.95	1.79	1.3	74.2	75.16	74.43	0.58
Ni	wt-%	0.04	0.06	-	0.02	11.45	11.11	11.1	0.03
	atm-%	0.04	0.06	-	0.02	8.3	8.04	8.07	0.01
Mo	wt-%	53.58	53.09	53.41	52.98	1.56	1.75	1.79	-
	atm-%	34.49	34.21	34.93	36.82	0.69	0.77	0.8	-
Al	wt-%	-	-	-	-	-	-	-	2.53
	atm-%	-	-	-	-	-	-	-	2.02
O	wt-%	-	-	-	-	-	-	-	32.18
	atm-%	-	-	-	-	-	-	-	45.28
Ca	wt-%	-	-	-	-	-	-	-	14.28
	atm-%	-	-	-	-	-	-	-	7.68
Si	wt-%	-	-	-	-	-	-	-	35.45
	atm-%	-	-	-	-	-	-	-	32.84

A13: The point analysis of mixed sample sintered at 1330 °C for 1h.

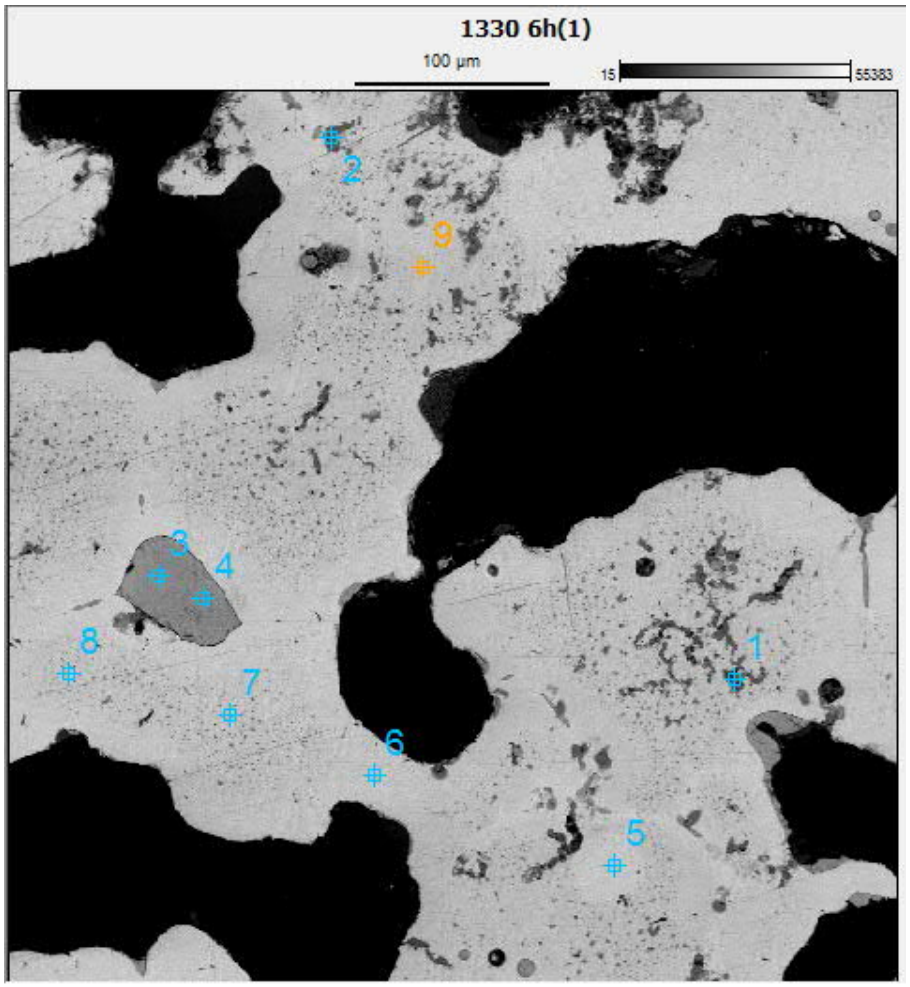

Elements		1	2	3	4	5	6	7	8	9
C	wt-%	2.76	2.1	1.52	1.2	2.57	2.2	2.77	2.14	2.05
	atm-%	10.3	9.12	6.62	5.47	9.47	9.71	9.14	9.02	9.4
Si	wt-%	0.56	0.71	-	0.2	0.19	0.14	0.13	0.14	0.14
	atm-%	0.69	0.81	-	0.36	0.3	0.2	0.18	0.2	0.21
Cr	wt-%	3.03	2.14	38.22	32.72	4.84	4.52	4.68	4.3	3.7
	atm-%	2.02	1.33	48.27	46.99	3.98	3.56	3.63	3.3	2.93
Mn	wt-%	0.07	0.03	1.69	3.22	-	0.03	0.07	0.09	0.04
	atm-%	0.04	0.02	1.6	2.97	-	0.02	0.05	0.06	0.03
Fe	wt-%	84.74	82.32	4.4	12.38	81.03	81.81	80.62	81.66	82
	atm-%	81.85	82.24	4.1	11.22	78.38	79.03	79.39	79.91	79.48
Ni	wt-%	8.31	10.29	-	0.72	9.96	9.9	10.06	10.07	10.22
	atm-%	4.9	5.67	-	0.62	7.25	6.89	6.91	6.84	7.16
Mo	wt-%	0.53	2.42	56.18	49.57	1.4	1.4	1.66	1.61	1.85
	atm-%	0.19	0.81	39.41	32.37	0.62	0.6	0.7	0.67	0.79

A14: The point analysis of mixed sample sintered at 1330 °C for 6h.

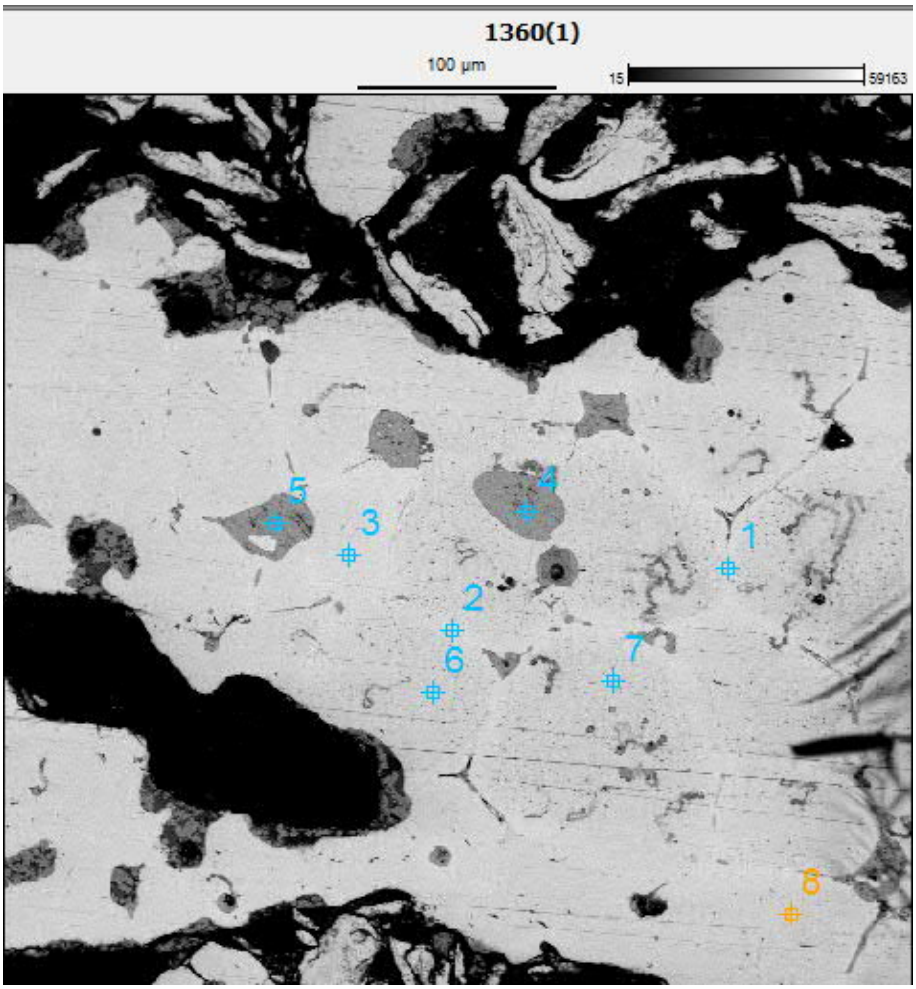

Elements		1	2	3	4	5	6	7	8
C	wt-%	2.05	2.08	1.98	1.03	1.83	2.04	1.99	3.44
	atm-%	9	9.08	8.65	5.85	9.99	8.9	8.68	14.31
Cr	wt-%	4.6	5.07	5.52	35	35.29	6.18	6.51	6.84
	atm-%	4.66	5.11	5.57	45.82	44.42	6.22	6.56	6.57
Mn	wt-%	0.04	-	0.01	2.87	0.53	-	0.05	-
	atm-%	0.04	-	0.01	3.56	0.63	-	0.05	-
Fe	wt-%	77.62	78.85	78.92	2.74	4.93	78.39	78.41	76.96
	atm-%	73.23	74	74.24	3.35	5.77	73.51	73.58	68.78
Ni	wt-%	12.79	11.98	11.8	0.06	0.04	11.72	11.56	11.22
	atm-%	11.48	10.7	10.56	0.07	0.05	10.45	10.32	9.54
Mo	wt-%	2.9	2.01	1.77	58.29	57.37	1.68	1.48	1.53
	atm-%	1.59	1.1	0.97	41.35	39.14	0.92	0.81	0.8

A15: The point analysis of mixed sample sintered at 1360 °C for 1h.

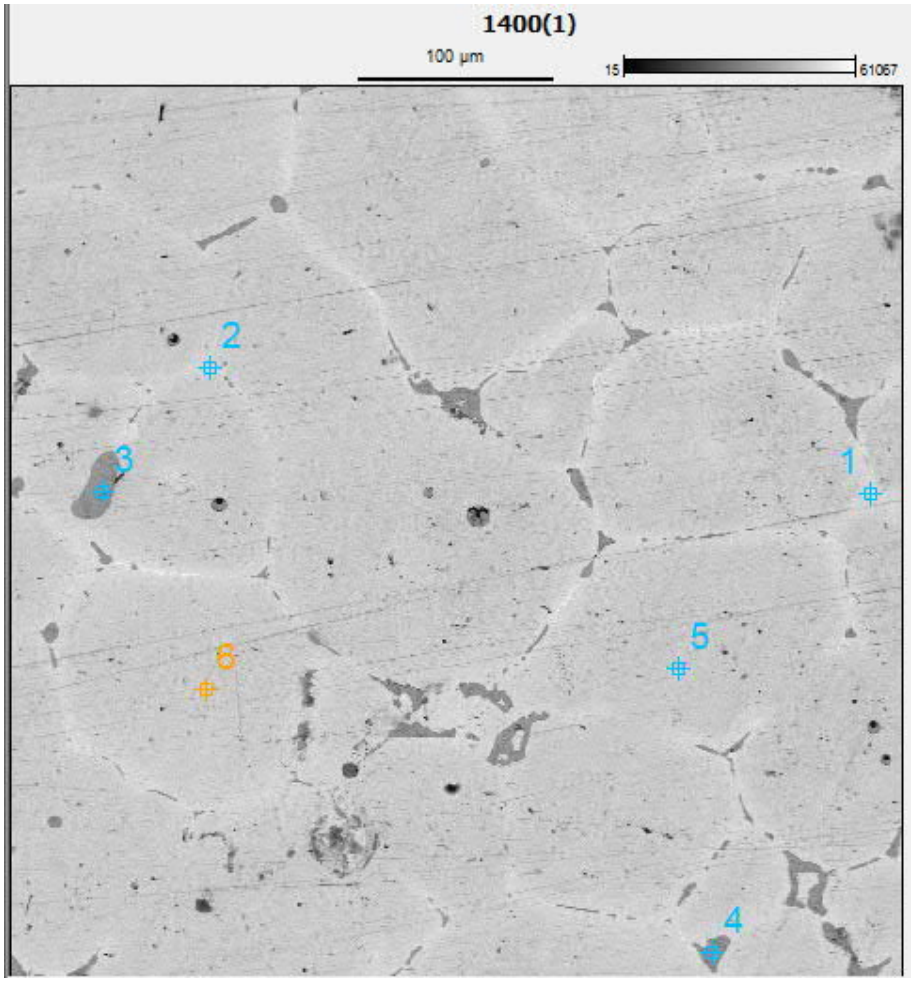

Elements		1	2	3	4	5	6
C	wt-%	2.37	2.24	1.87	1.1	2.51	2.66
	atm-%	9.12	9.93	5.54	5.97	8.76	8.64
Al	wt-%	-	-	0.11	0.12	0.01	0.01
	atm-%	-	-	0.2	0.23	0.01	0.01
Si	wt-%	0.61	0.31	1.1	0.56	0.44	0.88
	atm-%	0.87	0.45	1.94	1.05	0.62	1.26
Ca	wt-%	-	-	-	0.02	-	-
	atm-%	-	-	-	0.02	-	-
Cr	wt-%	1.45	2.35	30.89	32.87	5.04	4.72
	atm-%	1.12	1.85	45.65	45.43	3.82	3.64
Mn	wt-%	0.15	0.1	0.98	-	0.07	0.08
	atm-%	0.11	0.07	0.89	-	0.05	0.06
Fe	wt-%	76.99	81.04	8.65	7.39	80.19	80.18
	atm-%	78.01	78.57	7.67	6.89	79.22	78.91
Ni	wt-%	11.39	11.7	0.12	0.04	10.33	10.08
	atm-%	7.81	8.16	0.1	0.04	6.93	6.9
Mo	wt-%	7.04	2.26	56.28	57.9	1.41	1.4
	atm-%	2.95	0.96	38.01	40.36	0.58	0.59

A16: The point analysis of mixed sample sintered at 1400 °C for 1h.